

**NATIONAL UNIVERSITY OF SCIENCES & TECHNOLOGY
COLLEGE OF ELECTRICAL AND MECHANICAL ENGINEERING,
RAWALPINDI, PAKISTAN**



**Compression Ring Hydrodynamic and Elastohydrodynamic Lubrication
Modeling in the Initial Engine Start Up**

By

Mr. Ali Usman

MS-56 (Mechanical Engineering)

(2008-NUST-MS-Phd-Mech-02)

**Thesis submitted to the faculty of the Department of Mechanical Engineering,
National University of Sciences and Technology College of Electrical and Mechanical
Engineering, Rawalpindi PAKISTAN in partial fulfillment of the requirements for the
degree of Masters**

Thesis Supervisor

Prof. Dr. Muhammad Afzaal Malik

Compression Ring Hydrodynamic and Elastohydrodynamic Lubrication
Modeling in the Initial Engine Start Up

By
Mr. Ali Usman

Submitted to the Faculty of Department of Mechanical Engineering,
National University of Sciences and Technology College of Electrical and
Mechanical Engineering, Rawalpindi Pakistan, in partial fulfillment of
the requirement for the degree of
Master of Science in Mechanical Engineering

Candidate: _____
Mr. Ali Usman

Advisor: _____
Professor Dr. Muhammad Afzaal Malik

Committee Members:

1. Prof. Dr. Mahmood Anwar Khan
2. Associate Prof. Dr. Riaz A Mufti
3. Assistant Prof. Raja Amir Azim

National University of Sciences and Technology
College of Electrical & Mechanical Engineering
Rawalpindi

27 Jan, 2011

Publications

1. M. Afzaal Malik, Ali Usman, S. Adnan Qasim, Riaz Mufti, "Modeling of Piston Top Ring Lubrication by Considering Cylinder Out-Of-Roundness in Initial Engine Start Up", International Congress on Mechanical Engineering, London, 29 June-to- 3 July 2010
2. Ali Usman, M. Afzaal Malik, S. Adnan Qasim, Riaz Mufti, "Modeling Two-Dimensional Elastohydrodynamic Lubrication Fluid Flow Of Piston Top Ring Considering Elastic Deformation In Initial Engine Start Up", ASME International Mechanical Engineering Congress & Exposition, Vancouver Canada, 12- 18 Nov 2010
3. Ali Usman, M. Afzaal Malik, S. Adnan Qasim, Riaz Mufti, "Modeling the Energy Loss in the Two-Dimensional Lubrication of First Compression Ring in the Initial Engine Start-Up", IEEE International Conference on Energy Systems Engineering, Pakistan, 25-27 Oct 2010

ABSTRACT

Modern engine design demands better fuel economy, reduced exhaust emissions, increased recyclability, freedom from hazardous substances and enhanced operating life. To fulfill these requirements, automobile engine manufacturers ensured that piston ring design must reduce frictional power loss, oil transport into the combustion chamber, and wear, as piston ring account for majority of the mechanical power loss of the internal combustion engine. Aforementioned requirements and function can be fulfilled only and only if piston ring is fully flooded with controlled amount of lubricant oil at inlet region, to generate Elastohydrodynamic lubricating film between piston ring and cylinder liner to separate these sliding surfaces from each other, hence preventing adhesive wear and dry contact.

Oil starvation and absence of fully developed lubricating film results in dry contact followed by sequential formation of boundary, mixed, hydrodynamic and then elastohydrodynamic lubricating film in initial engine start up. This sequence of film development in engine startup period results in drastic increase in friction, power loss, wear and ultimately compromised engine operating life. Advancement in numerical and experimental investigation of static and dynamic analysis of piston ring performance showed that cylinder liner is not perfectly circular due to high combustion pressure forces, thermal distortion, variable load at major and minor thrust sides, wear, head clamping forces and manufacturing errors. This liner distortion results in reduction in magnitude of the minimum lubricating film thickness due to circumferential flow of lubricant oil, but decreased overall power loss and increased exhaust emissions due to oil transport in to the combustion chamber.

In this research work Two-Dimensional hydrodynamic and elastohydrodynamic model is developed and is simulated in initial engine startup conditions. Parametric study is conducted for piston ring running face profile, engine speed and degree of distortion in non-circular cylinder liner. Results show that parabolic ring running face profile is best suited for improved lubricating film thickness profile and performance. Results also show that with increase in speed, film thickness profile improves but ring performance decreases, and with increase in magnitude of bore distortion, film thickness profile and ring performance improve, except oil transport to combustion chamber, which also increases.

ACKNOWLEDGMENT

First and foremost, I would like to thank The Allah Almighty, Who lead this work to be completed in time and Whose blessings and help kept me sheltered all the time.

I would like to thank my advisor Dr. Prof. Afzaal Malik, for his contributions to both my work as well as my personal and professional development throughout my time at the NUST College of E&ME and for all of the technical insight he has provided on numerous occasions throughout the duration of the Thesis work. I would also like to thank Mr. Syed Adnan Qasim, the founder of Tribology research group in NUST College of E&ME. It was he, who introduced the concept of research groups in Mechanical department of the college, and his endless efforts made in possible to establish not only Tribology research group but also Micro-Air Vehicle research group. His never ending encouragement and guidance made it possible for me to conduct and complete this research work. Countless discussion with him on technical issues, Islamic, social and moral values gave me valuable insight to many aspects of professional and personal development.

I am indebted to the College of Electrical and Mechanical Engineering, National University of Sciences and Technology and Higher Education Commission of Pakistan for providing financial resources for this research work.

I would like to thank my beloved parents and family, who always guided me in the right way and whose endless effort and support made it possible for me, to be, what I am today. I would not forget to thank my dear friends like Mr. Abdul Wahab, Mr. Zubair Ahmed and Mr. Sheeraz Sabir, for always being there for me.

I have been fortunate to met and work with many wonderful people like Asst. Prof. Raja Amer Azim, Mr. Farooq Ahmad, Mr. Mumtaz Ali Khan, Mr. Usman Farooq, Mr. Munzer Shaheer, Mr. Barlas, Mr. Arsalan Jahangir, Mr. Mubashir Gulzar, Mr Muhammad Saif ullah Khaild, Mr. Azher Zeb, and Ms. Sadia Riaz. Who made my time at college enjoyable and whose continues encouragement made it possible for me to reach all the way to this point.

In the end I would like to thank the entire honorable faculty of Mechanical Department of the college, whose professional approach and vision groomed me.

Ali Usman
Jan 2011

Table of Contents

Abstract	1
Acknowledgment	2
Table of Contents	3
List of Figures	6
List of Tables	8
Chapter-1 Introduction	9
1.1. Back Ground	9
1.2. Previous Experimental and Theoretical Work on Ring/Liner Static and Dynamic Analysis	12
1.2.1. Hydrodynamic and Mixed Lubrication	12
1.2.2. Elastohydrodynamic Lubrication	16
1.3. Objective of the Thesis Work	18
1.3.1. Static Analysis	18
1.3.2. Dynamic Analysis	18
Chapter-2 Mathematical Modeling	20
2.1. Introduction	20
2.2. Principle of Hydrodynamic Pressure Generation	20
2.3. Derivation of Two-Dimensional Steady State Reynolds Equation	23
2.3.1. Equilibrium of Liquid Subjected to Viscous Shear	23
2.3.2. Reynolds Equation and Continuity of Flow in a Column Application of Flow Continuity Principle	27
2.3.3. Simplification to 3-D Reynolds Equation	29
2.4. Elastohydrodynamic Lubrication of Piston and Rings	31
2.4.1. EHL/EHD Theory	31
2.4.2. Contact Stresses and Hertz Theory	32
2.4.3. Stress Status in Lubricated Sliding Contact	33
2.4.4. EHD Lubricating Film	33
2.4.5. Theoretical EHL Film Thickness of Piston and Ring	34

Chapter-3	Piston Ring Lubrication	35
3.1.	Mathematical Model of Rigid Ring and Liner Lubrication	35
3.1.1.	Piston Ring Instantaneous Velocity	36
3.1.2.	Hydrodynamic Film Thickness	37
3.1.3.	Film Thickness in Sliding Direction	37
3.1.4.	Film Thickness in Circumferential Direction	39
3.1.5.	Resultant Hydrodynamic Load	40
3.2.	Mathematical Model of Elastic Ring and Liner Lubrication	42
3.2.1.	Elastohydrodynamic Lubricating Film Thickness	42
3.2.2.	Pressure Viscosity Relation	43
3.3.	Performance Parameters	44
3.3.1.	Friction Force	44
3.3.2.	Power Loss	45
3.3.3.	Flow Rate	45
Chapter-4	Non-Dimensionalisation and Numerical Procedure	47
4.1.	Non-Dimensional Reynolds Equation	47
4.2.	The Vogelpohl Parameter	47
4.2.1.	Finite Difference Equivalent of Reynolds Equation	48
4.3.	Algorithm for Numerical Simulation	51
4.3.1.	Hydrodynamic Lubrication	51
4.3.2.	Elastohydrodynamic Lubrication	52
Chapter-5	Results and Discussions	53
5.1.	Lubricating Film Thickness	53
5.2.	Hydrodynamic and Elastohydrodynamic Pressure Field	57
5.3.	Performance Parameters	65
5.3.1.	Friction Force and Power Loss	65
5.3.2.	Lubricant Flow Rate	66
Chapter-6	Sensitivity Analysis - Results and Discussions	68
6.1.	Parametric Study of Ring Face Profile	68

6.1.1.	Effect of Ring Running Face Profile on Lubricating Oil Film Thickness	68
6.1.2.	Effect of Ring Running Face Profile on Performance Parameters	69
6.2.	Parametric Study of Engine Speed	75
6.2.1.	Effect of Engine Speed on Lubricating Oil Film Thickness	75
6.2.2.	Effect of Engine Speed on Performance Parameters	79
6.3.	Parametric Study of Bore Distortion	81
6.3.1.	Effect of Bore Distortion on Lubricating Oil Film Thickness	81
6.3.2.	Effect of Bore Distortion on Piston Ring Performance	82
Chapter-7	Conclusions	84
	References	
	Annexure	

List of Figure

Figure 1.1	Piston assembly and piston ring pack of an internal combustion engine	9
Figure 2.1	Principle of hydrodynamic pressure generation between non-parallel surfaces	21
Figure 2.2	Equilibrium of an element of fluid from a hydrodynamic film	23
Figure 2.3	Velocity profile at the entry of hydrodynamic film	26
Figure 2.4	Continuity of flow in a column	27
Figure 2.5	Effect of local deformation on the lubricant film profile	34
Figure 3.1	Variable and coordinate systems	36
Figure 3.2	Cross-sectional view of the piston ring	37
Figure 3.3	Cross-sectional view of different symmetric ring face profile	38
Figure 3.4	Circumferential deformation of the cylinder liner	39
Figure 3.5	Gas pressure forces Vs crank angle	41
Figure 4.1	Finite difference operator and nodal scheme for numerical analysis of the Reynolds equation	49
Figure 4.2	Computational flow-chart for the hydrodynamic lubrication	52
Figure 4.2	Computational flow-chart for the elastohydrodynamic lubrication	53
Figure 5.1	Minimum hydrodynamic and elastohydrodynamic film thickness Vs Crank angle	56
Figure 5.2	Film thickness field as a function of the ring geometry	57
Figure 5.3-5.12	Hydrodynamic pressure fields	58-64
Figure 5.13	Hydrodynamic viscous friction force Vs Crank angle	65
Figure 5.14	Mechanical frictional power loss Vs Crank angle	66
Figure 5.15	Volumetric flow rate (m^3/s) Vs Crank angle	67
Figure 6.1 (a)	Minimum film thickness Vs crank angle	68
Figure 6.1 (b)	Maximum hydrodynamic pressure Vs Crank angle	69
Figure 6.2	Friction force Vs crank angle	70
Figure 6.3	Power loss Vs crank angle	72

Figure 6.4	Flow rate Vs crank angle	73
Figure 6.5	Minimum hydrodynamic film thickness Vs crank angle at different engine speeds	75
Figure 6.6 (a)	Minimum hydrodynamic film thickness in critical region	75
Figure 6.6 (b-e)	Hydrodynamic Pressure profiles over the ring face at 450 degree crank angle at different engine speeds	76-77
Figure 6.7	Minimum EHD lubricating film thickness Vs crank angle	78
Figure 6.8	Minimum EHD lubricating film thickness Vs crank angle in critical region	78
Figure 6.9	Viscous friction force Vs crank angle at different engine speeds	79
Figure 6.10	Mechanical power loss Vs crank angle at different engine speeds	79
Figure 6.11	Volumetric flow rate Vs crank angle at different engine speeds	80
Figure 6.12 (a-b)	Minimum film thickness at different degree of bore distortion	81
Figure 6.13	Viscous friction force Vs crank angle at different degree of bore distortion	82
Figure 6.14	Mechanical power loss Vs crank angle at different degree of bore distortion	82
Figure 6.15	Volumetric flow rate loss Vs crank angle at different degree of bore distortion	83

List of tables

Table 2.1	Summary of the simplifying assumptions in hydrodynamics	22
Table 4.1	Value of the parameters adopted for the calculations	51

CHAPTER-1

Introduction

1.1 Background

Piston ring pack is essentially a set of sliding seal which is used for several purposes, for instant: separate the combustion chamber from crank case, transfer, heat generated during combustion, to cylinder liner, distribute and control the Lubricating oil, stabilize the piston [1]. To perform aforementioned functions the conventional piston ring pack of the modern high speed automobile engine consists of three rings: the top or first compression ring, second compression or scrapper ring, oil control ring, as shown in Fig 1.1

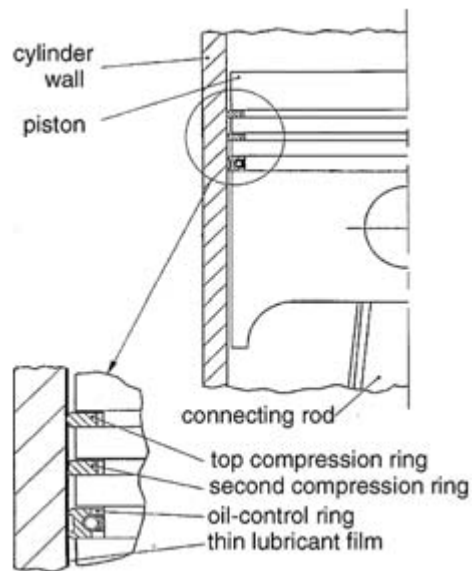


Fig 1.1: Piston assembly and piston ring pack of an internal combustion engine [1]

Top compression ring experiences the most severe operating conditions and alternating loads and its main function is to provide sealing function, that is, to prevent combustion gas leakage from combustion chamber to crank case. Top ring mostly have barrel or parabolic ring faced profile with wear resistant coating, such as flame sprayed molybdenum [1]. Parabolic profile has the advantage that it tends to be self-perpetuating under wear since the piston ring tends to rock inside its groove during reciprocating movement and causes preferential wear of

the edges of the ring [2]. Second compression ring is designed to assist first compression ring and to limit upward oil flow and is therefore tapered-faced, downward scraping profile or non-axisymmetric face profile and is normally not coated. Oil control ring limits the amount of the lubricating oil transport from the crank case to the combustion chamber and has no gas sealing function. Oil control ring has two running faces or lands and is usually chromium plated [1].

Modern automotive engines are designed and developed keeping in view five major factors: fuel economy, pollutant engine out emission, increased recyclability, freedom from hazardous substances, customer satisfaction [3].

For these design specification the piston rings have to meet six requirements: low friction, low wear, emission suppression, by limiting the flow of engine oil to combustion chamber, good sealing ability, good mechanical and thermal fatigue properties, and cost efficient and prolonged operating life [4]. Piston ring zone contributes 20% - 50% of the total mechanical frictional losses of an internal combustion engine [3, 6, 7]. So improvement in the performance of the piston ring will subsequently lead to fuel economy, prolonged live, low friction and reduced power loss.

In order to study aforementioned requirements one has to understand ring pack lubrication and dynamics. Among the efforts to understand piston ring performance, Numerical simulation has been advancing in many aspects and playing very important role. Numerical models can be categorized into Static analysis and Dynamic analysis. The static analysis refers to the study of the static interaction between a single ring and the power cylinder system, while the dynamic analysis includes ring-pack lubrication modeling, ring-pack dynamics and blow-by simulation during engine operation [8]. In the following sections, the existing modeling work and their limitations are reviewed.

Furthermore static analysis can be divided into two main streams: geometry-mechanical design and material coating design. The dynamic analysis of the piston ring-pack are usually further categorized into dynamics analysis and lubrication analysis. The major subject of dynamics analysis is to study the axial, radial and twist displacements of a ring during an engine cycle, while the main goal of lubrication analysis is to investigate the ring/liner friction and oil transport along the liner [8].

Under all of the above mentioned critical requirements, piston ring performance and limitations, Tribological study has been center of interest for many global researchers for decades.

1.2 Previous Experimental and Theoretical Work on Ring/Liner Static and Dynamic Analysis

1.2.1 Hydrodynamic and Mixed Lubrication

The serious appreciation of hydrodynamics in lubrication started at the end of the 19th century when Beauchamp Tower, an engineer, noticed that the oil in a journal bearing always leaked out of a hole located beneath the load. The leakage of oil was a nuisance so the hole was plugged first with a cork, which still allowed oil to ooze out, and then with a hard wooden bung. The hole was originally placed to allow oil to be supplied into the bearing to provide 'lubrication'. When the wooden bung was slowly forced out of the hole by the oil, Tower realized that the oil was pressurized by some as yet unknown mechanism. Tower then measured the oil pressure and found that it could separate the sliding surfaces by a hydraulic force [9]. At the time of Beauchamp Tower's discovery Osborne Reynolds and other theoreticians were working on a hydrodynamic theory of lubrication. By a most fortunate coincidence, Tower's detailed data was available to provide experimental confirmation of hydrodynamic lubrication almost at the exact time when Reynolds needed it. The result of this was a theory of hydrodynamic lubrication published in the Proceedings of the Royal Society by Reynolds in 1886 [10]. Reynolds provided the first analytical proof that a viscous liquid can physically separate two sliding surfaces by hydrodynamic pressure, resulting in low friction and theoretically zero wear.

In 1974 G.M Hamilton [11] measured oil film thickness between piston ring and liner of a small diesel engine using capacity gauges and found that behavior is essentially hydrodynamic throughout the stroke upon different seeps, loads and temperature variation. It was observed that oil film thickness increases with increase in speed and viscosity, where as it reduces with increasing load. Again in 1974 G.M Hamilton [12] compared measured and calculated lubricating oil film thickness between piston ring/liner and found that measured film thickness is considerably greater and is not in complete agreement with theoretical results. Author addressed the reason of this discrepancy in the measured and predicted results in 1977, S.R. Brown and G M Hamilton [13], stated that if care is taken to keep inlet region of the ring fully

flooded the film thickness obeys the theory and such starvation is an essential feature of the lubrication of the ring in a ring pack. Capacitance film thickness measuring gauges and pressure gauges were used to conduct experimental study and found that if aforementioned instruments are used in conjunction with each other then it is possible to account for the behavior of a piston ring even at the central portion of the stroke. In 1980 SL Moore and GM Hamilton [14] extended their previous experimental investigation of oil film thickness behavior at TDC using capacitance transducers and diesel engine, authors focused on the change in film thickness along the ring face over long period of running engine and found that film thickness profile at a fixed location on the liner (TDC), and observed oil film thickness is dependent upon time of measuring from the moment engine started. Authors also showed that film thickness profile varies along the circumferential axis by measuring oil film thickness profile along the ring face at five different circumferential positions. Asperity heights were observed to be reduced and peak to peak surface roughness decreases in running engine than that of before running.

In 1986, Sherrington and E.H. Smith [15] proposed different experimental methods for measuring the oil film thickness between piston ring and cylinder liner of internal combustion (IC) engine and critically analyzed optical and electrical method of measuring oil film thickness considering accuracy, installation issues and localized film thickness as investigating criteria. In 1992 Y. Wakuri et al [16], presented a comparative study regarding piston ring friction in internal combustion engine, authors stated that piston assembly accounts for majority of mechanical power loss in the engines. Authors used the hydrodynamic regime as lubricating regime for complete stroke and considered only change in film thickness in the sliding direction and also incorporated shear thinning effects as modern SAE oil are all non-Newtonian. Results predicted oil film thickness of the top compression ring is remarkably reduced over the complete cycle and cyclic change in oil film thickness is reduced when oil starvation with in the ring pack is taken into account. In 1995 M. T. Ma et al [17], developed a three-dimensional mathematical model to analyze piston ring lubrication, author considered parabolic ring shape, elliptical and four lobe distorted bore, oil damping forces at TDC and BDC and piston ring fluttering inside the groove. Main focus of these researchers was to investigate effect of bore-out-of-roundness on oil film thickness, power loss and oil flow rate. This work concluded that

oil film thickness values and profile reduces in four lobe bore than that of in elliptical bore and than that of circular cylinder liner. Bore out of roundness can reduce the energy consumption despite the effect of ring liner interaction. It was also observed that when a simple model of the ring-liner interaction is adopted, the predicted energy consumption is likely to be about twice than that of predicted by using fully hydrodynamic lubrication for the entire strokes. However, it can be concluded from this work that although the model used does not give precise numerical results for friction and power loss, the trends observed still give a remarkable indication of the behavior of these variables at the interface. In 1995, Masaaki Takiguchi et al [18] conducted experiments on engine with different ring packs using Laser Induced Florescence probe as measuring instrument at normal operation condition and stated that oil film thickness of ring pack having two rings, is thinner than that of three rings due to greater amount of blow by through the piston, as a result oil consumption of two ring piston was kept to the low level of the conventional ring pack. Piston friction force can be reduced using low tension of piston ring but lube oil consumption will increase in this case.

In 1996, Qingmin Yang and Theo G. Keith [19] adopted a hydrodynamic cavitations algorithm to analyze piston ring performance. Two-dimensional piston ring with elliptically distorted cylinder liner was used by authors to investigate circumferential flow effect. Results showed that hydrodynamic pressure dramatically decreases with increase in film thickness in circumferential direction because of deformed cylinder liner.

In 1996, G R Paul and IJ sixsimith [20], experimentally measured friction and energy losses in motored and firing engine and found that friction increases with increase in speed and magnitude of friction force almost doubles its value the moment engine firing starts. In 1998, Mohsen Esfahanian et al [21], conducted two-dimensional theoretical analysis on low speed two stroke diesel engine considering film thinness changes in sliding direction and squeeze film effects at TDC and BDC, authors concluded that minimum film thinness occur few degree crank angle after TDC in the combustion stroke and magnitude of film thickness was found to be in fraction of micron, pointing that chances of wear are sufficiently prominent in this zone. In 1998, Kliu et al [22], developed a theoretical model considering change in the film thickness in sliding and circumferential direction, considering surface roughness in account along with

piston tilt motion. Authors found that lubricating film thickness is non uniform along the circumferential direction. Parametric study was also conducted by authors on piston ring geometry and found that power loss and ring height are directly proportional to each other.

In 1999, Sanjay D. Gulwandi [23], conducted a detailed study of tribological performance of piston ring pack with the objective of studying the behavior and inter relation of key engine parameters, such as oil consumption, blow by/blow back, power loss and wear load, for typical normal operating conditions. The computation was conducted considering high speed 4-stroke gasoline engine at different loads and engine speeds and at different inlet/exit conditions. In first case, 1st, 2nd and 3rd rings were computed independent of each other. In second case oil left over by trailing edge of leading ring was taken as inlet for leading edge of trailing ring, authors found that for both cases behavioral trend of film thickness is almost same and for increasing speed and loads, engine losses increases. In 1999 Zeng Yong et al [7], conducted a theoretical study in hydrodynamic and mixed regime with effect of variable viscosity depending upon temperature and pressure in mixed and hydrodynamic regime. It was found that film thickness is highly dependent on shear rate.

In 2000, Sung woo et al [24], published experimental results and finding on the frictional model of barrel shaped piston ring under flooded condition and under controlled lubricant oil temperature and piston secondary motion. Authors stated that frictional behavior of piston ring can be classified into five modes by lubrication regimes evaluated at mid-stroke and dead centers; transition between the lubrication regimes is easily achieved at mid-stroke where the piston speed is high, but the transition is more difficult at dead centers where the piston speed approaches zero. Mode I: Boundary lubrication is dominant throughout the entire stroke. This mode can be seen when the engine speed is slow and oil viscosity is very low. Mode II, III: Transition to mixed lubrication begins at the mid-stroke region where piston speed is high. Transition progresses towards dead centers, where piston speed approaches zero. Mode IV, V: Transition to hydrodynamic lubrication starts at the mid-stroke region, and the position of transition progresses towards the dead center region.

In 2000, Jinglei Chen and D.E. Richardson [25], used Cummins single cylinder research base engine with intense degree of instrumentation including pressure sensors and ring motion

sensors at eight different positions on piston and cylinder over six sets of different operating conditions and concluded that blow by and inter ring pressure predicted correlates well with measured results but small change in inter ring pressure can sometime cause complete differently ring motion.

1.2.2 Elastohydrodynamic Lubrication

As an icon in field of tribology, D. Dowson, B.L Ruddy and PN Economou [26], in 1982 conducted a piston ring lubrication study in Elastohydrodynamic regime using one dimensional model with squeeze film effects and found that elastic consideration plays a significant role in the lubrication of the top compression ring, near top dead center (TDC). This study was one of the very few studies in which elastic effects were considered along with hydrodynamic lubrication theory of piston rings, author strongly recommended that elastic deformation must be taken in account when investigating lubrication problem of piston ring near TDC in the combustion stroke.

Later on in 1991 Chu-Jung and Cheng-I Weng [27], used non linear Finite Element Method (FEM) scheme based on Newtonian Raphson Mutry algorithm to analyze piston ring lubrication problem under EHL and Hydrodynamic regime. Results were consistency with those presented by D. Dowson and Ruddy and conclusions regarding lubricating film thickness were approximately same as were concluded by D. Dowson.

In 1996 Qumingmin Yang and Theo G. Keith JR [28] extended their previous hydrodynamic model by incorporating elastic deformation and cavitations in their previous two-dimensional model and found that elastic deformation are only prominent in power stroke when gas pressure is high enough and net hydrodynamic film profile offsets with a positive shift. When compression is made between one-dimensional and two-dimensional results, film thickness values sere also observed to be reduced due to circumferential flow.

In 2009, Chensbo Ma and Hua Zhu [29], adopted Partial Elastohydrodynamic phenomena to simulate minimum film thickness in the piston ring cylinder contact, with pezo-density and pezo-viscosity in One-dimensional mathematical model, and concluded that in closed vicinity to

the TDC the minimum film thickness is less than one micron and to consider elastic deformation whether partial or compound, must be taken in account while calculating oil film thickness

1.3 Objective of the Thesis Work

As discussed earlier, piston ring performance is core of IC engine performance, and numerical simulation is the key to investigate and improve static and dynamic issues of the piston ring. It is also clear from above discussion that piston ring performance is being mathematically modeled and simulated for more and less a century, but very few researchers incorporated liner deformation and circumferential flow, which has high influence upon piston ring performance parameters (friction force, power loss, flow rate, blow by/blow back, lube oil consumption, operating life and environmental pollution). It is also evident from literature review that engine performance specifically piston ring performance has been analyzed in almost any possible operating condition at different speeds, loads and temperature, but none of previous research work investigated piston ring performance in initial engine startup condition where chances of wear are definite hence compromising fuel efficiency, power loss, piston ring and liner operating life.

In this study, a two dimensional lubrication model is presented for hydrodynamic and elastohydrodynamic for a first few cycles in the initial engine start up therefore exploring the effect of ring face geometry and deformed cylinder line on performance of the piston ring in initial engine start up conditions.

1.3.1 Static analysis

To meet the practical requirements of the ring manufacturers, the static analysis needs to function as an analytical tool for piston ring design, which can be used in the early stage of ring design. Different piston ring running face profiles are modeled (see section 3.1.3) and analyzed regarding performance parameters (see section 6.1).

1.3.2 Dynamic analysis

For the dynamic analysis, three-dimensional models need to be developed in order to address non-axisymmetric characteristics of the power cylinder system. To avoid the complexity of ring lubrication, two two-dimensional mass conserved hydrodynamic and elastohydrodynamic models are developed to analyze lubricating oil film thickness,

hydrodynamic and elastohydrodynamic pressure profiles, friction force, power loss, flow rate and elastic deformation in initial engine startup condition.

CHAPTER-2

Mathematical Modeling

2.1. Introduction

As stated by Stachowiak [2], that serious appreciation of hydrodynamics in lubrication started at the end of the 19th century when Beauchamp Tower, an engineer, noticed that the oil in a journal bearing always leaked out of a hole located beneath the load. The leakage of oil was a nuisance so the hole was plugged first with a cork, which still allowed oil to ooze out, and then with a hard wooden bung. The hole was originally placed to allow oil to be supplied into the bearing to provide 'lubrication'. When the wooden bung was slowly forced out of the hole by the oil, Tower realized that the oil was pressurized by some as yet unknown mechanism. Tower then measured the oil pressure and found that it could separate the sliding surfaces by a hydraulic force [9]. At the time of Beauchamp Tower's discovery Osborne Reynolds and other theoreticians were working on a hydrodynamic theory of lubrication. By a most fortunate coincidence, Tower's detailed data was available to provide experimental confirmation of hydrodynamic lubrication almost at the exact time when Reynolds needed it. The result of this was a theory of hydrodynamic lubrication published in the Proceedings of the Royal Society by Reynolds in 1886 [10]. Reynolds provided the first analytical proof that a viscous liquid can physically separate two sliding surfaces by hydrodynamic pressure, resulting in low friction and theoretically zero wear.

2.2. Principle of Hydrodynamic Pressure Generation

All hydrodynamic lubrication can be expressed mathematically in the form of an equation which was originally derived by Reynolds and is commonly known throughout the literature as the 'Reynolds equation'. There are several ways of deriving this equation. Since it is a simplification of the Navier-Stokes momentum and continuity equation it can be derived from this basis. It is, however, more often derived by considering the equilibrium of an element of

liquid subjected to viscous shear and applying the continuity of flow principle, as is derived by Stachowiak [2]. There are two conditions for the occurrence of hydrodynamic lubrication

- Two surfaces must move relatively to each other with sufficient velocity for a load carrying lubricating film to be generated and,
- Surfaces must be inclined at some angle to each other, i.e., if the surfaces are parallel a pressure field will not form in the lubricating film to support the required load.

There are two exceptions to this last rule: hydrodynamic pressure can be generated between parallel stepped surfaces or the surfaces can move towards each other (these are special cases and are discussed later). The principle of hydrodynamic pressure generation between moving non-parallel surfaces is schematically illustrated in Figure 4.1. It can be assumed that the bottom surface, sometimes called the 'runner', is covered with lubricant and moves with a certain velocity. The top surface is inclined at a certain angle to the bottom surface. As the bottom surface moves it drags the lubricant along it into the converging wedge. A pressure field is generated as otherwise there would be more lubricant entering the wedge than leaving it. Thus at the beginning of the wedge the increasing pressure restricts the entry flow and at the exit there is a decrease in pressure boosting the exit flow. The pressure gradient therefore causes the fluid velocity profile to bend inwards at the entrance to the wedge and bend outwards at the exit, as shown in Figure 4.1. The generated pressure separates the two surfaces and is also able to support a certain load.

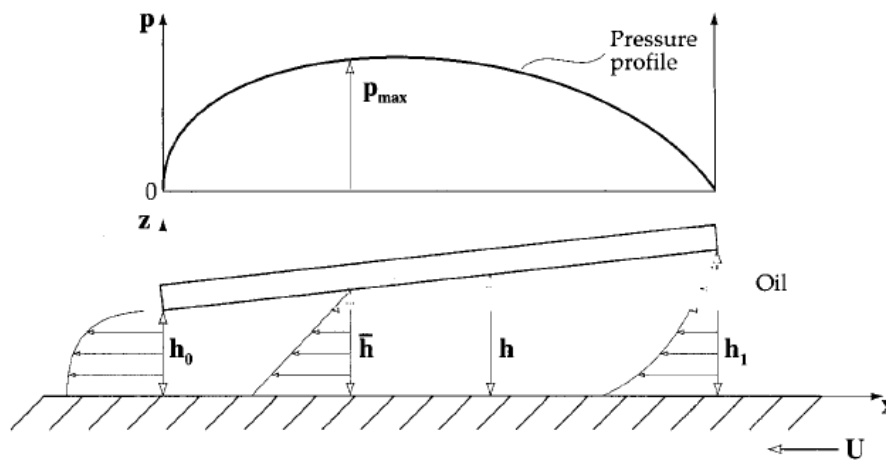


Fig 2.1: Principle of hydrodynamic pressure generation between non-parallel surfaces [2]

There are some simplifying assumptions, which are required in the derivation of Reynolds equation, and are as follows

Table 2.1: Summary of Simplifying Assumptions in Hydrodynamics [2].

	Assumption	Comments
1	Body forces are neglected	Always valid, since there are no extra outside fields of forces acting on the fluids with an exception of magnetohydrodynamic fluids and their applications.
2	Pressure is constant through the film	Always valid, since the thickness of hydrodynamic films is in the range of several micrometers. There might be some exceptions, however, with elastic films.
3	No slip at the boundaries	Always valid, since the velocity of the oil layer adjacent to the boundary is the same as that of the boundary.
4	Lubricant behaves as a Newtonian fluid	Usually valid with certain exceptions, e.g., polymeric oils.
5	Flow is laminar	Usually valid, except large bearings, e.g., turbines.
6	Fluid inertia is neglected	Valid for low bearing speeds or high loads. Inertia effects are included in more exact analyses.
7	Fluid density is constant	Usually valid for fluids when there is not much thermal expansion. Definitely not valid for gases.
8	Viscosity is constant throughout the generated fluid film	Crude assumption but necessary to simplify the calculations, although it is not true. Viscosity is not constant throughout the generated film.

2.3. Derivation of Two-Dimensional Steady State Reynolds Equation

The equilibrium of an element of fluid is considered as shown in figure 2.2, to obtain an expression of the continuity of flow in a column. For Simplicity, assume that the forces on the element are acting initially in the 'x' direction only.

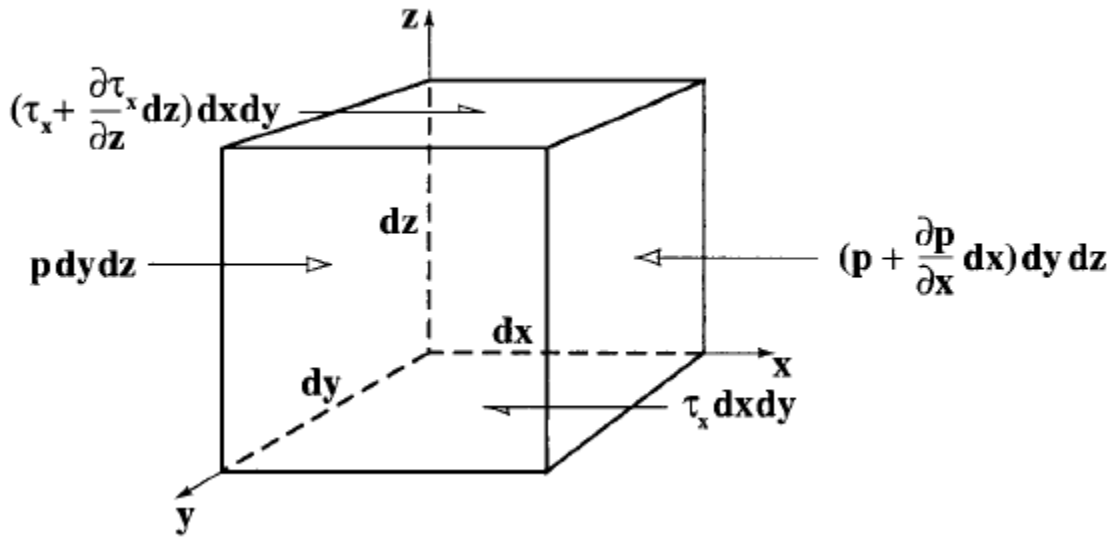


Fig 2.2 Equilibrium of an element of fluid from a hydrodynamic film [2]

2.3.1. Equilibrium of an Element of Liquid Subjected to Viscous Shear

Since the fluid element is in equilibrium condition, hence the forces acting on it must balance out, so

$$p dy dz + \left(\tau + \frac{\partial \tau}{\partial z} dz \right) dx dy = \left(p + \frac{\partial p}{\partial x} dx \right) dy dz + \tau_x dx dy \quad (2.1)$$

which after simplifying gives

$$\frac{\partial}{\partial z} \tau_x dx dy dz = \frac{\partial p}{\partial x} dx dy dz \quad (2.2)$$

Assuming non-zero volume i.e., $dx dy dz \neq 0$

$$\frac{\partial \tau_x}{\partial z} = \frac{\partial p}{\partial x} \quad (2.3)$$

Forces that are acting in the outward direction must balance the forces that are acting in the inward direction, hence

$$p dx dz + \left(\tau_y + \frac{\partial}{\partial z} \tau_y dz \right) dx dy = \left(p + \frac{\partial p}{\partial y} dy \right) dx dz + \tau_y dx dy \quad (2.4)$$

Again assuming non-zero volume i.e., $dx dy dz \neq 0$

$$\frac{\partial}{\partial z} \tau_y = \frac{\partial p}{\partial y} \quad (2.5)$$

According to Assumption No. 2, Pressure is constant throughout the film. Hence, $\frac{\partial p}{\partial z} = 0$

So shear stress can be expressed in terms of shear rate and lubricant viscosity, and is given as

$$\tau_x = \eta \frac{u}{h} = \eta \frac{\partial u}{\partial z} \quad (2.6)$$

$$\tau_y = \eta \frac{v}{h} = \eta \frac{\partial v}{\partial z} \quad (2.7)$$

Putting the x component of Shear stress into equation (2.3), we obtain:

$$\frac{\partial}{\partial z} \left[\eta \frac{\partial u}{\partial z} \right] = \frac{\partial p}{\partial x} \quad (2.8)$$

Similarly, putting the y component of shear stress into equation (2.4), we obtain

$$\frac{\partial}{\partial z} \left[\eta \frac{\partial v}{\partial z} \right] = \frac{\partial p}{\partial y} \quad (2.9)$$

According to assumption # 8, viscosity is considered constant in the entire fluid film. Hence it has no component in the 'z' direction. So equation (2.5) can be rearranged to give

$$\frac{\partial p}{\partial x} \partial z = \partial \left[\eta \frac{\partial u}{\partial z} \right]$$

Taking Integral on both sides of the above equation:

$$\frac{\partial p}{\partial x} z + c_1 = \eta \frac{\partial u}{\partial z}$$

Integrating the above expression will give

$$\frac{\partial p}{\partial x} \left(\frac{z^2}{2} \right) + c_1 z + c_2 = \eta u \quad (2.10)$$

Boundary Conditions: As there is no slip or velocity changes between the liquid film and solid surface at the boundaries of the wedge. Hence the boundary conditions are defined as

$$u = U_2 \text{ at } z = 0; u = U_1 \text{ at } z = h$$

Applying $u = U_2$ at $z = 0$ in equation (2.10)

$$C_2 = \eta U_2 \quad (2.11)$$

Applying $u = U_1$ at $z = h$ in equation (2.10)

$$C_1 = (U_1 - U_2) \frac{\eta}{h} - \frac{\partial p}{\partial x} \frac{h}{2} \quad (2.12)$$

Solving equations (2.10), (2.11) and (2.12) we obtain

$$u = \frac{\partial p}{\partial x} \left[\frac{z^2 - zh}{2\eta} \right] + (U_1 - U_2) \frac{z}{h} + U_2 \quad (2.13)$$

Equation (2.13) defines the velocity in the 'x' direction. Velocity profiles at the entry of the hydrodynamic film are shown in figure 2.3.

According to assumption # 8, fluid viscosity is assumed constant. Therefore it is not a function of 'z' Equation So eq (2.9) after double integration can be written as

$$\eta v = \frac{\partial p}{\partial y} \left(\frac{z^2}{2} \right) + C_1 z + C_2 \quad (2.14)$$

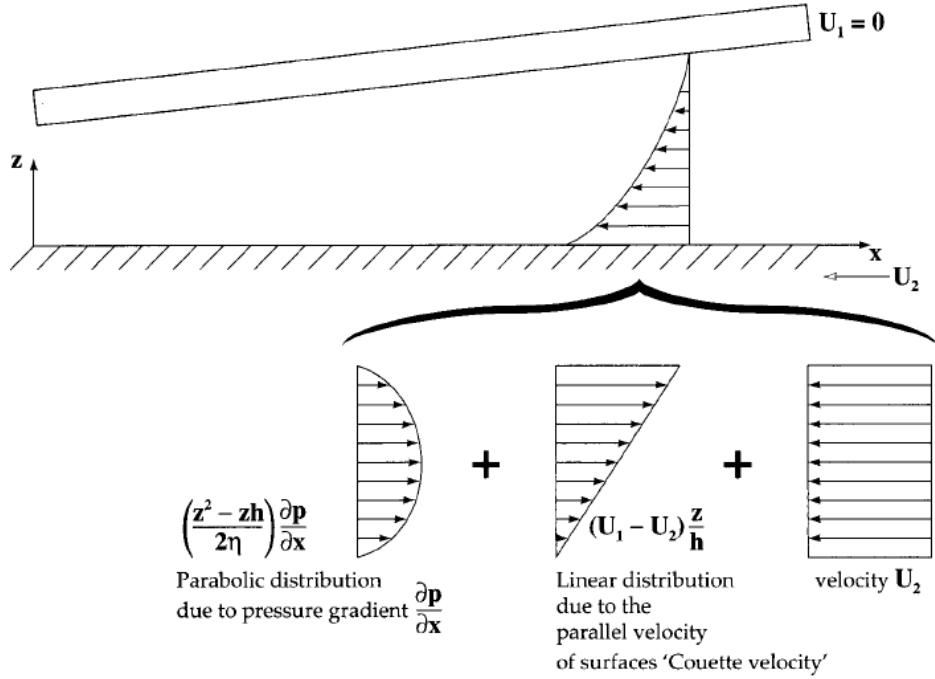


Fig 2.3: Velocity profiles at the entry of the hydrodynamic film [2]

Keeping in view the third assumption that there is no slip or velocity change between the liquid and solid at the boundaries of the wedge, hence the boundary conditions are defined as

$$v = V_2 \text{ at } z = 0 ; v = V_1 \text{ at } z = h$$

Put $v = V_2$ at $z = 0$ in equation (2.14)

$$C_2 = \eta V_2 \quad (2.15)$$

Put $v = V_1$ and $z = h$ and $C_2 = \eta V_2$ in equation (2.14)

$$C_1 = \frac{\eta}{h} (V_1 - V_2) - \frac{\partial p}{\partial y} \frac{h}{2} \quad (2.16)$$

Solving equations (2.14), (2.15) and (2.16), we get

$$v = \frac{\partial p}{\partial y} \left[\frac{z^2 - zh}{2\eta} \right] + (V_1 - V_2) \frac{z}{h} + V_2 \quad (2.17)$$

2.3.2. Reynolds Equation & Continuity of Flow in a Column - Application of Continuity of Flow Principle

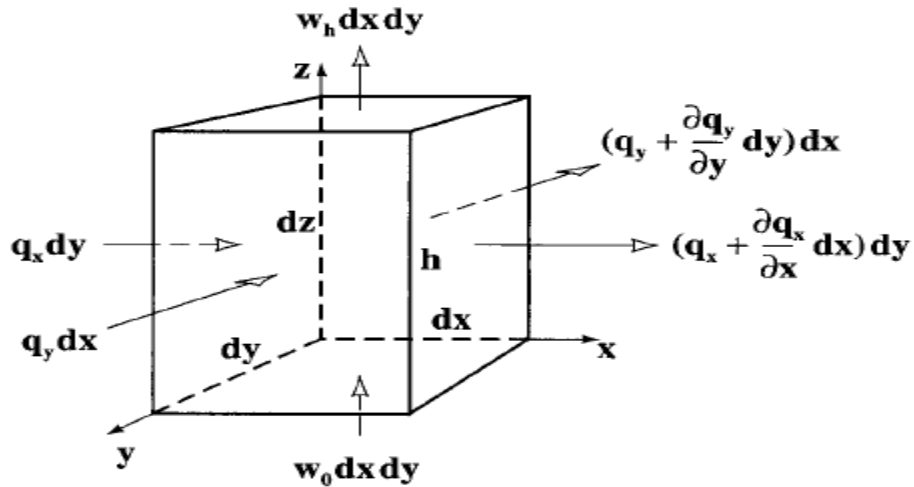


Fig 2.4: Continuity of flow in a column [2]

Consider the lubricant film such that the film flows into the column horizontally at the rates of q_x and q_y as shown in figure 2.4 and in the vertical direction the lubricant flows into the column at the rate of ' $w_0 dx dy$ ' and flows out at the rate of ' $w_h dx dy$ '. The principle of continuity of flow states that "the inflow of a liquid must be equal to outflow from the control volume under steady conditions". Hence following relation applies:

$$q_x dy + q_y dx + w_0 dx dy = \left(q_x + \frac{\partial q_x}{\partial x} dx \right) dy + \left(q_y + \frac{\partial q_y}{\partial y} dy \right) dx + w_h dx dy$$

$$\frac{\partial q_x}{\partial x} dx dy + \frac{\partial q_y}{\partial y} dx dy + (w_h - w_0) dx dy = 0$$

$$dx dy \left(\frac{\partial q_x}{\partial x} + \frac{\partial q_y}{\partial y} + (w_h - w_0) \right) = 0$$

Since film area = $dx dy \neq 0$, hence

$$\frac{\partial q_x}{\partial x} + \frac{\partial q_y}{\partial y} + (w_h - w_0) = 0 \quad (2.18)$$

If 'h' is the oil film thickness and 'u' is the oil film velocity then oil flow rate per unit length in the 'x' & 'y' direction is given by

$$q_x = \int_0^h u dz \quad (2.19)$$

$$q_y = \int_0^h v dz \quad (2.20)$$

Solving equations (2.13) & (2.17), we obtain:

$$u = \frac{\partial p}{\partial x} \left[\frac{z^2 - zh}{2\eta} \right] + (U_1 - U_2) \frac{z}{h} + U_2$$

$$v = \frac{\partial p}{\partial y} \left[\frac{z^2 - zh}{2\eta} \right] + (V_1 - V_2) \frac{z}{h} + V_2$$

Put 'u' in equation (2.19)

$$q_x = - \left[\frac{-h^3}{12\eta} \frac{\partial p}{\partial x} \right] + \frac{h}{2} (U_1 + U_2) \quad (2.21)$$

which is the expression of the flow rate per unit length in the 'x' direction. Also after putting 'v' from equation (2.17) in to equation (2.20), we obtain

$$q_y = \frac{-h^3}{12\eta} \frac{\partial p}{\partial y} + \frac{h}{2} (V_1 + V_2) \quad (2.22)$$

which is the expression for the flow rate per unit length in the 'y' direction. Solving equations (2.18), (2.21) and (2.22),

$$\frac{\partial}{\partial x} \left[- \frac{h^3}{12\eta} \frac{\partial p}{\partial x} + \frac{h}{2} (U_1 + U_2) \right] + \frac{\partial}{\partial y} \left[- \frac{h^3}{12\eta} \frac{\partial p}{\partial y} + \frac{h}{2} (V_1 + V_2) \right] + (w_h - w_0) = 0 \quad (2.23)$$

In order to further simplify the expression of the continuity equation of flow in a column, we define oil velocities in the 'x' and 'y' directions as follows:

$$U = U_1 + U_2 ; \quad V = V_1 + V_2$$

Assuming that there is no variation in surface velocity in the 'x' and 'y' directions, i.e.,

$$U \neq f(x) \quad ; \quad V \neq f(y)$$

Hence equation (2.23) becomes

$$\frac{\partial}{\partial x} \left(\frac{h^3}{\eta} \frac{\partial p}{\partial x} \right) + \frac{\partial}{\partial y} \left(\frac{h^3}{\eta} \frac{\partial p}{\partial y} \right) = 6 \left(\frac{Udh}{dx} + \frac{Vdh}{dy} \right) + 12(w_h - w_0) \quad (2.24)$$

Equation (2.24) is the final expression of the 3-D Reynolds Equation.

2.3.3. Simplifications to 3-D Reynolds Equation

Further simplifying the 3-D Reynolds equation, we make certain approximations.

1. **Unilateral Velocity Approximation:** Assuming that one of the velocities is equal to zero i.e., $V = 0$, hence equation (2.24) becomes

$$\frac{\partial}{\partial x} \left(\frac{h^3}{\eta} \frac{\partial p}{\partial x} \right) + \frac{\partial}{\partial y} \left(\frac{h^3}{\eta} \frac{\partial p}{\partial y} \right) = 6 \frac{Udh}{dx} + 12(w_h - w_0) \quad (2.25)$$

Steady Film Thickness Approximation: Assuming that there is no vertical flow over the oil film, i.e. $w_h - w_0 = 0$. This assumption requires that the distance between the two film surfaces remains constant during the operation. In that case equation (2.25) becomes

$$\frac{\partial}{\partial x} \left(\frac{h^3}{\eta} \frac{\partial p}{\partial x} \right) + \frac{\partial}{\partial y} \left(\frac{h^3}{\eta} \frac{\partial p}{\partial y} \right) = 6 \frac{Udh}{dx} \quad (2.26)$$

2. **Iso-viscous Approximation:** Neglecting shear heating effects and assuming that lubricant viscosity is constant over the film, i.e., η is constant.

$$\frac{1}{\eta} \left[\frac{\partial}{\partial x} \left(h^3 \frac{\partial p}{\partial x} \right) + \frac{\partial}{\partial y} \left(h^3 \frac{\partial p}{\partial y} \right) \right] = 6 \frac{Udh}{dx}$$

$$\frac{\partial}{\partial x} \left(\frac{h^3 \partial p}{\partial x} \right) + \frac{\partial}{\partial y} \left(\frac{h^3 \partial p}{\partial y} \right) = 6U\eta \frac{dh}{dx} \quad (2.27)$$

This equation (2.27) will be used in later chapter for piston ring lubrication.

2.4. Elastohydrodynamic Lubrication (EHD/EHL) of Piston & Rings

2.4.1. EHL/EHD Theory

Elastohydrodynamic lubrication can be defined as a form of lubrication where the elastic deformation of the contacting bodies and the changes of viscosity with pressure play fundamental roles. The influence of elasticity is not limited to second-order changes in load capacity or friction. Instead, the elastic deformation of the bodies has to be included in the basic model of EHL. The same refers to the changes in viscosity due to pressure. It has been found that the combination of three effects namely hydrodynamics, elastic deformation of the metal surfaces and the increase in the viscosity of oil under extreme pressures are instrumental to EHL or EHD mechanism. It has been initially been shown theoretically that under conditions of intense contact stress a lubricating oil film can be formed. The lubricated contacts in which the above three effects take place are said to be operating elastohydrodynamically, which effectively means that contacting surfaces deform elastically under the hydrodynamic pressure generated in the layer of lubricating film. The exact analysis of piston and rings EHL involves a simultaneous iterative numerical solution of the equations describing hydrodynamic film formation, elastic deformation and piezo-viscosity in a lubricated Hertzian contact. The lubricating film is very thin, in the range of 0.1 to 1 micron but manages to separate the interacting surfaces, resulting in a significant reduction of wear and friction in general and reducing adhesive wear to almost zero in particular.

A particular characteristic of conventional dynamically loaded slider bearings like piston and rings is the high degree of geometrical conformity between the bearing components, a feature, which enables substantial loads to be carried by relatively small oil film pressures. Some of the assumptions employed in the analysis of normal fluid bearings cannot be made in the EHD theory as applicable to piston and rings. In particular the influence of high pressure on the viscosity of oil lubricants is most marked and the effect must be fully considered in any analysis of highly loaded piston/cylinder liner and rings/cylinder liner contacts. Furthermore, the application of high contact loads can lead to substantial local deformation of the elastic piston & rings surfaces; an effect which may drastically change the geometry of the lubricating film.

Since the shape of the lubricating film in turn determines the pressure distribution, it is at once apparent that a solution to the EHD problem of piston and rings must simultaneously satisfy the governing elastic and lubrication equations. Elastic bodies like piston and rings, in contact deform and the contact geometry, load and material properties determine the contact area and stresses. The shape of the piston/liner and rings/liner contact areas depends on the shape of piston and rings. The evaluation of piston/liner and rings/liner contact parameters is very essential for EHL analysis. The more frequently used contact parameters are the following

1. Piston and rings contact area dimensions.
2. Maximum contact pressure, often termed as Hertzian stress.
3. The maximum deflection at the center of the contacting surfaces.
4. The position of the maximum shear stress under the surface.

2.4.2. Contact Stresses & Hertz Theory

We know that two contacting surfaces under load deform, which may be either plastic or elastic depending on the magnitude of the applied load and the material's hardness. Hertz's theory of elasticity as applicable to determining contact stresses of piston/liner and rings/liner contacts forms the basis of the model of EHD lubrication. Hertz's model of contact stress as is based on the following simplifying assumptions

1. The materials in contact are homogeneous and the yield stress is not exceeded.
2. Contact stress is caused by the load, which is normal to the contact tangent plane. It means that there are no tangential forces acting between the solids.
3. The contact area is very small compared with the dimensions of the contacting solids.
4. The contacting solids are at rest and in equilibrium.
5. The effect of surface roughness is negligible.

2.4.3. Stress Status in Lubricated Sliding Contacts

In lubricated sliding contacts between piston & cylinder liner and rings & cylinder liner, the lubricating film separating the opposing surfaces and the level of sliding affects the contact stresses. The hydrodynamic film generated under these conditions and the relative movement of the surfaces causes significant changes to the original stress distribution. The sliding piston & rings exert the most critical influence on the subsurface stress fields. When a piston is sliding against the cylinder liner surface frictional forces are the inevitable results and cause a shear stress to act along the interface of piston & liner surfaces. There is a gradual increase in shear stress acting at the interface as the friction force increases.

2.4.4. EHD Lubricating Film

The term EHD lubricating film refers to the lubricating oil, which separates the opposing surfaces of concentrated contacts of piston & liner and rings & liner. The three following effects act simultaneously and play a major role in the formation of lubrication films in EHL:

1. The hydrodynamic film formation.
2. The modification of film geometry by elastic deformation.
3. The transformation of the lubricant's viscosity and rheology under pressure.

The geometry of interacting piston/liner and rings/liner surfaces in Hertzian contacts contains converging and diverging wedges so that some form of hydrodynamic lubrication occurs. Unlike classical piston hydrodynamics, both the piston and rings contact geometry with the liner and lubricant viscosity are a function of hydrodynamic pressure. It is therefore impossible to specify precisely a film geometry and viscosity before proceeding to solve the Reynolds equation. The principal effect of elastic deformation on the lubricant film geometry profile is to interpose a central region of quasi-parallel surfaces between the inlet and outlet wedges. The elastic deformation effects on film profile are shown in figure 2.5 below.

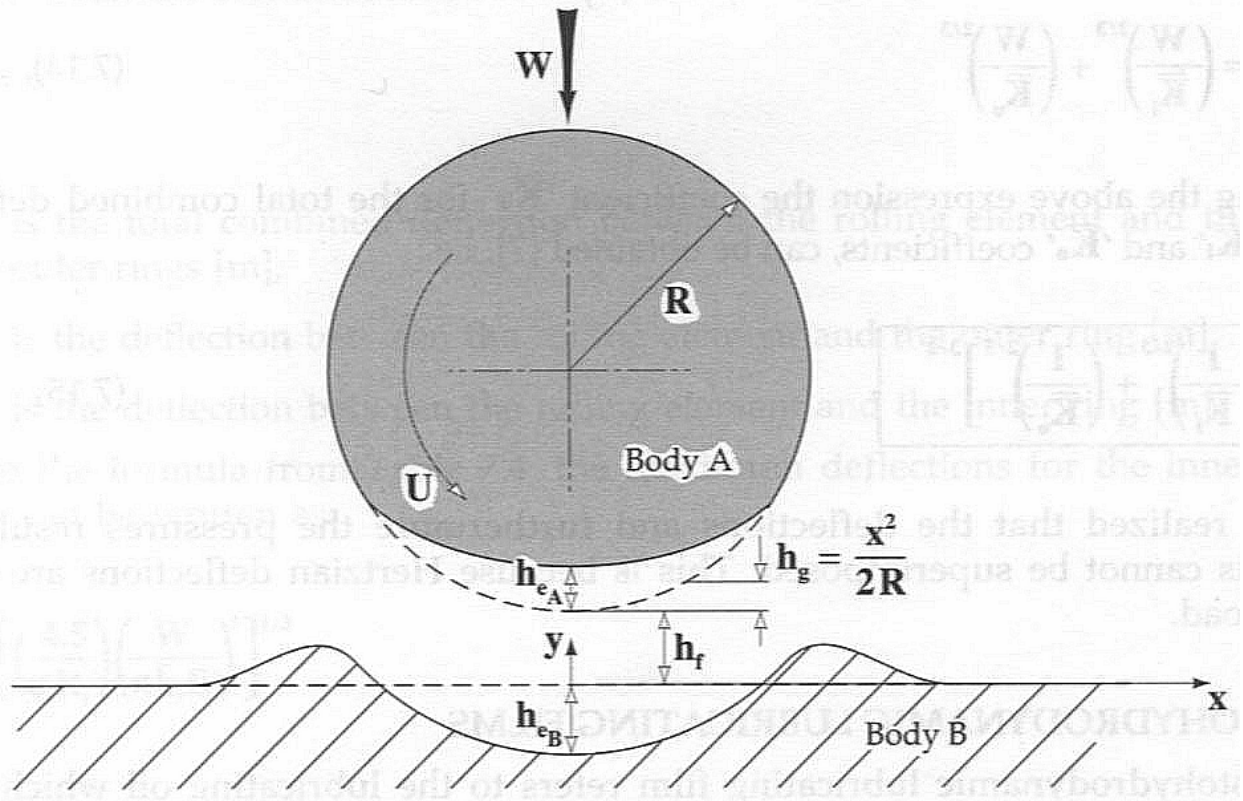


Figure 2.5: Effect of Local Deformation on the Lubricant Film Profile [2]

2.4.5. Theoretical EHL Film Thickness of Piston & Rings

To solve the EHD problem of piston and rings in the initial engine start up, the problem is to calculate the pressure distribution in the contact, allowing at the same time for the effects that this pressure will have on the properties of engine lubricating oil and on the geometry of piston and rings. The solution will also provide the shape of the lubricant film, in particular the minimum clearance between piston & cylinder liner walls and rings & cylinder liner walls. In order to do this it is imperative to set down some assumptions here, which are the following

1. The displacements are initially calculated for a semi-infinite solid (piston & rings).
2. Side leakage is neglected.
3. The boundary conditions for pressure at the inlet are zero.
4. The lubricant is incompressible.
5. Thermal effects are neglected.

CHAPTER-3

Piston Ring/Liner Lubrication

3.1. Mathematical Model of Rigid Ring and Liner Lubrication

Two dimensional Hydrodynamic and Elastohydrodynamic piston ring/liner lubrication model is presented in this chapter, following assumptions are taken to develop mathematical model

1. The lubricant is an incompressible Newtonian fluid and the flow is laminar.
2. Side leakage, oil starvation and surface roughness factors are neglected.
3. No relative motion between piston ring and its groove.
4. Piston secondary motion and ring twist are neglected.
5. An iso-viscous case, that is, viscosity is same in the circumferential and sliding directions.
6. The fully flooded inlet and Reynolds exit conditions are applied.
7. The surfaces of the ring and the liner are perfectly smooth.
8. Thermal effects are neglected.

According to afore mentioned assumptions steady state Reynolds equation 2.27 as described in previous chapter fits in well for this model

$$\frac{\partial}{\partial x} \left(\frac{h^3 \partial p}{\partial x} \right) + \frac{\partial}{\partial y} \left(\frac{h^3 \partial p}{\partial y} \right) = 6U\eta \frac{dh}{dx} \quad (3.1)$$

Where x is sliding direction of the piston ring and y is the circumferential direction, U is the sliding velocity of the piston ring and can be expressed as in equation (3.2), p is hydrodynamic pressure and h is lubricating film thickness which separates the ring and liner surface as is shown below in Fig 3.1, where U is the sliding velocity of the piston ring, B is the ring width, x_1 and x_2 are leading and trailing edge depending upon the sliding direction of the piston ring, q_{x2} is the flow rate of the lubricant.

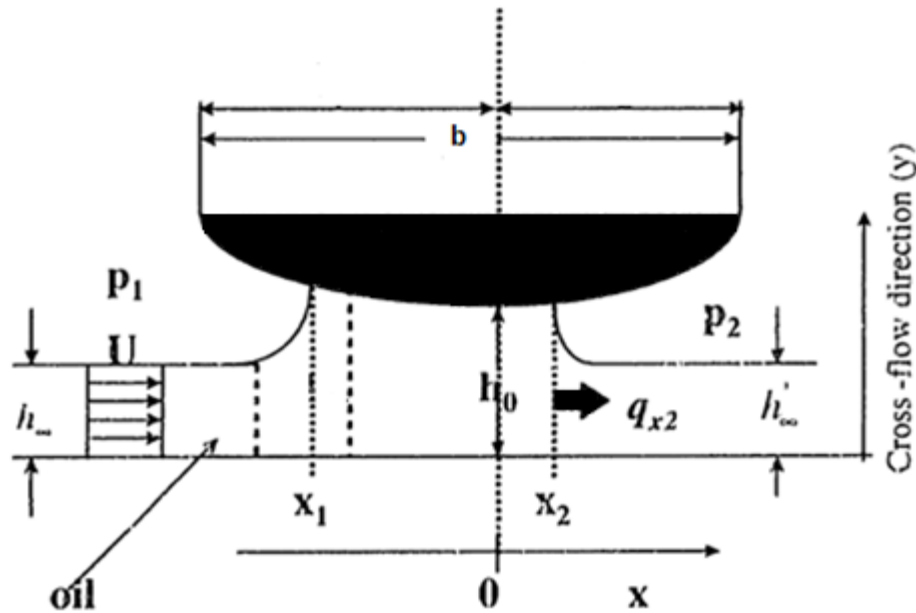


Fig 3.1: Variables and Coordinate system [8]

3.1.1. Piston Ring Instantaneous Velocity

According to assumption No. 3, there is no relative motion between piston ring and its groove, or piston ring and piston is one body, therefore sliding speed of piston ring is same as that of piston itself, the primary motion of the piston rings is equal to the reciprocating piston motion. In an analysis of the piston ring lubrication, it is necessary to determine the velocity of the piston ring as a function of the crank angle. The instantaneous speed of the reciprocating piston motion can be estimated with decent accuracy by the following equation (3.2), as in [31]

$$U = r\omega \sin\theta + r\omega(C_p + r\sin\theta)\cos\theta(l^2 - (C_p + r\sin\theta)^2)^{0.5} \quad (3.2)$$

where U , r , C_p and l are piston velocity in axial direction, crank radius, wrist pin off-set and connecting rod length respectively. ω is angular velocity of crank shaft and can be represented as follows

$$\omega = V/r \quad (3.3)$$

where V is engine speed (rpm)

3.1.2. Hydrodynamic Film Thickness

In the current model, change in film thickness in the sliding direction and in the circumferential direction, both are taken into account to analyze the change in minimum film thickness due to circumferential flow of the lubricant, a flexible mathematical model is developed for the ring face profile and circumferential change in bore out-of-roundness so that parametric study can be conducted upon different critical parameters, as is described in upcoming sections. So we can write film thickness as sum of change in sliding and circumferential direction as in equation (3.4), as in [17]

$$h(x, y) = h_1(x) + h_2(y) + h_0 \quad (3.4)$$

where $h_1(x)$ is film thickness in sliding direction, $h_2(y)$ is film thickness in circumferential direction, and h_0 is important adjustable factor to iterate during computation to converge solution to desired criteria and is described in section 4.3.

3.1.3. Film Thickness in the Sliding Direction

According to the ring face profile as is shown Fig 3.2, film thickness in the sliding direction can be expressed in the form of piece wise continues function, and can be expressed as is in [32] by following equation (3.5)

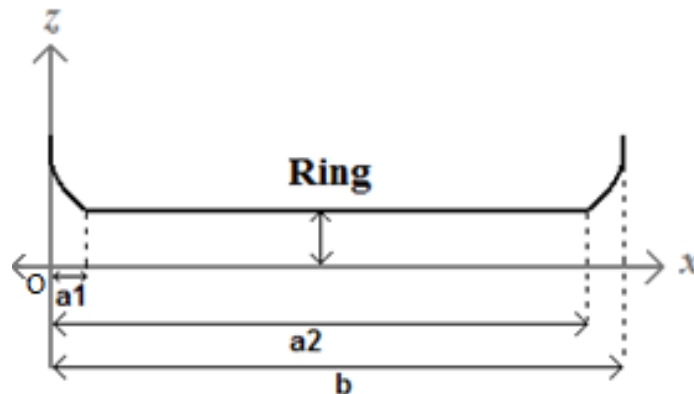


Figure 3.2: Cross-sectional view of the piston ring

$$h_1(x) = \begin{cases} S_1(x^2 - 2a_1x + a_1^2) & 0 \leq x \leq a_1 \\ 0 & a_1 < x < a_2 \\ S_2((x^2 - 2a_1x + a_2^2)) & a_2 \leq x \leq b \end{cases} \quad (3.5)$$

Where a_1 , a_2 , s_1 s_2 are the geometric parameter of the ring face profile and by changing these parameters ring face profile can be changed to analyze effect of ring geometry on lubricating film thickness and other performance parameters like friction, power loss and flow rate, for symmetric ring a_1 and a_2 are equal but not for asymmetric rings. Four different symmetric ring face profile as shown in Fig. 3.3 are analyzed in this work and results are discussed in section 6.1

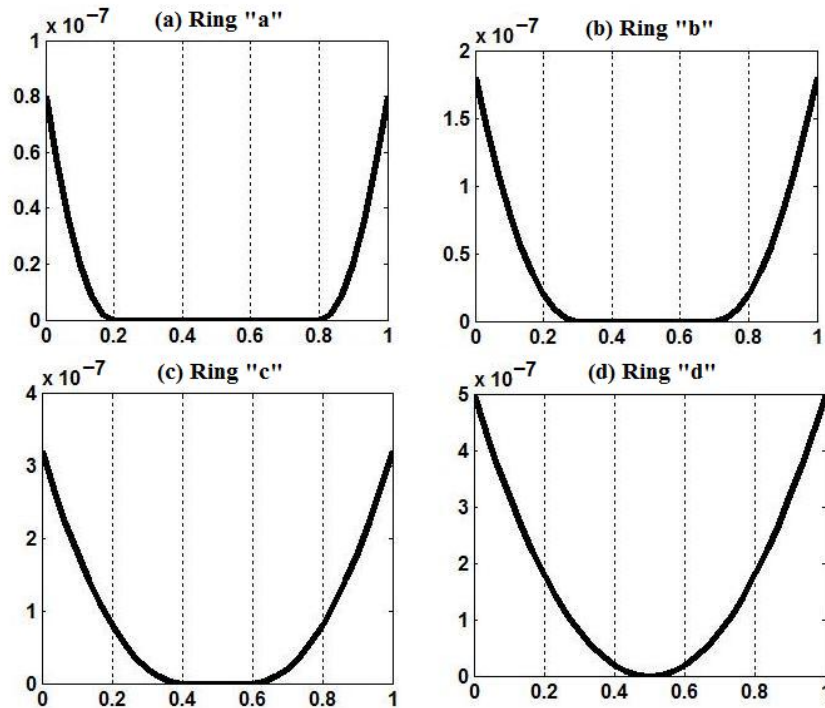


Fig 3.3: Cross sectional view of different Symmetric Ring face profiles

Fig. 3.3 represents Ring 'a', with flat spam or 60% of the total ring width, similarly Fig. 3.3 (b), (c) and (d) represents, Ring 'b', Ring 'c', and Ring 'd', with flat spam of 40%, 20% and 0% of total ring width respectively. Ring face profile shown in Fig 3.3 (d) is known as fully parabolic

profile, which is shown by this research, as a suitable candidate for reduced frictional power loss and increased fuel efficiency and is discussed in section 6.1.2.

3.1.4. Film Thickness in the Circumferential Direction

Most of the earlier research on the Piston ring lubrication was carried out by considering the cylinder liner as perfectly circular but in reality it is not so, due to the high pressures, thermal and variable loads at the thrust and non-thrust sides, wear of the liner, manufacturing errors and head clamping force [17]. By incorporating noncircular elliptical or four lobe bore, lubricant film thickness was found to be significantly reduced [7, 17, 19, 28] and more realistic numerical result are achieved. Circumferentially cylinder liner deform and can be mathematically modeled as elliptically deformation , 3 lobes, 4 lobes, 5 lobes up to n-lobes deformation. Elliptical Bore Distortion as Cylinder/liner Out-of-Roundness is take in the current research work for the simplicity and ease of numerical computation, and is shown in Fig 3.4, where Δc is maximum deformation of the cylinder liner and by changing it, its effect is analyzed on film thickness and other performance parameters and results are discussed in section 6.3. Mathematically can be expressed as in equation (3.6)

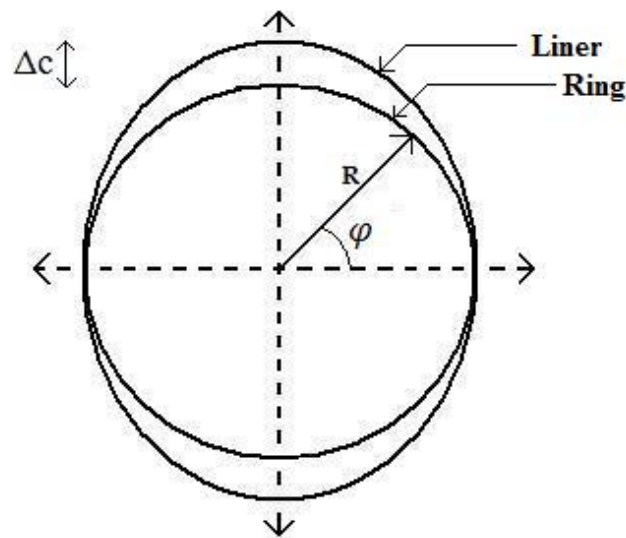


Figure 3.4: Circumferential Deformation of the cylinder liner

$$h_2(y) = R \left\{ \frac{1}{\sqrt{1 - \left[1 - \left(\frac{R}{R + \Delta c}\right)\right] \sin \varphi}} - 1 \right\} \quad (3.6)$$

Where φ can be represented as follows

$$\varphi = \frac{y}{R} ; 0 < y < 2\pi R \quad (3.7)$$

3.1.5. Resultant Hydrodynamic Load

In order to calculate normal force ' W ', hydrodynamic pressures in the lubricating film which separates piston ring and liner are required; this hydrodynamic pressure distribution is obtained by solving the 2-Dimensional Reynolds equation (3.1). After getting the required hydrodynamic pressure distribution, the normal force ' W ' can be calculated by integrating these pressures over the ring face area and can be expressed as equation (3.8)

$$W = \int_0^L \int_0^b p(x, y) dx dy \quad (3.8)$$

Where L is the ring length

Equilibrium condition is supposed to be satisfied when net resultant hydrodynamic force (W) and Gas-pressure force (FG) satisfy the following equation (3.9)

$$FG - W = 0 \quad (3.9)$$

where FG is Gas pressure forces at the back of ring due to combustion chamber pressures. Simulated data of combustion gas force is used as a function of crank angle, as shown in Fig 3.5, as in [31].

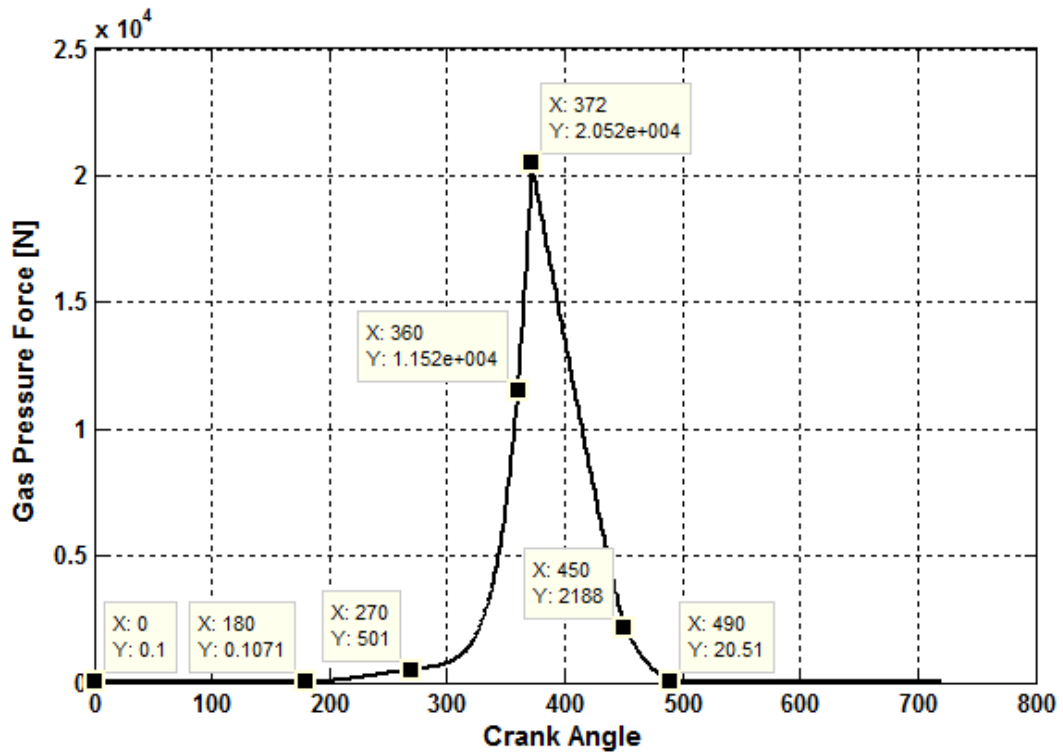


Figure 3.5: Gas Pressure Force Vs Crank Angle [31]

3.2. Mathematical Model of Elastic Ring and Liner Lubrication

Under the hydrodynamic pressure in the combustion stroke the piston ring deform elastically to an amount equivalent to the magnitude of film thickness based on the elasticity theory. This deformation is determined as in [28], and can be expressed as in equation (3.10)

$$dv = \frac{1}{\pi E'} \frac{p(x, y) dy dy}{r} \quad (3.10)$$

where

$$r = \sqrt{(x - x_0)^2 + (y - y_0)^2} \quad (3.11)$$

$$\frac{1}{E'} = \frac{1}{2} \left[\frac{(1 - \nu_1^2)}{E_1} + \frac{(1 - \nu_2^2)}{E_2} \right] \quad (3.12)$$

At a specific point (x_0, y_0) , the elastic deformation can be calculated by equation (3.13), as in [28]

$$v(x_0, y_0) = \frac{1}{\pi E'} \iint_A \frac{p(x, y) dx dy}{r} \quad (3.13)$$

3.2.1 Elastohydrodynamic Lubricating film thickness

The film thickness in Elastohydrodynamic regime applied to piston ring liner system can be expressed as follows [28, 29]

$$h(x, y) = h_1(x) + h_2(y) + v(x, y) + h_0 \quad (3.14)$$

where $h_1(x)$ is film thickness in sliding direction, $h_2(y)$ is film thickness in circumferential direction, $v(x, y)$ is elastic deformation and h_0 is important adjustable factor to iterate during computation to converge solution to desired criteria. $h_1(x)$, $h_2(y)$ and h_0 are the same as were in the rigid hydrodynamic (section 3.1.2).

3.2.2 Pressure Viscosity Relationship

The viscosity of the lubricant is assumed to vary with the pressure according to Barus equation as shown in following equations (3.15), as is in [31]

$$\eta = \eta_0 e^{\alpha p} \quad (3.15)$$

where

$$\alpha = \alpha p_0 \quad (3.16)$$

where p is hydrodynamic pressure, p_0 is atmospheric pressure and η_0 is viscosity at zero shear rate.

3.3 Performance Parameters

3.3.1 Friction Force

We know that, shear stress is defined in terms of dynamic viscosity (η) and shear rate $\left(\frac{du}{dz}\right)$ Hence

$$\tau = \eta \frac{du}{dz} \quad (3.17)$$

$$u = \left(\frac{z^2 - zh}{2\eta}\right) \frac{\partial p}{\partial y} + (U_1 + U_2) \frac{z}{h} + U_2 \quad (3.18)$$

where, η = Dynamic viscosity; h is Fluid film thickness, $\frac{\partial p}{\partial y}$ is Pressure gradient in the 'y' direction, U_1 is cylinder liner surface, U_2 is Velocity of Piston ring surface, Hence in this case $U_1 = 0$ and $U_2 = U$, thus velocity equation, that is, equation 3.18 can be written as

$$u = \left(\frac{z^2 - zh}{2\eta}\right) \frac{\partial p}{\partial y} - \frac{Uz}{h} + U \quad (3.19)$$

Differentiating equation (3.19) with respect to 'z' gives shear rate $\frac{du}{dz}$

$$\frac{du}{dz} = (2z - h) \frac{1}{2\eta} \frac{dp}{dy} - \frac{U}{h} \quad (3.20)$$

$$\frac{du}{dz} = \left(z - \frac{h}{2}\right) \frac{1}{\eta} \frac{dp}{dy} - \frac{U}{h} \quad (3.21)$$

Substituting equation (3.21) in equation (3.17) to get

$$\tau = \eta \left[\left(z - \frac{h}{2}\right) \frac{1}{\eta} \frac{dp}{dy} - \frac{U}{h} \right] \quad (3.22)$$

$$\tau = \left(z - \frac{h}{2} \right) \frac{dp}{dy} - \frac{\eta U}{h} \quad (3.23)$$

$$\tau = \left(-\frac{h}{2} \right) \frac{dp}{dy} - \frac{\eta U}{h} \quad (3.24)$$

The average shear stress acting on the surface of piston ring can be expressed as equation (3.24), so viscous shear force can be evaluated by integrating shear stress over the ring face area as shown by equation (3.26)

$$\tau = \eta \frac{U}{h} - \frac{h}{2} \frac{\partial p}{\partial x} \quad (3.25)$$

$$F_{visc} = \int_0^L \int_0^b \left(\eta \frac{U}{h} - \frac{h}{2} \frac{\partial p}{\partial x} \right) dx dy \quad (3.26)$$

3.3.2 Power Loss

Instantaneous Power loss due to viscous friction force is product of sliding velocity of piston ring and viscous shear force, and can be expressed as equation (3.27), as in [17]

$$P_{loss} = F_{visc} U \quad (3.27)$$

3.3.3 Flow rate:

Flow rate which is need at the inlet of the ring to maintain the lubricating film thickness out of boundary and mixed lubrication regime for each crank angle, q_x passing the ring in the sliding or axial direction lubricant can be evaluated by following equation as in [17, 33]

$$q_x|_{x=x_t} = \frac{U h_t}{2} - \frac{h_t^3}{12\eta} \frac{\partial p}{\partial x} \Big|_{x=x_t} \quad (3.28)$$

where subscript "t" represents the trailing edge position of the piston ring.

Hence the total flow rate Q passing the ring can be evaluated by integrating q_x over the ring length as in [6]

$$Q = \int_0^L q_x dy \quad (3.29)$$

CHAPTER-4

Non-Dimensionalisation & Numerical Procedure

4.1. Non-Dimensional Reynolds Equation

To solve steady state Reynolds equation numerically, equation 3.1 is non-dimensionalised by following four non-dimensional variables

$$\begin{aligned} h^* &= \frac{h}{c} & x^* &= \frac{x}{R} \\ y^* &= \frac{y}{L} & p^* &= \frac{pc^2}{6U\eta R} \end{aligned}$$

where R is the piston radius [m], L is the piston axial length [m], p is the hydrodynamic pressure [Pa], U is the piston entraining velocity [m/s], η is the dynamic viscosity of the piston [Pas] and x, y are the hydrodynamic film co-ordinates [m]. After substituting aforementioned variables in equation (3.1), Two-dimensional steady state Reynolds equation can be written as follows

$$\frac{\partial}{\partial x^*} \left(h^{*3} \frac{\partial p^*}{\partial x^*} \right) + \left(\frac{R}{L} \right)^2 \frac{\partial}{\partial y^*} \left(h^{*3} \frac{\partial p^*}{\partial y^*} \right) = \frac{\partial h^*}{\partial x^*} \quad (4.1)$$

4.2. The Vogelpohl Parameter

The Vogelpohl parameter was introduced in the 1930's with the aim to improve the accuracy of numerical solutions of the Reynolds equation. The Vogelpohl parameter ' M_v ' is defined as follows

$$M_v = p^* h^{*1.5} \quad (4.2)$$

Substitution into the non-dimensional form of Reynolds equation (4.1), gives the 'Vogelpohl equation', that is, equation 4.3

$$\frac{\partial^2 M_v}{\partial x^{*2}} + \left(\frac{R}{L}\right)^2 \frac{\partial^2 M_v}{\partial y^{*2}} = FM_v + G \quad (4.3)$$

where parameters 'F' and 'G' for the piston as well as rings are as follows

$$F = \frac{0.75 \left[\left(\frac{\partial h^*}{\partial x^*} \right)^2 + \left(\frac{R}{L} \right)^2 \left(\frac{\partial h^*}{\partial y^*} \right)^2 \right]}{h^{*2}} + \frac{1.5 \left[\frac{\partial^2 h^*}{\partial x^{*2}} + \left(\frac{R}{L} \right)^2 \frac{\partial^2 h^*}{\partial y^{*2}} \right]}{h^*} \quad (4.4)$$

$$G = \frac{\left(\frac{\partial h^*}{\partial x^*} \right)}{h^{*1.5}} \quad (4.5)$$

The Vogelpohl parameter facilitates computing by simplifying the differential operators of the Reynolds equation. Furthermore, it does not show high values of higher derivatives in the final solution. We know that large values of higher derivatives cause significant truncation error in numerical analysis.

4.2.1 Finite Difference Equivalent of the Reynolds Equation

Piston rings lubrication problems will be solved here by 'finite difference' method, therefore

$$\left(\frac{\partial M_v}{\partial x^*} \right) = \frac{M_{v,i+1} - M_{v,i-1}}{2\delta x^*} \quad (4.6)$$

where the subscripts i-1 and i+1 denote positions immediately behind and in front of the central position 'i' and 'δx*' is the step length between nodes. A similar expression results for second differential $\partial^2 M_v$. The computational molecule is shown in figure 4.1

The second differential $\partial^2 M_v / \partial x^{*2}$ is found by subtracting the expression for $\partial M_v / \partial x^*$, at the i-0.5 nodal position from the i+0.5 nodal position and dividing by δx^* , that is,

$$\left(\frac{\partial^2 M_v}{\partial x^{*2}} \right)_i = \frac{\left(\frac{\partial M_v}{\partial x^*} \right)_{i+0.5} - \left(\frac{\partial M_v}{\partial x^*} \right)_{i-0.5}}{\delta x^*} \quad (4.7)$$

where

$$\left(\frac{\partial M_v}{\partial x^*}\right)_{i+0.5} \approx \frac{M_{v,i+1} - M_{v,i}}{\delta x^*} \quad (4.8)$$

$$\left(\frac{\partial M_v}{\partial x^*}\right)_{i-0.5} \approx \frac{M_{v,i} - M_{v,i-1}}{\delta x^*} \quad (4.9)$$

Substituting into equation (4.8) yields

$$\left(\frac{\partial^2 M_v}{\partial x^{*2}}\right)_i \approx \frac{M_{v,i+1} - M_{v,i-1} - 2M_{v,i}}{(\delta x^*)^2} \quad (4.10)$$

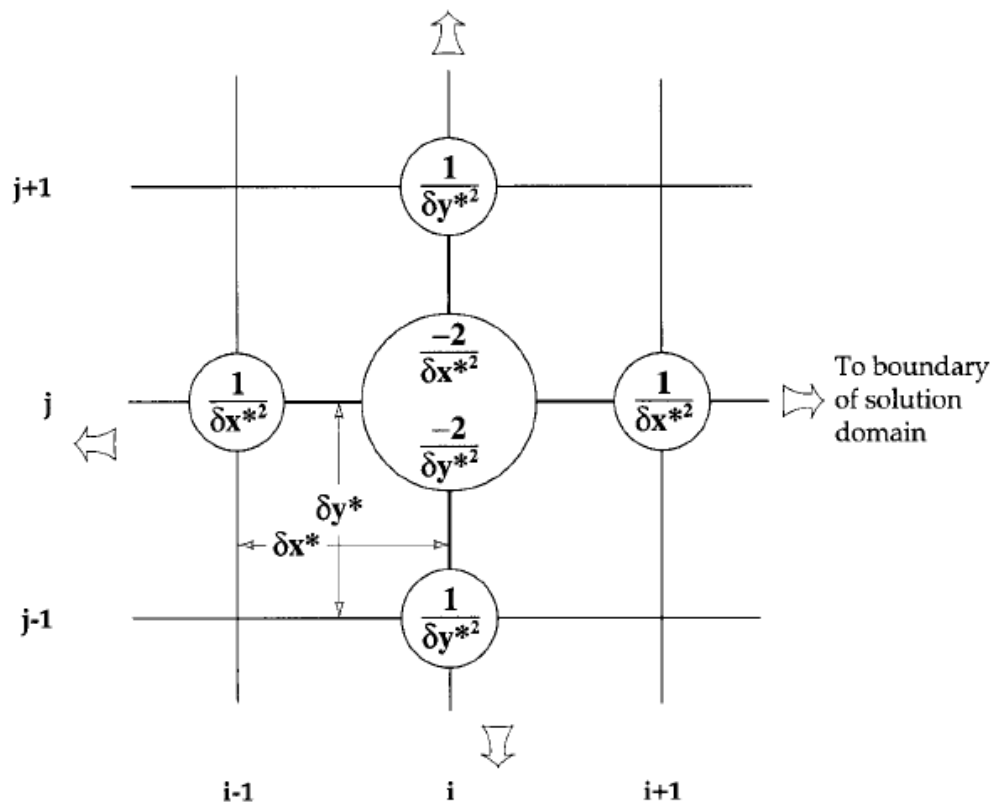


Figure 4.1: Finite Difference Operator and Nodal Scheme for Numerical Analysis of the Reynolds Equation [2]

The finite difference equivalent of $\partial^2 M_v / \partial x^{*2} + \partial^2 M_v / \partial y^{*2}$ is found by considering the nodal variation of 'M_v' in two axes, i.e. the 'x' and 'y' axes. A second nodal position variable is

introduced along the 'y' axis, the 'j' parameter. The expressions for $\partial M_v / \partial y^*$ and $\partial^2 M_v / \partial y^{*2}$ are exactly the same as the expressions for the 'x' axis but with 'i' substituted by 'j'. The coefficients of 'M_v' at the 'i'-th node and adjacent nodes required by the Reynolds equation which form a 'finite difference operator' are illustrated as a 'computing molecule' as shown in figure 4.1.

The finite difference operator is convenient for computation and does not create any difficulties with boundary conditions. When the finite difference operator is located at the boundary of a solution domain, special arrangements may be required with imaginary nodes outside of a boundary. In our case the solution domain is the range over which our solution is applicable, i.e. the dimensions of piston skirts as well as rings. The terms 'F' and 'G' can be included with the finite difference operator to form a complete equivalent of the Reynolds equation. The equation is then rearranged to provide an expression for 'M_{v,i,j}' i.e.:

$$M_{v,i,j} = \frac{C_1(M_{v,i+1,j} + M_{v,i-1,j}) + \left(\frac{R}{L}\right)^2 C_2(M_{v,i,j+1} + M_{v,i,j-1}) - G_{i,j}}{2C_1 + 2C_2 + F_{i,j}} \quad (4.11)$$

where

$$C_1 = \frac{1}{\delta x^{*2}} \quad C_2 = \frac{1}{\delta y^{*2}}$$

This expression forms the basis of the finite difference method for the solution of the Reynolds equation. Its solution gives the required nodal values of 'M_v'.

4.3 Algorithm for Numerical Simulation

4.3.1 Hydrodynamic Lubrication

While computing, the initial value of ' h_0 ' is assumed and hydrodynamic pressures are calculated accordingly. Then resultant hydrodynamic pressures are integrated over ring face area to determine the net resultant hydrodynamic force (W). If equilibrium condition is satisfied, instantaneous friction force, power loss and flow rate is calculated, crank angle gets new increment and the whole procedure is repeated for updated crank angle. If equilibrium condition is not satisfied, then the value of ' h_0 ' is updated according to the following expressions as in [6]

$$h_{0, approx}^{(k)} = \left(\frac{FG}{W}\right)^\gamma h_{0, old}^{(k)} \quad (4.12)$$

$$h_{0, new}^{(k)} = h_{0, old}^{(k)} + \lambda_1(h_{0, approx}^{(k)} - h_{0, old}^{(k)}) \quad (4.13)$$

Where γ is empirical coefficient ranging from 0.1 to 0.2, λ_1 is an under-relaxation factor equal to 0.15-0.5 and k denotes the crank angle position as in [6]. If gas pressure force and the net resultant hydrodynamic force differ by 0.5% then it is assumed that the convergence criterion is satisfied. Flow chart for the aforementioned procedure is given in Fig. 4.2.

Table 2: Values of Parameters Adopted For the Calculation

Bore diameter	83.00mm
Compression ratio	9.05:1
Ring axial width, b	0.0015m
Wrist pin offset, C_p	1mm
Elastic modulus of ring, E_1	113.79 GPa
Elastic modulus of liner, E_2	200 GPa
Ring length, L	0.15m
Ring radius, R	0.0415m
Geometrical parameters of ring face profile, $S_{1,2}$	2e-6
Crank radius, r	0.0418m
Error term, ϵ	0.001
Poisson's ratio of ring and liner, $\nu_{1,2}$	0.3

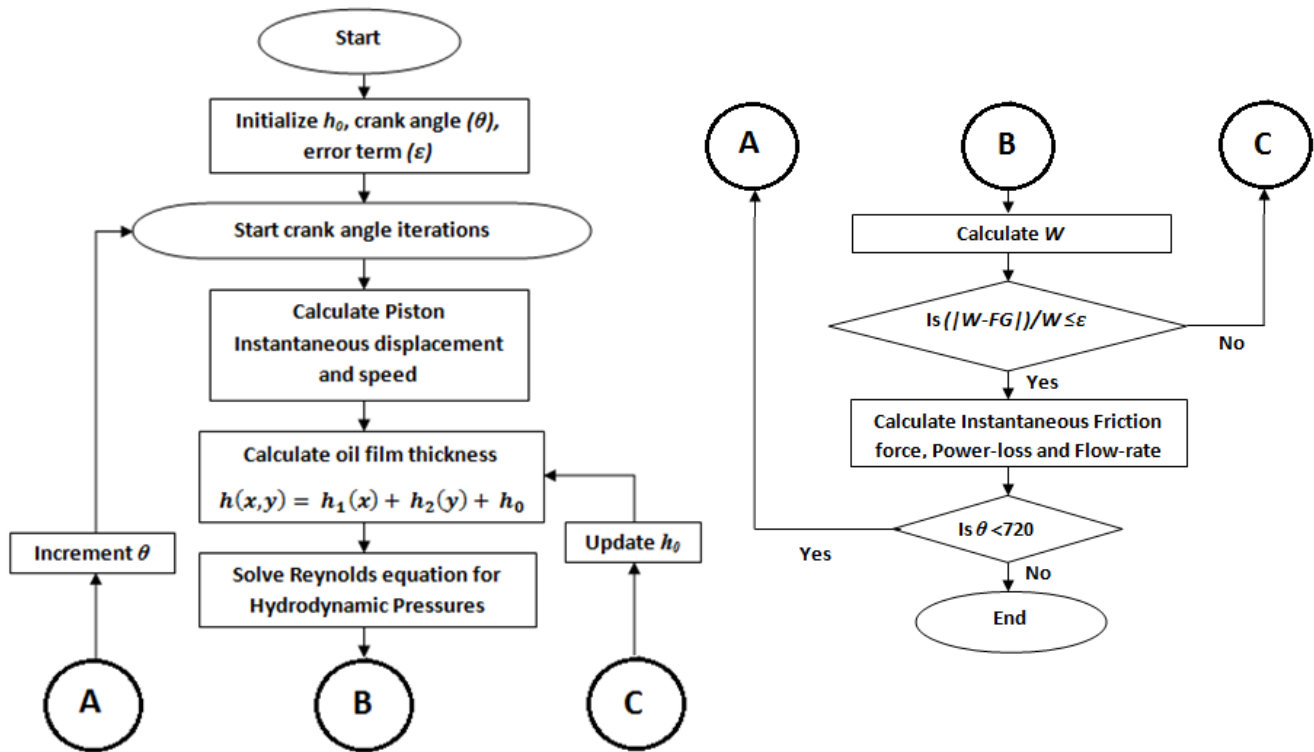


Figure 4.2: Computational Flow-chart for Hydrodynamic Lubrication

4.3.2. Elastohydrodynamic Lubrication

Finite difference approach is adopted to solve the governing equations. While computing, the initial value of ' h_0 ' is assumed and hydrodynamic pressures are calculated accordingly. Then elastic deformation is calculated and added in film thickness and Reynolds equation is solved again, then net resultant hydrodynamic pressures are integrated over ring face area to determine the net resultant load W . If equilibrium condition is satisfied, crank angle gets new increment and the whole procedure is repeated for updated crank angle. If equilibrium condition is not satisfied, then the value of h_0 is updated according 4.10 and 4.11, sequence of numerical simulation is illustrated in following flowchart

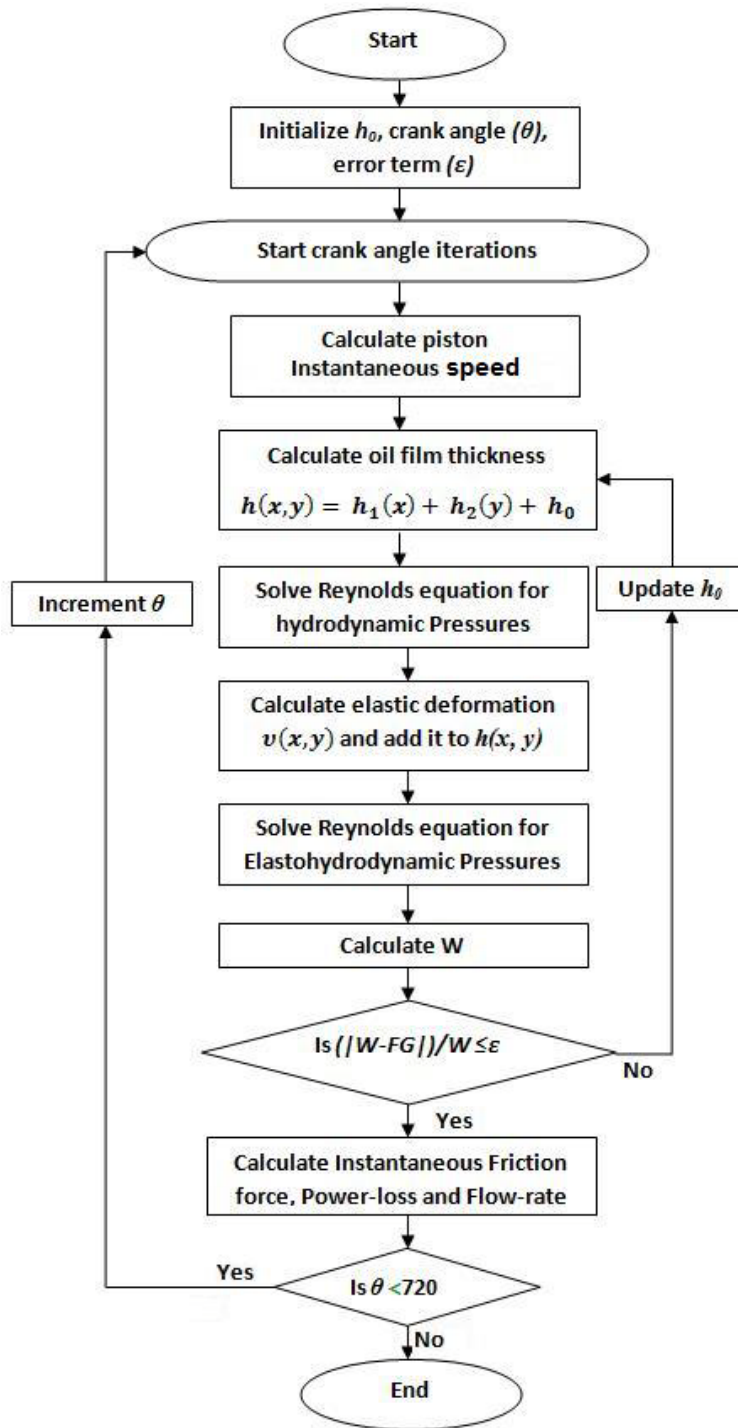


Figure 4.3: Computational Flow Chart for Elastohydrodynamic Lubrication

CHAPTER-5

Results and Discussions

To model two-dimensional lubrication in a comprehensive manner, the piston ring lubrication is evaluated at 600 rpm initial engine start up speed such that all aspects contributing directly or indirectly towards the ring performance regarding lubrication are covered and their effects are simulated for an objective analysis. The profiles are plotted against the 720 degree crank rotation angle corresponding to the 4-stroke engine cycle with induction stroke commencing at 0 degree followed by compression, expansion and exhaust strokes such that each stroke has an equal length of 180 degree.

5.1 Lubricating Film Thickness

Hydrodynamic and elastohydrodynamic lubricating film thickness profiles between the barrel-faced piston ring and the cylinder liner surfaces in a 4-stroke piston cycle in the initial engine start up speed of 600 rpm are shown in figure 5.1. The film thickness profiles show the different film thickness values at various piston positions in terms of 720 degree crank rotation cycle. The minimum hydrodynamic film thickness is the value which carries the hydrodynamic load.

In the induction stroke, the hydrodynamic film thickness rises with the increasing piston cyclic speed till it reaches the mid-stroke region when the film thickness is more than 2 microns. After attaining the maximum cyclic velocity, the piston crosses the mid-stroke region and travels towards the bottom dead center (BDC). During the piston travel from the mid-stroke to BDC, its cyclic speed starts decreasing and with it the hydrodynamic film thickness also reduces such that at 180 degree angle, when cyclic velocity of the piston is minimum, the film thickness goes down to as low as 0.1 micron. In the induction stroke the gas pressure force effect is negligible due to its magnitude as could be seen in figure 3.5. Moreover, the generated hydrodynamic pressures remain very low, which contribute towards an increase in the film thickness. The parabolic shaped film thickness curve in the induction stroke is

essentially hydrodynamic due to the contact geometry of the piston ring and the cyclic piston speed effect.

The film thickness curve show very low values in the compression and exhaust strokes. The commencement of piston motion from BDC towards the top dead center (TDC) is again cyclic, causing a rise in the film thickness at 180 degree but the hydrodynamic pressure increase causes the film thickness to decrease. In the compression stroke, the intake valves are closed due to which the gas pressure force and hydrodynamic friction force start increasing to transfer the load due to which hydrodynamic pressures start increasing appreciably. The combined effect of increasing magnitudes of gas pressure force and hydrodynamic friction force do not let the film thickness to increase during the compression stroke. In the first half of the compression stroke of piston, the hydrodynamic pressure rise due to the stated force effects is not very high due to which, although the minimum film thickness is reduced yet the regime remains the rigid hydrodynamic lubrication regime.

After the piston moves past the mid-stroke region, the hydrodynamic pressure rise is so high that it causes the elastic deformation of the interacting first compression ring and the liner surfaces. The piston travel in the last quarter of the compression stroke results in the creation of EHL domain between the piston ring and the liner surfaces, which is essentially the region of extremely high pressures and lasts till the piston travel up to the mid of the expansion stroke. This elastic deformation creates additional space, which under the fully flooded conditions, is occupied by the lubricant, causing an increase in its magnitude as shown in figure 5.1.

The lowest value of the minimum hydrodynamic film thickness is found at the end of compression stroke when the magnitude of gas pressure force is very high. In the region of very low film thickness, the magnitudes of gas pressure force and hydrodynamic friction force are very high. There is significant reduction in the magnitudes of the respective forces as the piston travels past the mid-point of expansion stroke, causing the reformation of the interacting piston ring and liner surfaces and the regime changes to rigid hydrodynamic lubrication of the ring. At 490 degree crank angle in the expansion stroke, the combustion gas force and the friction force effects subside to such an extent that the magnitude of

hydrodynamic pressures is reduced from hundreds of thousands of Pascal to less than 100 Pascal. It causes an exponential rise in the film thickness from the fraction of a micron to around 2 microns.

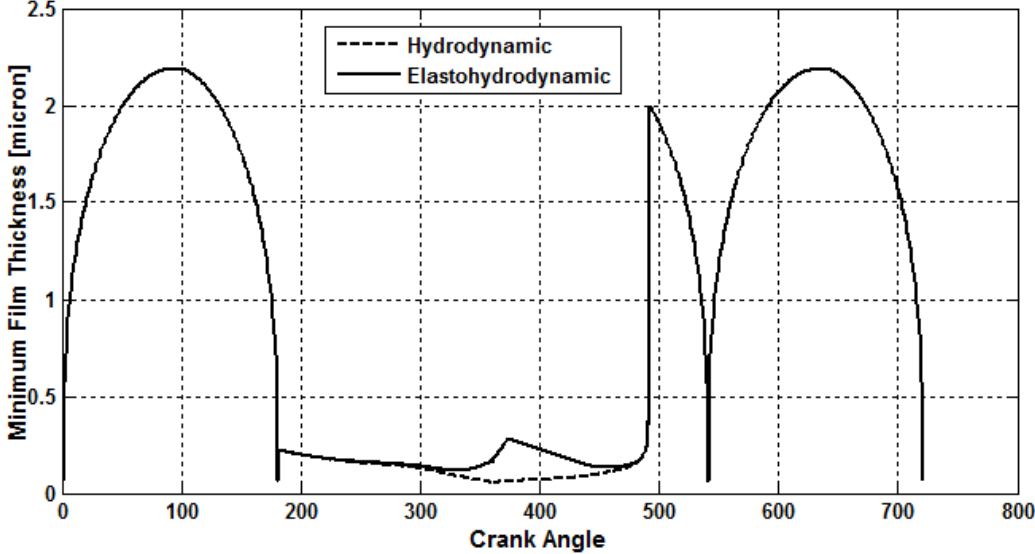


Figure 5.1: Minimum Hydrodynamic and EHL Film thickness Vs Crank Angle

During the piston stroke from 490 degree to 540 degree, the magnitude of hydrodynamic pressures further reduces to some extent but very small magnitude of gas pressure force and slowing down of piston as it approaches BDC results in yet another reduction in the hydrodynamic film thickness such that an instantaneous value is achieved at the end of the expansion stroke. In the exhaust stroke, the opening of the exhaust valves, the absence of significant gas pressure force effect and very low hydrodynamic pressures generate hydrodynamic film thickness profile similar to the case in the induction stroke. In this case the piston cyclic motion and the parabolic shape of the piston ring become the major contributors in generating such film thickness profile. Figure 6 shows hydrodynamic film profile as a function of the first compression ring contact geometry with the elliptical liner to highlight the out-of-roundness effect of cylinder liner on the hydrodynamic film thickness.

5.2 Hydrodynamic Elastohydrodynamic Pressure Field

In the initial engine start up the hydrodynamic pressures are generated due to the barrel faced profile of the piston ring, which generates the desired wedging action.

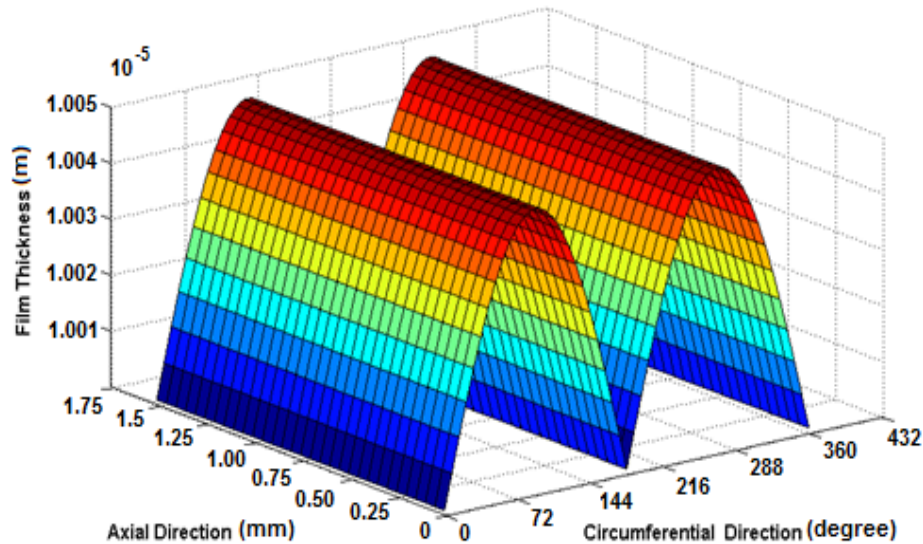


Figure 5.2: Film Thickness Field as a Function of the Ring Geometry.

The magnitude and profiles of the hydrodynamic pressure fields generated over the ring surface are critically significant as very high pressures may affect the film thickness to change the lubrication regime and in extreme cases may contribute towards the film rupture and subsequent damage to the first compression ring. In view of this, the pressure fields at each degree of 720 degree crank rotation cycle were plotted, some of which show major changes at different crank angles, as shown in figures 5.3-5.12

The hydrodynamic pressure field at 90 degree crank angle is shown in figure 5.3. At this instant, the maximum cyclic speed of the piston with negligible effect of gas pressure force and the maximum hydrodynamic film thickness facilitate generation of very low hydrodynamic pressures with peak values only a fraction of a Pascal. At this instant, the film thickness as a function of the geometry of the piston ring is at its maximum value as shown in figure 6.

At the end of induction stroke at 180 degree crank angle, the hydrodynamic pressure profiles are shown in figure 5.4. At this instant, the hydrodynamic pressures rise from a fraction

of a Pascal to more than one Pascal. Due to minimum cyclic speed of piston and minimum gas pressure force effect, a slight increase in the hydrodynamic pressures causes the film thickness to drop to very low value as shown in figure 5.1. The maximum magnitude rise is seen at 180 degree, which corresponds to the minimum film thickness value as a function of the piston ring geometry as shown in figure 5.2. The ring geometry against the non-axisymmetric elliptical bore has its effect visible in the low magnitude hydrodynamic pressures generated as is the case here.

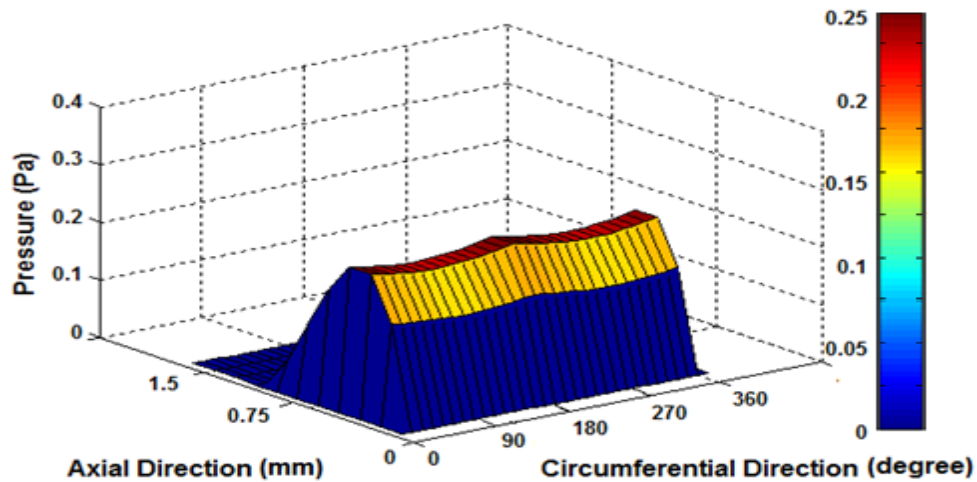


Figure 5.3: Hydrodynamic pressure profile at the mid-point of the induction stroke.

At the commencement of compression stroke, the cyclic speed of the piston starts increasing and the net cumulative effects of various factors as discussed earlier, cause the hydrodynamic pressures to rise. Such an increase in the pressures at 190 degree crank angle is shown in figure 5.5. The maximum hydrodynamic pressure of 80Pa is at 180 degree angle in the circumferential direction. It is followed by pressure values at zero and 360 degree crank angle. At all these three points on the piston ring, the film thickness as a function of ring geometry has minimum value as shown in figure 5.2. Due to the elliptical bore as shown in figure 2, the hydrodynamic pressures between 0-180 degree and between 180 and 360 degree do not rise to attain peak values. These effects do not allow the hydrodynamic film thickness to rise again to its maximum value as shown in figure 5.1.

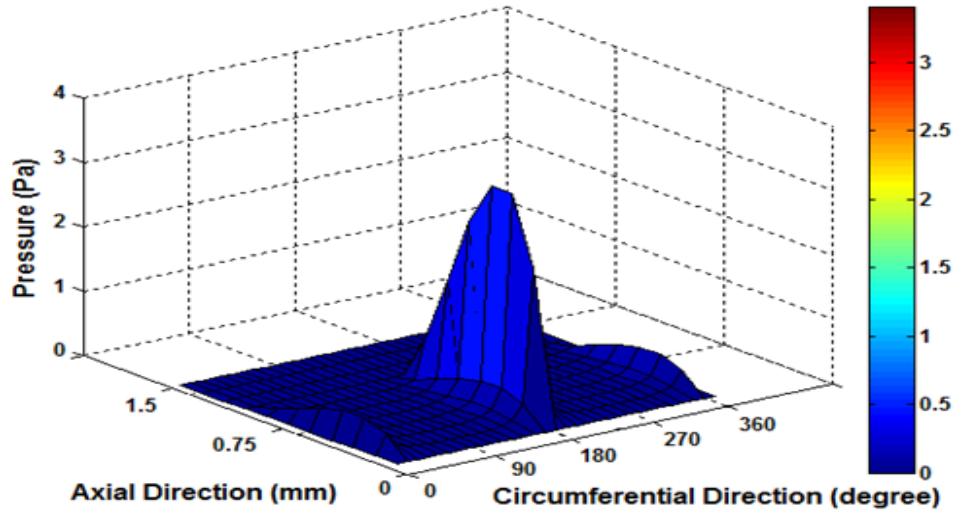


Figure 5.4: Hydrodynamic pressure profile at the end of the piston induction stroke.

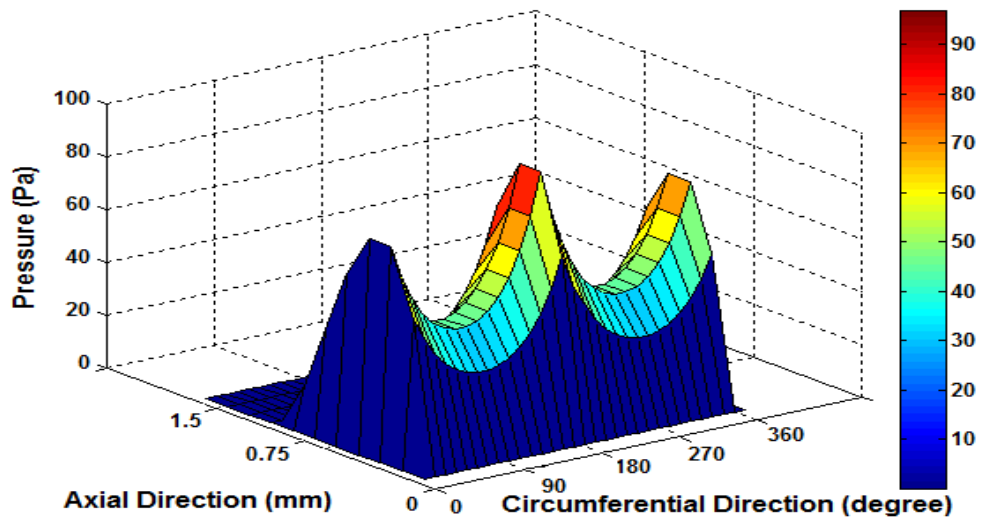


Figure 5.5: Hydrodynamic pressure profile at 190 degree crank angle

In the compression stroke, the increasing magnitudes of gas pressure force and cyclic speed of piston till the maximum speed is attained at the mid-stroke, coupled with an increase in the friction coefficient make the hydrodynamic pressures to rise to around 2 kPa from 80 Pa at 190 degree, which is quite substantial. The effects of the hydrodynamic film geometry due to the bore out-of-roundness, on hydrodynamic pressures are evident as shown in figure 5.6.

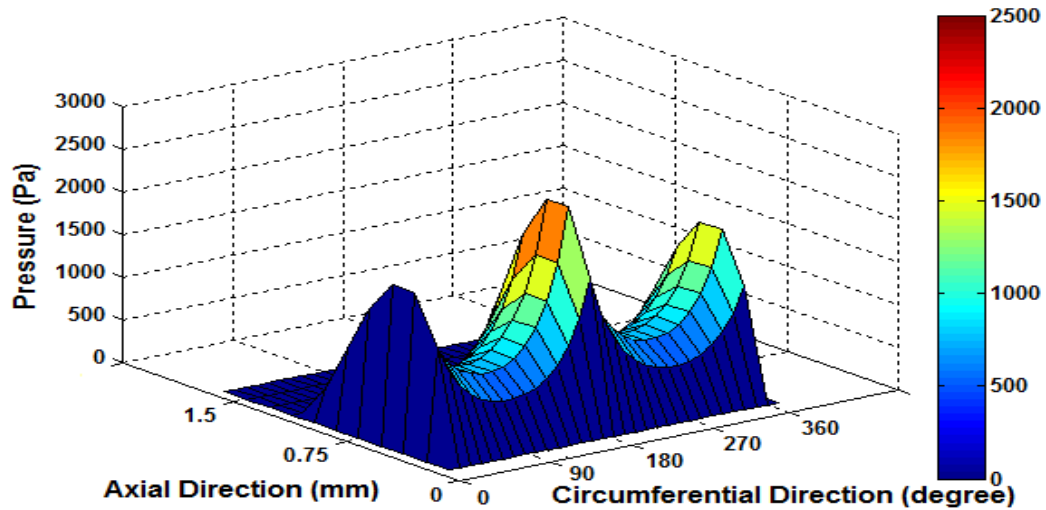


Figure 5.6: Hydrodynamic pressure profile at 270 degree crank angle

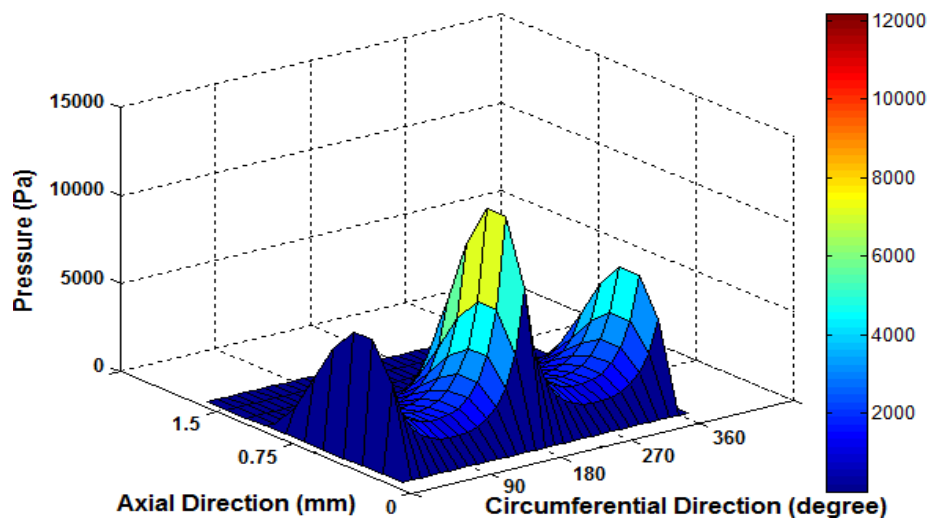


Figure 5.7: Hydrodynamic pressure profile at 320 degree crank angle

After the piston has crossed the mid-point in the compression stroke, there is a substantial rise in the gas pressure force due to which an equally substantial increase in the hydrodynamic pressures is witnessed at 320 degree crank angle as shown in figure 5.7. There is a real fourfold increase in the magnitude of pressure, which is 8kPa from 2 kPa. The effect of the bore-out-of-roundness is still evident despite such a pressure increase. There is a sharp rise in the magnitude of the gas pressure force, causing the hydrodynamic pressures to increase many times from a few kPa to hundreds of kPa. It not only reduces the hydrodynamic film thickness

to barely a fraction of a micron but very high pressure rise causes the interacting ring and liner surfaces to elastically deform, transforming the regime into EHD lubrication regime. In this regard, figure 5.8 shows generation and rise to very high pressures at 360 degree crank angle. Corresponding reduction in the film thickness is shown in figure 5.1. At these high pressures the effect of the elliptic cylinder liner subsides and instead, the elastic deformation of piston ring and liner surfaces becomes more pronounced.

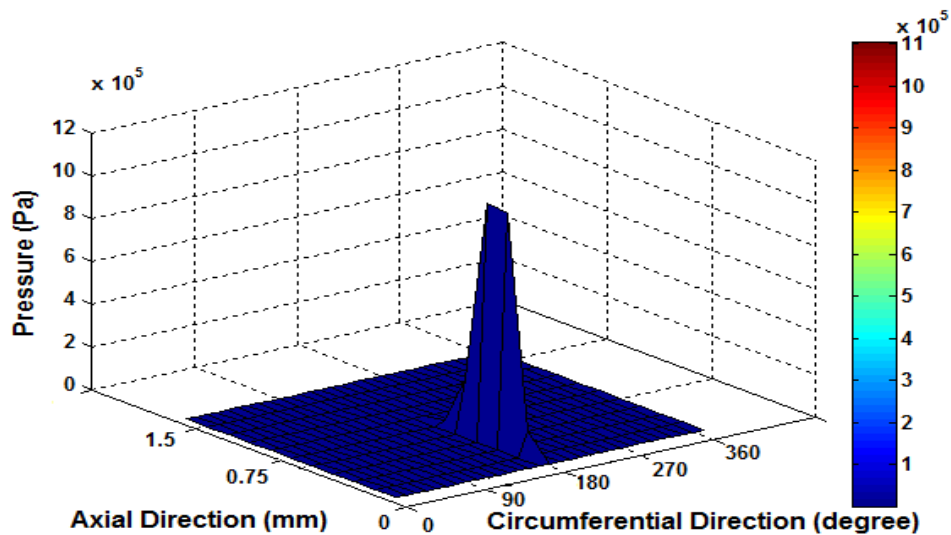


Figure 5.8: Hydrodynamic pressure profile at 360 degree crank angle

At the beginning of the expansion stroke, despite a slight reduction in its magnitude, the hydrodynamic pressure is very high, which is shown in figure 5.9 when the piston is at 380 degree crank rotation angle. At this point the hydrodynamic pressure rise is so high that they cause maximum elastic deformation of the interacting surfaces, as shown in figure 5.1.

At the piston position corresponding to 410 degree of crank rotation angle, the peak hydrodynamic pressures with slightly reduced intensity are in the high range and cause a decrease in the intensity of load acting on the piston ring surface as shown in figure 5.10. When seen in the context of figure 5.2, the rising pressure profiles show that maximum pressure rise is at 180 degree in the circumferential direction of the ring compared to low pressure increase at zero and 360 degree. It causes reduced elastic deformation of the interacting ring and liner surfaces resultantly increasing the hydrodynamic film thickness with corresponding decrease in the EHL film as shown in figure 5.1.

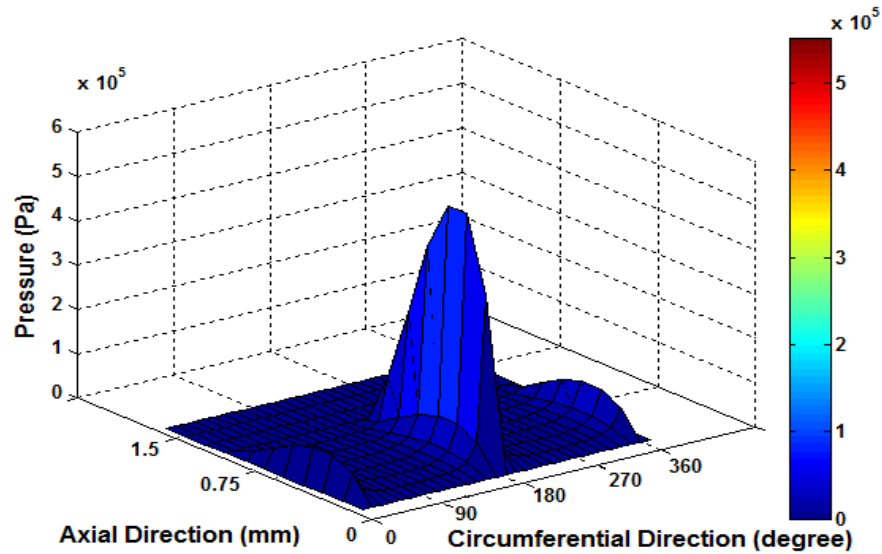


Figure 5.9: Hydrodynamic pressure profile at 380 degree crank angle

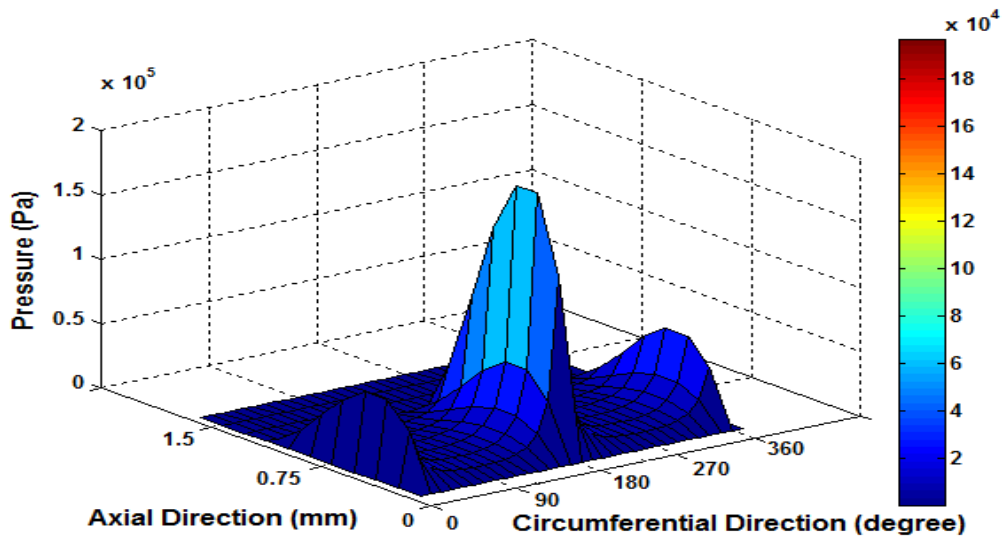


Figure 5.10: Hydrodynamic pressure profile at 410 degree crank angle

In the expansion stroke, the piston travel from TDC to BDC generates very high pressures between the piston ring and the liner causing elastic surface displacements. The effects of elastic deformation become negligible as the piston completes its mid-stroke at 450 degree

crank rotation angle. The hydrodynamic pressure profiles are shown in figure 5.11. Comparing these pressures with those at 360 degree in figure 5.8, 380 degree in figure 5.9, and 410 degree in figure 5.10, it becomes evident that with the gradual decrease in the hydrodynamic pressures the peak pressures acting on the ring surface at 0, 180 and 360 degree in the circumferential direction also have reduced intensities as hydrodynamic pressures in the non-axisymmetric bore out-of-round region emerge with comparable magnitudes.

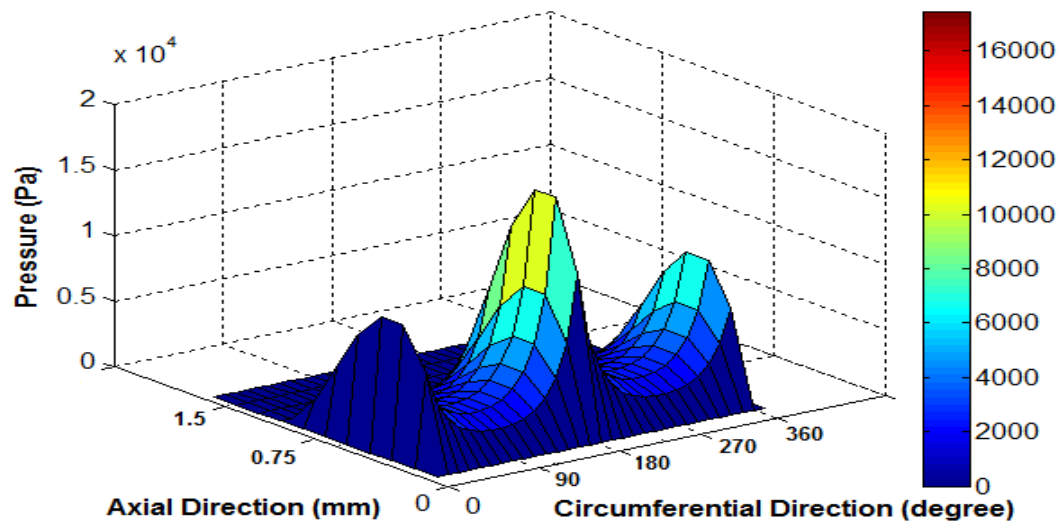


Figure 5.11: Hydrodynamic pressure profile at 450 degree crank

The hydrodynamic pressure drops down to lower values as piston travels towards the BDC in the expansion stroke. A case in point is when the piston is at 490 degree crank angle, as shown in figure 5.12. At this point, the cumulative effect of decreasing the cyclic speed, negligibly low gas pressure force, the instantaneous hydrodynamic film thickness rise and the effect of distorted cylinder bore facilitate the generation of low hydrodynamic pressures.

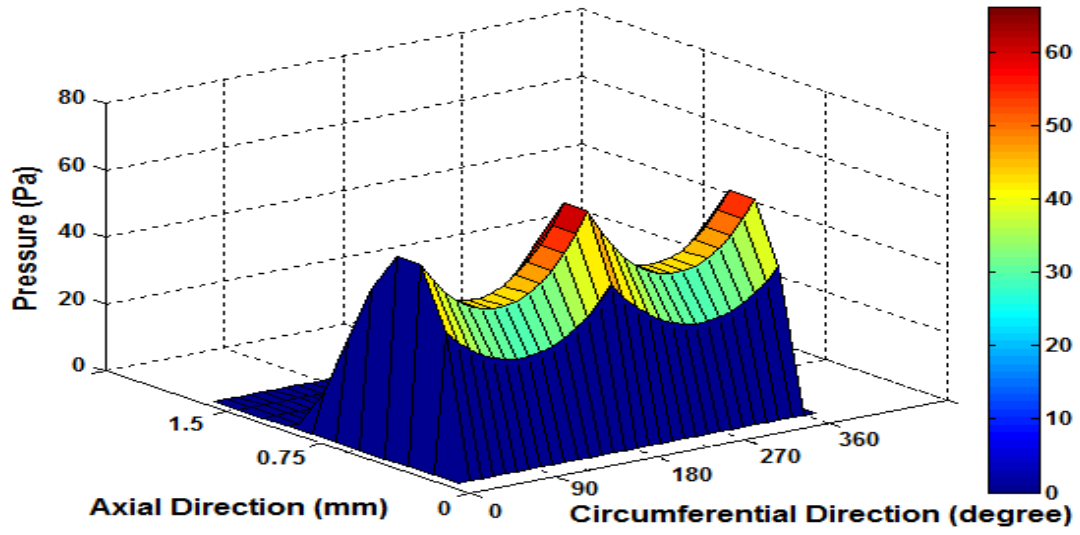


Figure 5.12: Hydrodynamic pressure profile over the ring surface at 490 degree crank angle

5.3 Performance Parameters

5.3.1 Friction Force and Power Loss

The hydrodynamic friction force is generated as the fluid flows and piston ring surface is lubricated in the hydrodynamic and EHL regime while the piston completes the 4-stroke cycle. Friction affects the ring lubrication by contributing towards energy dissipation, power losses and viscous shearing during a few initial cycles of cold engine start up. The friction force generated during the 720 degree crank rotation cycle is plotted and shown in figure 5.13. In the induction stroke, the minimum loading results in the generation of corresponding friction force of very low magnitude. In the compression stroke, the hydrodynamic friction force increases due to the combustion gas force effect, the hydrodynamic pressure rise, viscosity of the lubricant, cyclic speed of piston and the effect of the piston compressing the air-fuel charge. At the time of commencement and completion of induction, compression, expansion and exhaust strokes the cyclic velocity of the piston is minimum, due to which, the hydrodynamic friction force is also minimum.

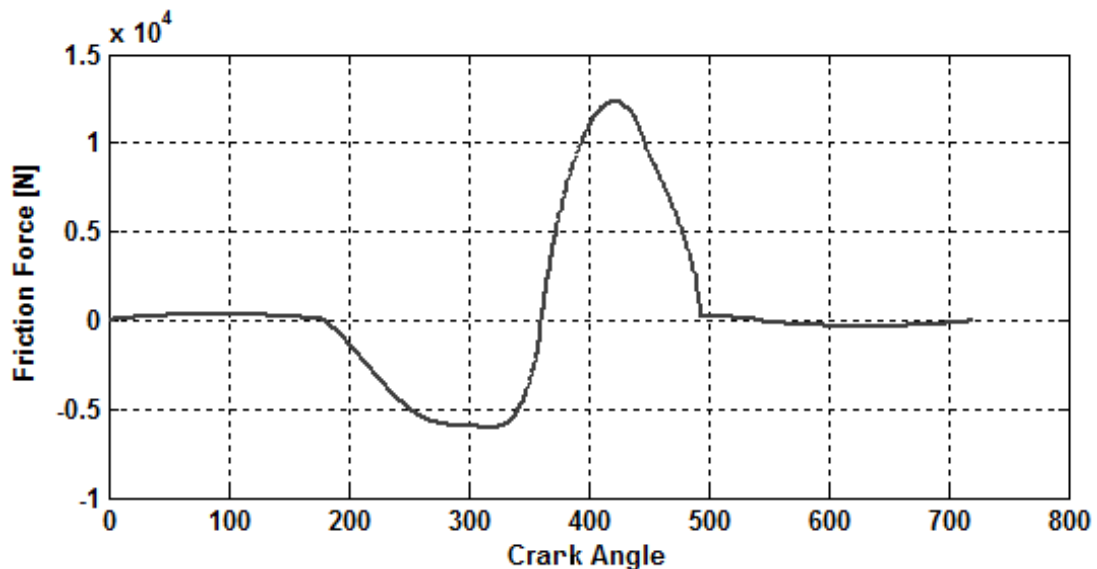


Figure 5.13: Hydrodynamic Viscous Friction Force Vs Crank Angle

Since maximum changes in the hydrodynamic pressures, film thickness, gas pressure force etc. occur during the compression and expansion strokes, hence cumulative effects of the same

cause an appreciable increase in the magnitude of the hydrodynamic friction force. Figure 5.13 highlights these effects such that the maximum hydrodynamic friction is generated in the expansion stroke at 420 degree crank angle. A drastic reduction in the combustion gas force effect and low hydrodynamic pressure keep the friction force to be of low magnitude in the exhaust stroke in the initial engine start up.

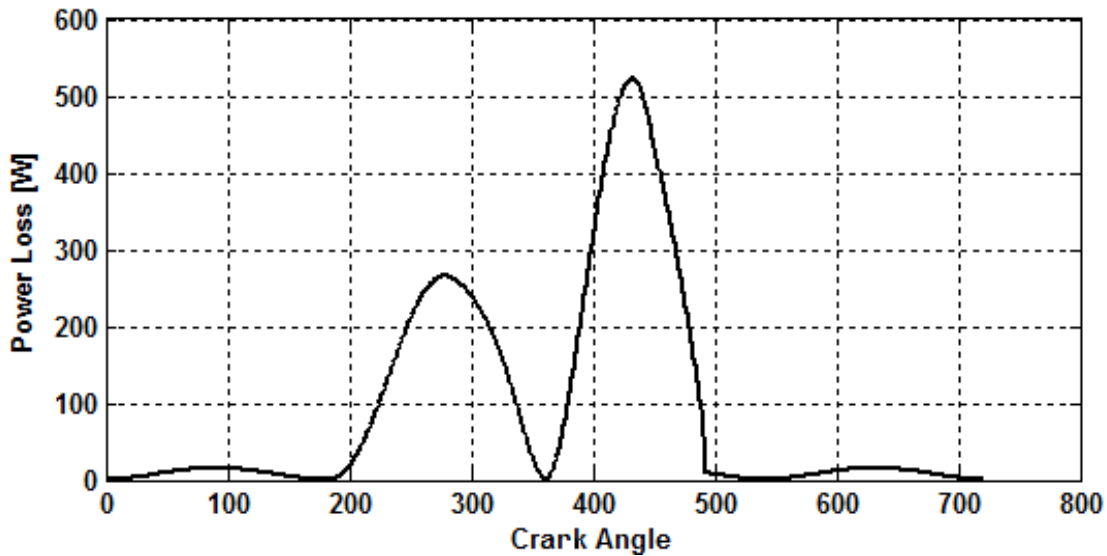


Figure 5.14: Mechanical Frictional Power Loss Vs Crank Angle

The hydrodynamic friction force and EHL of piston ring during the piston motion in the initial engine start up generate power loss, the profile of which is plotted in figure 5.14. The power loss during the 4-stroke cycle follow similar trend as that of hydrodynamic friction force. The power loss remains minimum during the intake and exhaust strokes, whereas it is maximum during the expansion stroke.

5.3.2 Lubricant Flow

In the lubrication of the first compression ring in the initial engine start up one of the important assumption is the oil flooding. In reality, it becomes difficult to maintain a continuous lubricant supply, especially at the time of the engine start up. To prevent the occurrence of lubricant starvation and ensure continuity of lubricant flow it is essential to calculate its volumetric flow rate as a function of 720 degree of crank rotation cycle. In this case the

volumetric flow rate is calculated and plotted against the crank rotation angle, as shown in figure 5.15. This graph also shows the amount of oil leaving the trailing edge of the piston ring and contributing in the pollutant exhaust emissions.

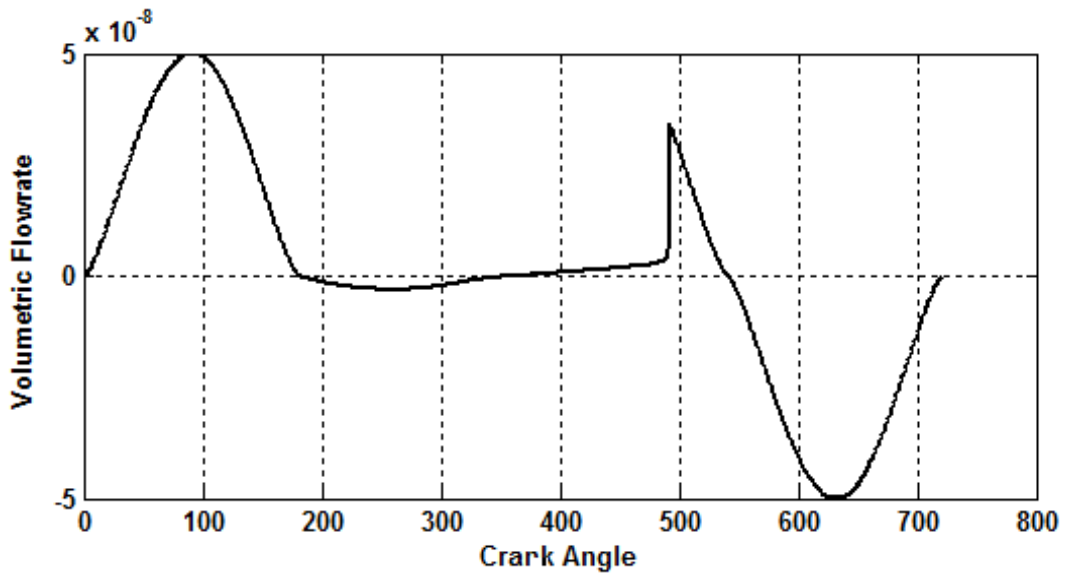


Figure 5.15: Volumetric Flow rate (m³/s) Vs Crank Angle

In the induction and exhaust strokes, flow rate makes the bell and inverted bell shape curve respectively, this is because of the low hydrodynamic pressures (see figure 5.3-5.4) and relatively higher amount of lubricating oil film thickness in the respective strokes as shown in figure 5.1, so more oil is required at inlet portion of the piston ring to establish subjected lubricating film thickness. In the compression and combustion stroke due to high hydrodynamic pressures and relatively low lubricating oil film thickness, flow rate required at inlet region is relatively less in compression and combustion strokes as compared to intake and exhaust strokes. Hence, a continuous lubricant supply and continuity of flow must be ensured under the stated conditions to establish hydrodynamic oil film thickness as shown in figure 5.1.

CHAPTER-6

Sensitivity Analysis - Results and Discussions

6.1 Parametric Study of Ring Face Profile

A parametric study is conducted for four different symmetric ring face profiles shown in Fig 3.3, with different flat spam, extending from completely flat ring face to completely parabolic ring face in 3 steps with reduction of 20% in flat zone in each step. The analysis of the numerical results lead towards optimizing the flat spam of the ring face by plotting and evaluating the profiles of hydrodynamic film thickness, friction force effect, the anticipated power loss and the flow rate under the stated conditions. It is followed by analysis of aforementioned different proportions of the flat spam of the ring for optimizing its face profile to minimize the mechanical energy loss in the initial engine start up conditions.

6.1.1 Effect of Ring Running Face Profile on Lubricating Oil Film Thickness

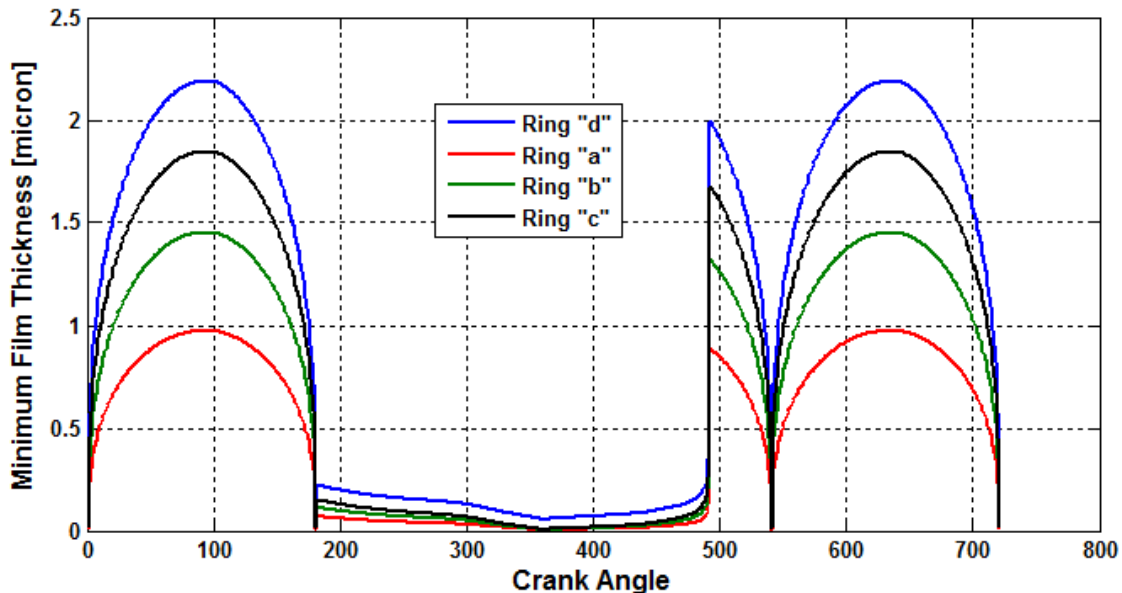


Figure 6.1(a): Minimum Film Thickness Vs Crank Angle

The significant aspect to analyze is the fact that despite following a similar trend in all the stated cases as is described in section 5.1, the film thickness magnitude keeps improving as the ring face profile is altered from a flat spam of 60% (*Ring a*) down to 0% (*Ring d*), as shown in

figure 6.1. An improved film thickness significantly reduces the mechanical sliding friction between the ring and the liner thereby aiding in the reduction of mechanical energy loss. The face profile of *Ring "d"* at which the film thickness remains maximum as compared to the minimum thickness of *Ring "a"* and intermittent thickness of the other two face profiles.

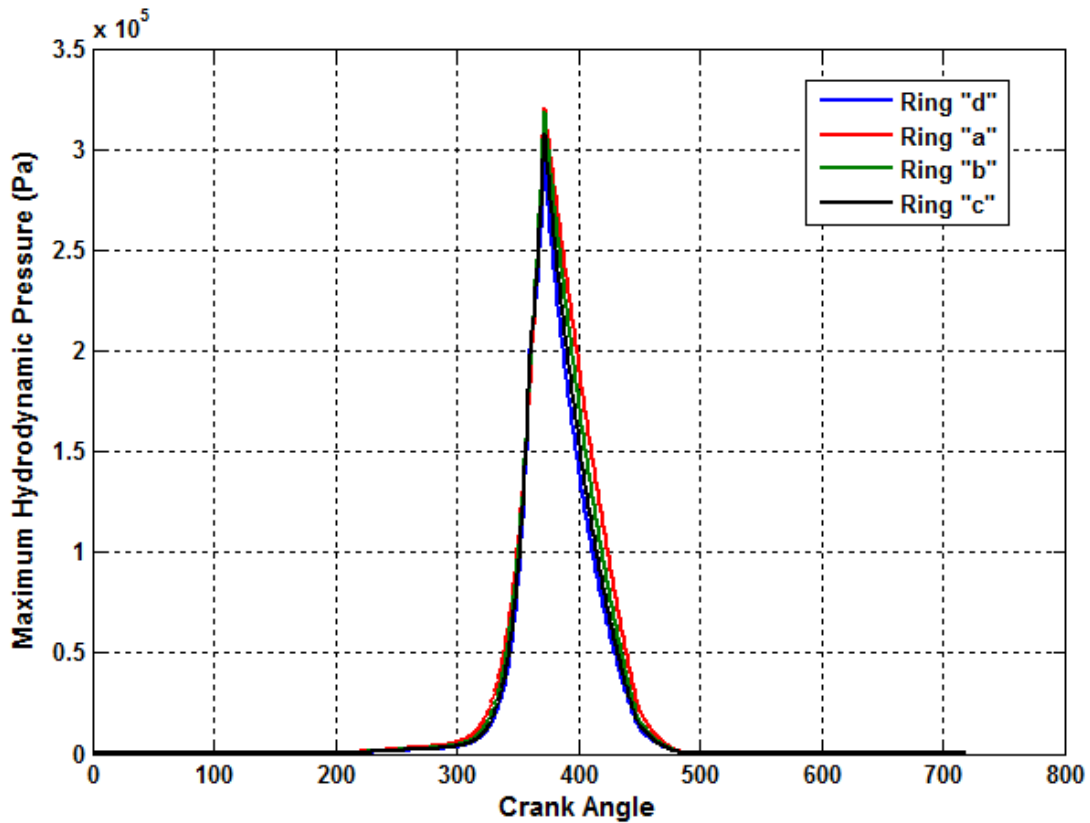


Figure 6.1(b): Maximum Hydrodynamic Pressures Vs Crank Angle

6.1.2 Effect of Ring Running Face Profile on Piston Ring Performance

6.1.2.1 Friction Force

After analyzing the hydrodynamic film thickness and volume flow rate using respective compression ring face profiles, it is imperative to discuss their effects on mechanical friction generated between the interacting compression ring and the cylinder liner surfaces during the engine cycle in the initial engine start up case. Figure 6.2 shows the profiles of the magnitude of friction force in respect of the four different ring faces. In the initial engine start up conditions the sliding friction between the ring and the liner surfaces is expected to be very high as

compared to the normal engine operation when high engine speeds and volume flow rates significantly contribute towards reducing this friction. In the induction and expansion strokes, the high volume flow rate, maximum film thickness, and absence of thermal loading keep the sliding friction to a minimum. On the other hand a sharp reduction in the volumetric flow, very small film thickness and effects of the very high combustion gas force increase the sliding friction to several orders of magnitude such that the maximum value of the friction force is seen in the expansion stroke followed by a similar profile of reduced magnitude in the compression stroke. It indicates maximum cumulative friction and energy losses in the compression and expansion strokes. The cyclic nature of the magnitude of the friction force is attributed to the cyclic speed of the piston such that at the commencement of the compression stroke the piston speed is minimum and as it starts its travel from the bottom dead center (BDC), its velocity also starts increasing. The piston attains maximum speed as it reaches the mid-point of the compression stroke. The rise in the magnitude of the gas pressure force due to the piston compressing the air fuel mixture, a sharp drop in the film thickness due to very low volume flow of the lubricant causes an increase in the magnitude of the friction force, which corresponds to the increasing cyclic speed of the piston in the first half of the compression stroke.

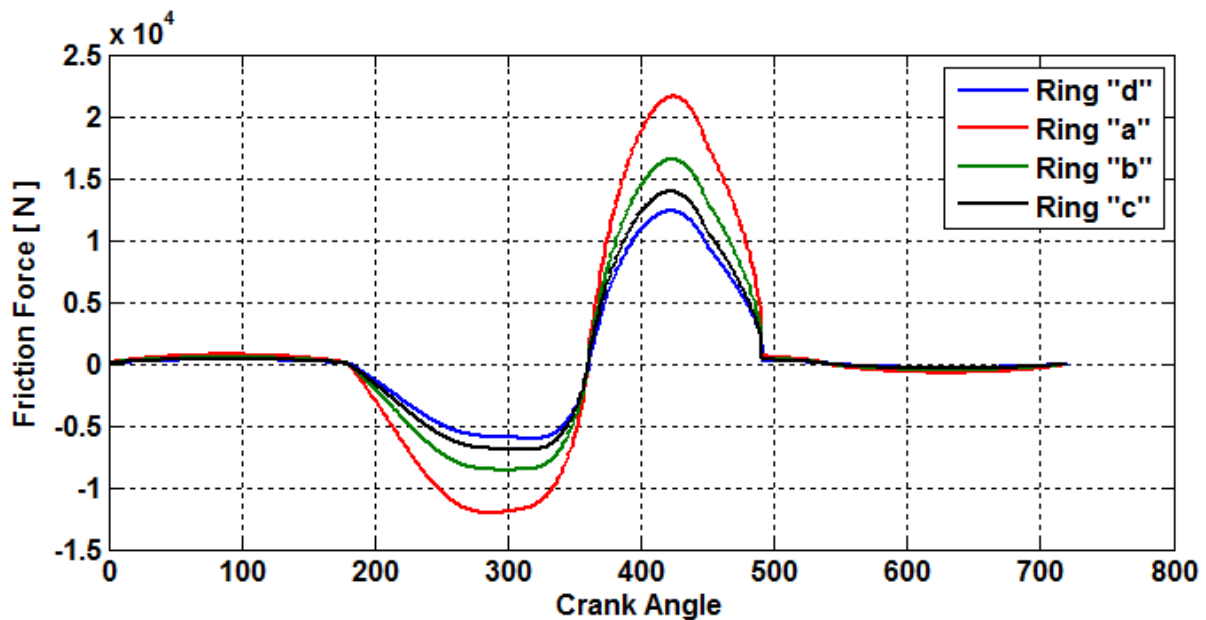


Figure 6.2: Friction Force Vs Crank Angle

After attaining the maximum cyclic speed at the mid-point, the piston starts slowing down as it displaces from the mid-stroke region to the end of the compression stroke at the top dead center (TDC). The slowdown of the piston in the second half of the compression stroke results in the corresponding reduction in the friction force magnitude, until it is negligible as piston comes to a near halt at TDC. The friction force profile shown in the negative quadrant in figure 6.2 indicates its magnitude in the reverse direction. The magnitude of the friction force rises and falls in a similar fashion during the expansion stroke but it is more than the force magnitude in the compression stroke with a pointed apex riding over the sharp ascending and descending slopes. It is obvious that the face profile of the first compression ring is one of the major contributors in altering the magnitude of sliding friction. Despite the respective friction force profiles showing a somewhat similar trend, the conventional face profile of the ring offers maximum friction in the critical zones of the compression and expansion strokes as compared to the other profiles. Keeping in view the significance and the vulnerabilities of piston in the compression and expansion strokes due to the minimum film thickness and very low volume flow rate the rising magnitude of the friction force is detrimental to the concept of saving the energy implying energy wastage under the stated conditions. In this context, a gradually reduced friction force magnitude by a corresponding reduction in the ratio of the flat span as the face profile shifts from *Ring a* to *Ring b*, to *Ring c* and then to *Ring d* is indicative of a gradual reduction in the energy loss in a similar manner.

6.1.2.2 Power Loss

The most crucial aspect of modeling the energy loss in the 2-D lubrication of the first ring is the cyclic power loss during the 4-stroke cycle of a piston. The profile of the magnitude of mechanical power loss as a function of 720 degree crank rotation cycle is shown in figure 6.3. In the absence of thermal loading of significant value, the cyclically changing piston motion in the induction stroke generates the cyclic power loss but its magnitude fails to go beyond a few watts at the mid-stroke region where the piston has maximum cyclic speed. The few watts of power loss are reduced to a negligibly small value as the piston approaches the end of induction stroke.

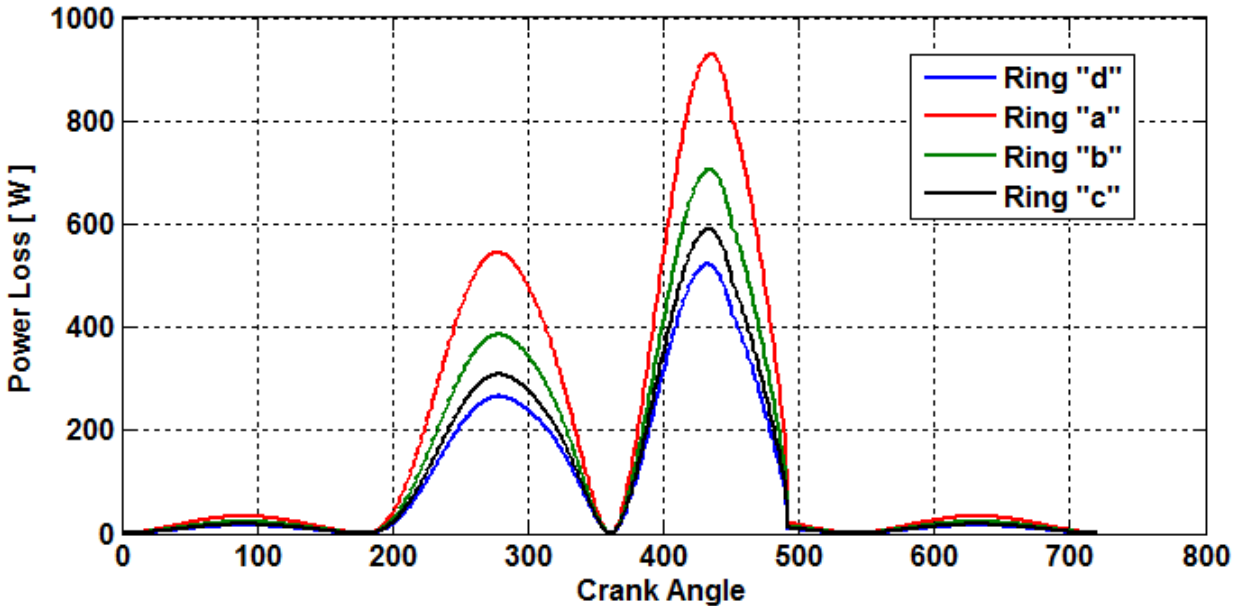


Figure 6.3: Power Loss Vs Crank Angle

There is a significant increase in the magnitude of power loss in the compression stroke but the trend remains cyclic. Power losses increase sharply in the expansion stroke such that the peak losses are double the losses during the compression stroke, as shown in figure 6.3. A sharp increase in the power loss is followed by a corresponding reduction as the piston reaches at the end of the expansion stroke. In the 4-stroke cycle, the exhaust valve opens before the piston completes the expansion stroke. It generates an instantaneous local turbulence in the expanding burnt out gases i.e., the product of combustion, resulting in the reversal of their flow path to the exit at the exhaust valve due to pressure differential caused by the opening. By the time the piston commences its journey in the exhaust stroke, the burnt out gases have almost changed their direction of flow and are on their way out.

The magnitude of the effort required by the piston to push the exhaust gases out of the cylinder is considerably reduced as a little push of the piston crown accelerates the already exiting gases, causing substantial energy savings, as evident in figure 6.3 by the profile of the power loss curve in the exhaust stroke. When making a comparison between the conventional ring face with the other face profiles in terms of the power loss it becomes very important to contain the energy and power losses to a minimum in the compression and exhaust strokes. By

reducing the flat spam from 60% of the total ring width to 40%, 20% and 0%, the power loss is decreased by 28.6%, 42.8% and 50.47% in the compression stroke and 22.4%, 35.52% and 44.3% in the expansion stroke, respectively. These savings in the energy are quite substantial and impressive under the stated conditions.

6.1.2.3 Lubricant Flow Rate

The discussion on film thickness profile for the different face profiles of the top ring is incomplete if the volume flow rate of the lubricant is not analyzed under the assumption of oil flooding conditions. Figure 6.4 shows the respective volume flow rates as a function of 720 degree crank rotation angle. The volume flow rate is directly related to the film thickness as an increased lubricant flow aids in enhancing the film thickness, ensures continuity of flow and maintains the conservation principle.

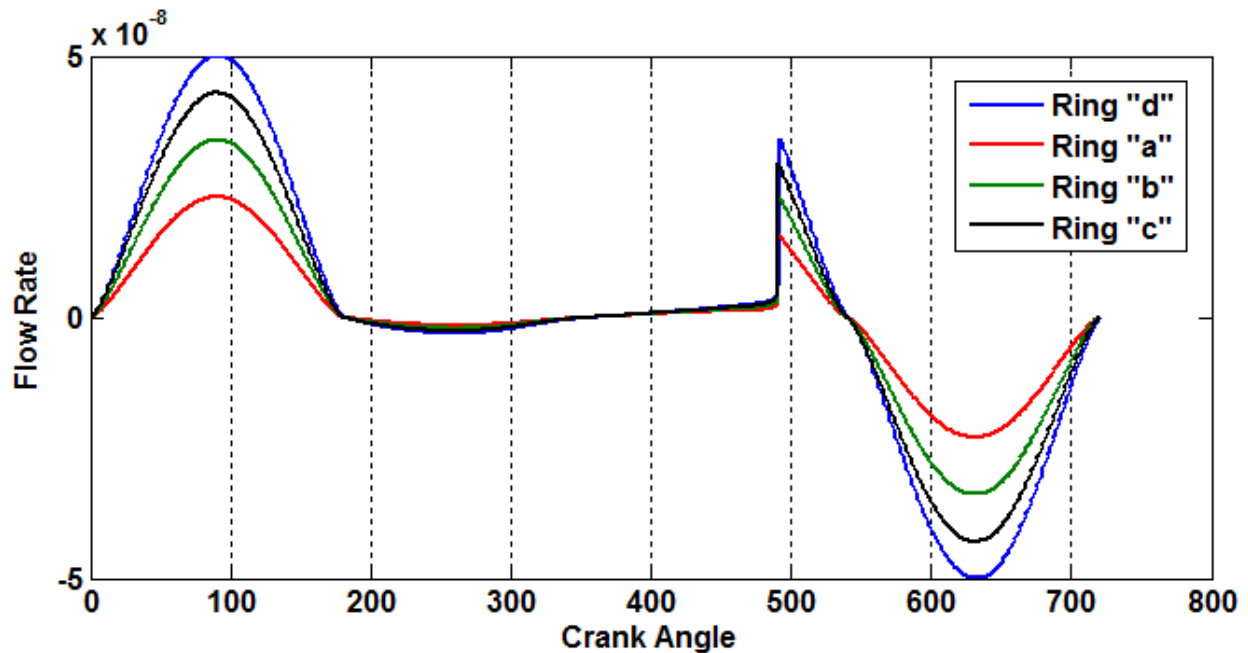


Figure 6.4: Flow-rate (m^3/s) Vs Crank Angle

The flow rate profiles of respective ring faces generally follow a similar trend of maximum flow rate during the induction and expansion strokes due to the absence of the gas pressure force of significant magnitude and minimum flow rates during the compression and expansion stroke of the piston due to the sharply rising magnitude of the gas force as shown in figure 3.5.

In the face profile of conventional *Ring a*, the maximum flow rate remains abysmally low throughout the 4-stroke cycle as compared to the other ring profiles, which is the major contributing factor behind the minimum film thickness profile between this conventional ring and the liner. A comparison of the face profiles of the three other rings indicates that the flow rate may not improve considerably in the compression and expansion strokes, which implies that the ring remains vulnerable to the possibility of contact and wear.

6.2 Parametric Study of Engine Speed

6.2.1 Effect of Engine Speed on Lubricating Oil Film Thickness

As is discussed in previous section and chapters the process of hydrodynamic lubricating film thickness and pressures. Similarly in this section hydrodynamic film thickness is plotted for different engine speed, as shown in figure 6.5. Upon increasing speed film thickness profile improves in induction, exhaust stroke and about half of expansion stroke because of low load of gas pressure forces.

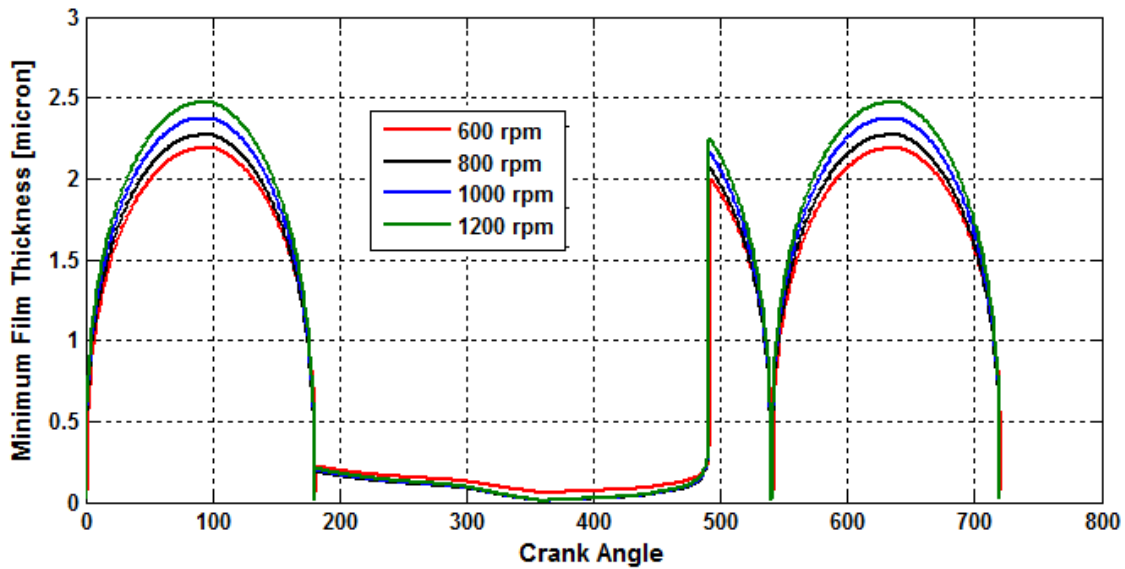


Fig 6.5: Minimum Hydrodynamic Film Thickness Vs Crank Angle at Different Engine Speeds

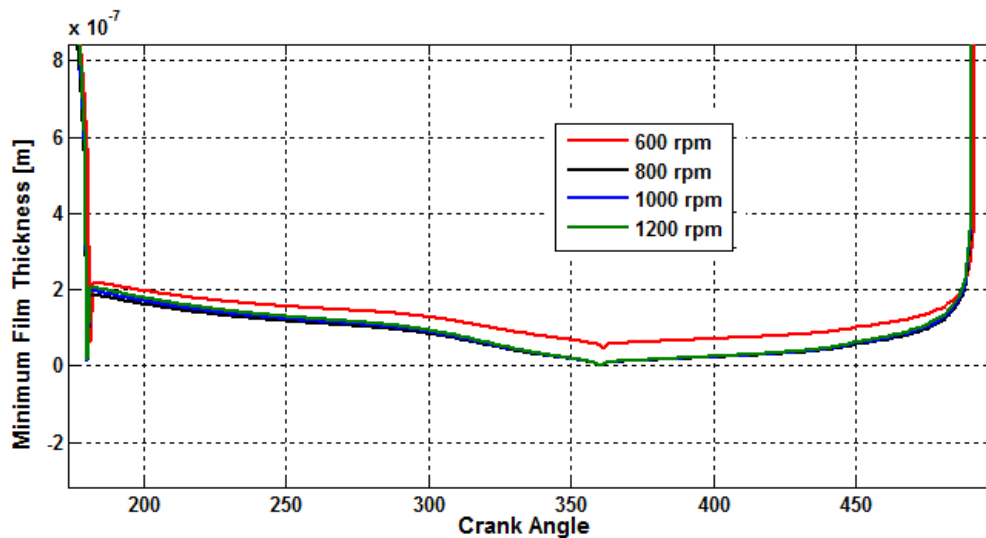


Fig 6.6(a): Minimum Hydrodynamic Film Thickness in Critical Region Vs Crank Angle

As is stated by many researchers (see section 1.2), film thickness increases with increase in speed and decrease with increase in load. In compression and half of combustion stroke gas pressures are sufficiently high to suppress film thickness, and minimum film thickness lies in this critical zone. It is also to be noted that, with increase in speed film thickness decreases in compression and expansion stroke, as is shown in figure 6.6(a).

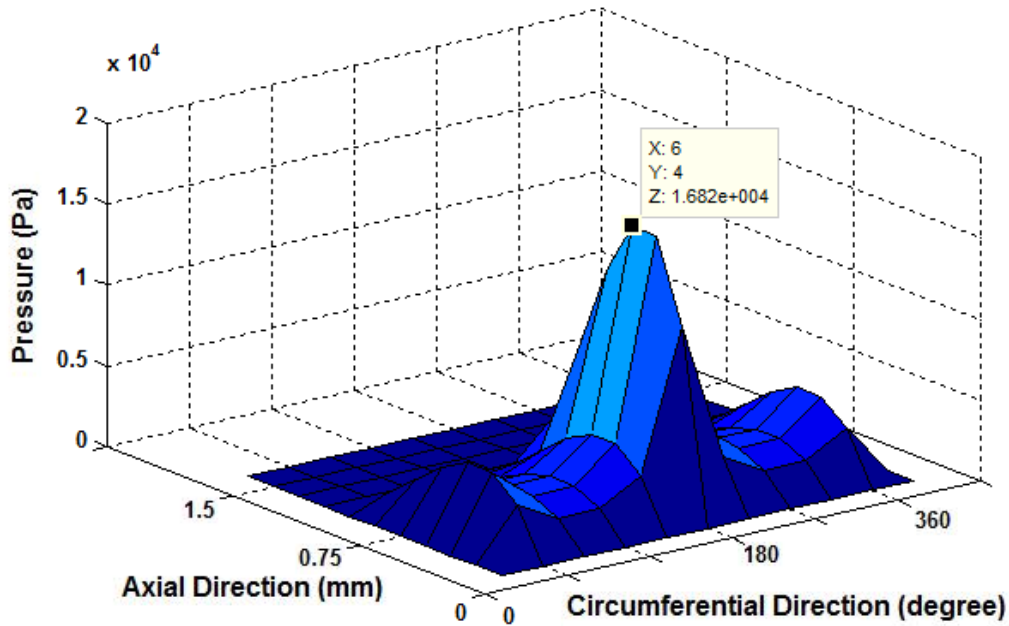


Fig 6.6(b): Hydrodynamic Pressures Profile over the ring face at 450 degree Crank Angle and 600 rpm

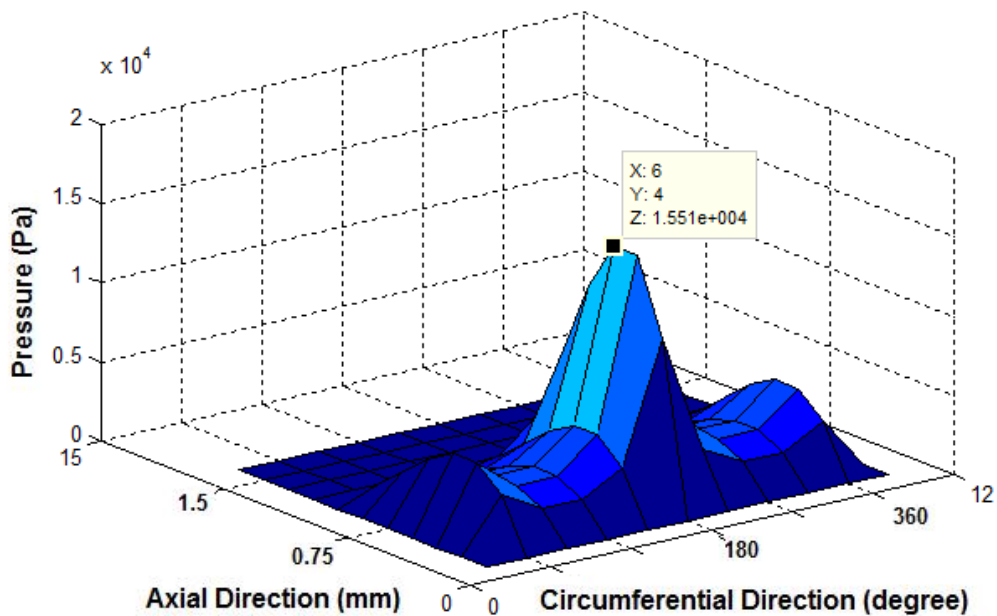


Fig 6.6(c): Hydrodynamic Pressures Profile over the ring face at 450 degree Crank Angle and 800 rpm

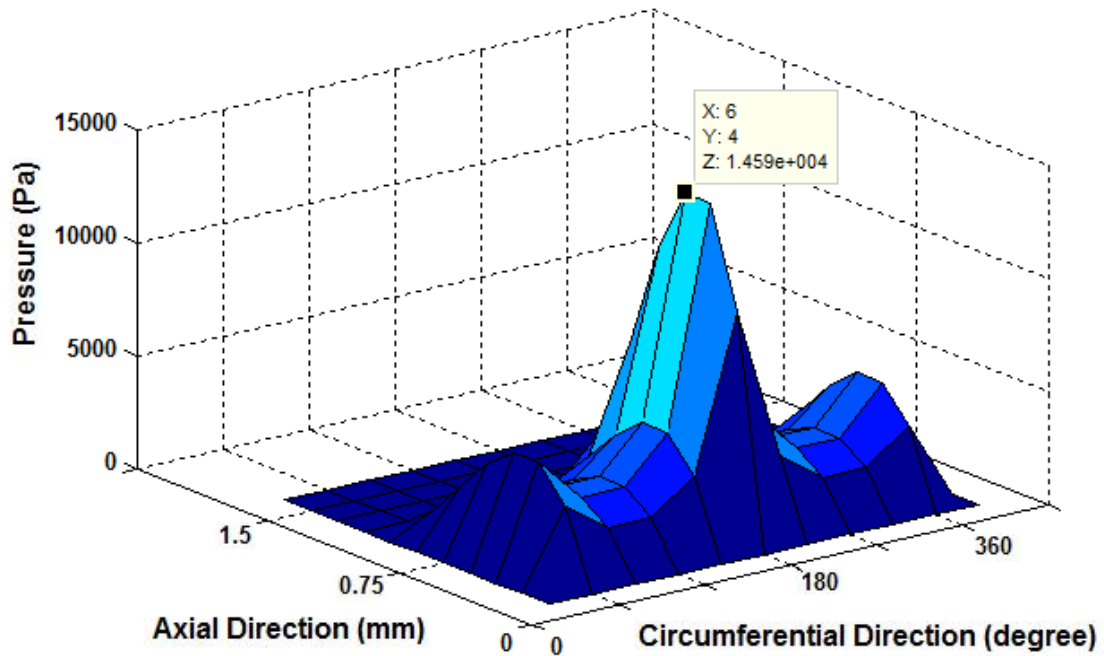


Fig 6.6(d): Hydrodynamic Pressures Profile over the ring face at 450 degree Crank Angle and 1000 rpm

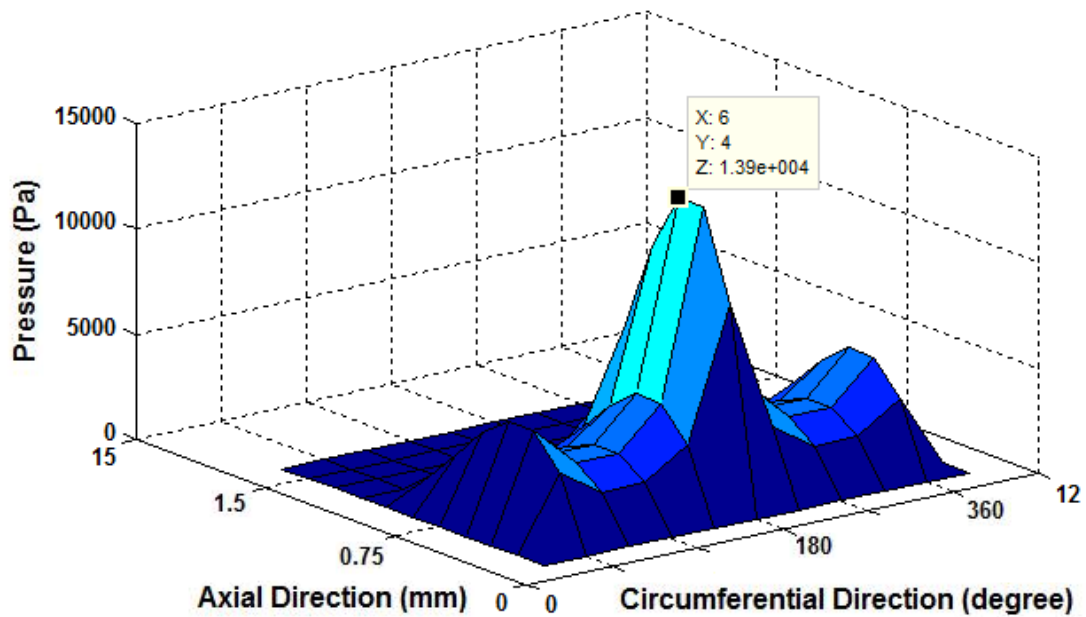


Fig 6.6(e): Hydrodynamic Pressures Profile over the ring face at 450 degree Crank Angle and 1200 rpm

Whereas, in elastohydrodynamic regime, due to increase in gas pressure and resultant hydrodynamic pressures, piston ring and cylinder liner surfaces deform elastically, hence increasing clearance between them and lubricating film thickness increases with increase in speed throughout the entire engine cycle in elastohydrodynamic regime, as is shown in figure 6.7 and figure 6.8.

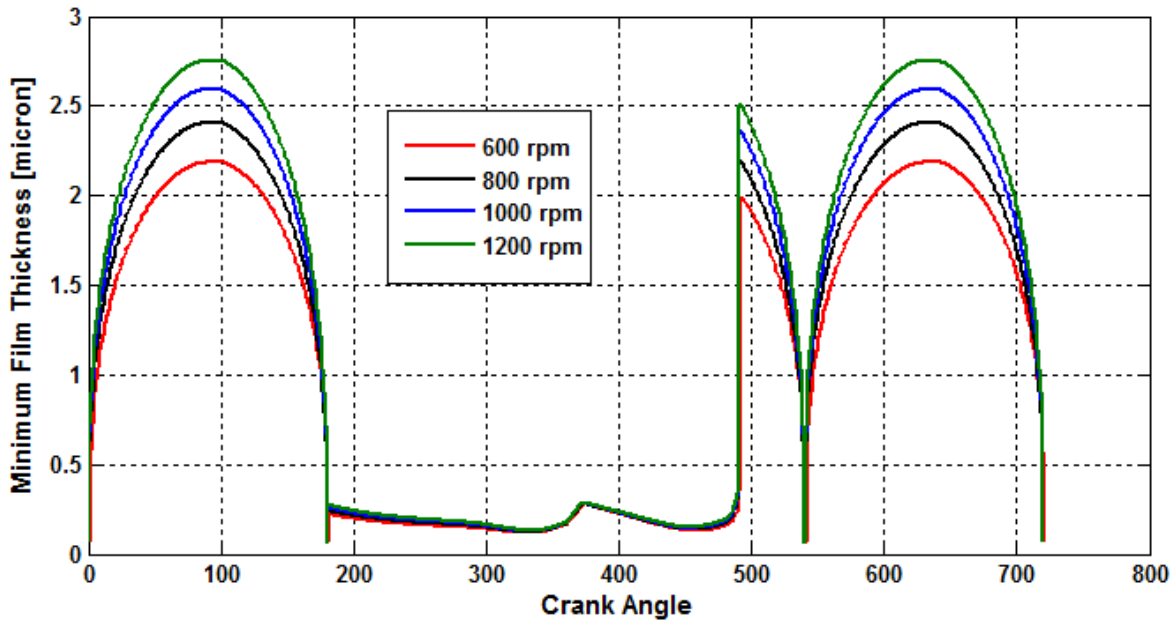


Fig 6.7: Minimum EHD Lubricating Film Thickness Vs Crank Angle

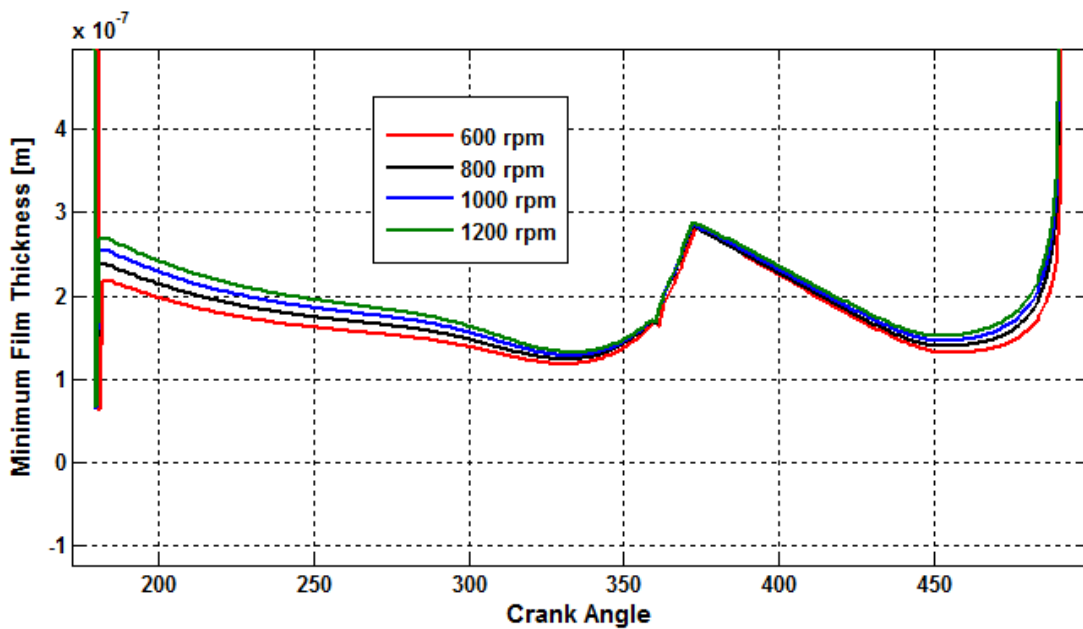


Fig 6.8: Minimum EHD Lubricating Film Thickness Vs Crank Angle in critical region

6.2.2 Effect of Engine Speed on Piston Ring Performance

6.2.2.1 Friction Force and Power Loss

According to mathematical model presented in chapter 3, viscous friction force is directly proportional to the engine speed, as is shown by figure 6.9 and figure 6.10. Hence if engine speed is increased friction force and power loss will increase resulting in reduced fuel efficiency.

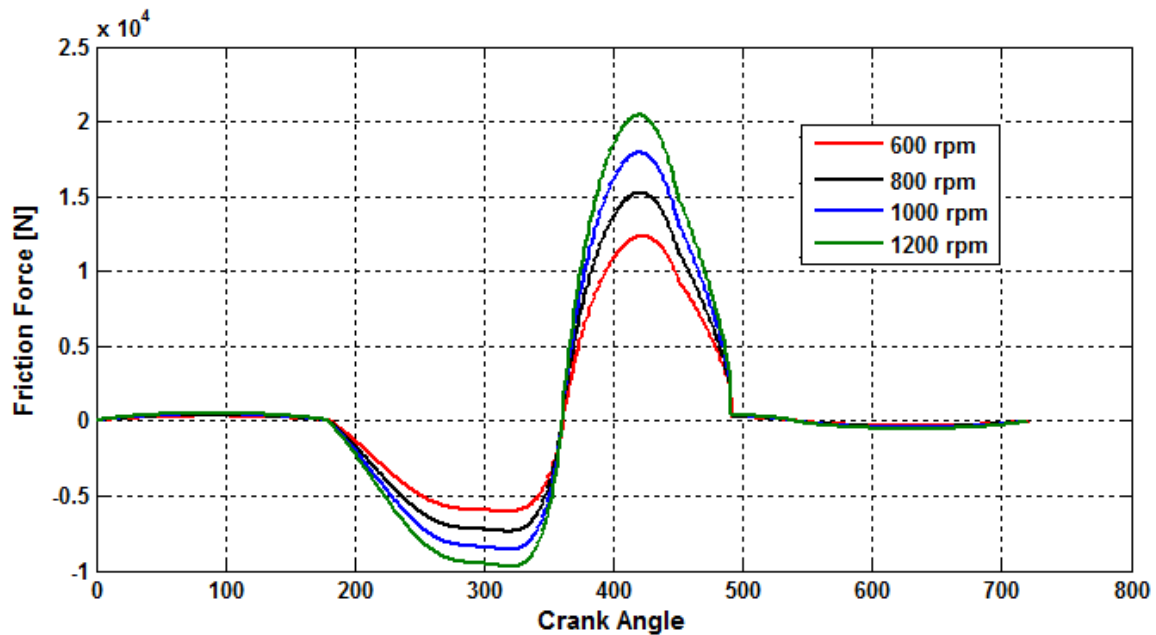


Fig 6.9: Viscous Friction Force Vs Crank Angle at Different Engine Speed

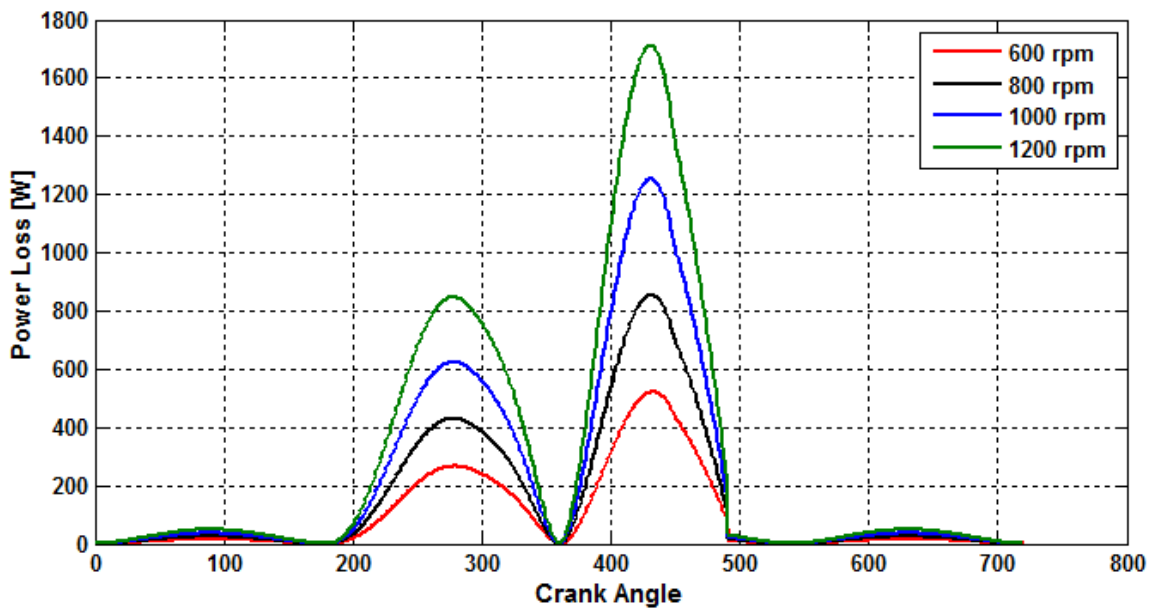


Fig 6.10: Mechanical Power Loss Vs Crank Angle at Different Engine Speed

6.2.2.2 Volumetric Flow-rate

With increase in speed lubricant flow rate will increase, as is shown by figure 6.11, hence not only increasing the amount of oil required at inlet, but also increase in oil transport to the combustion chamber resulting in increase in health hazardous exhaust emission.

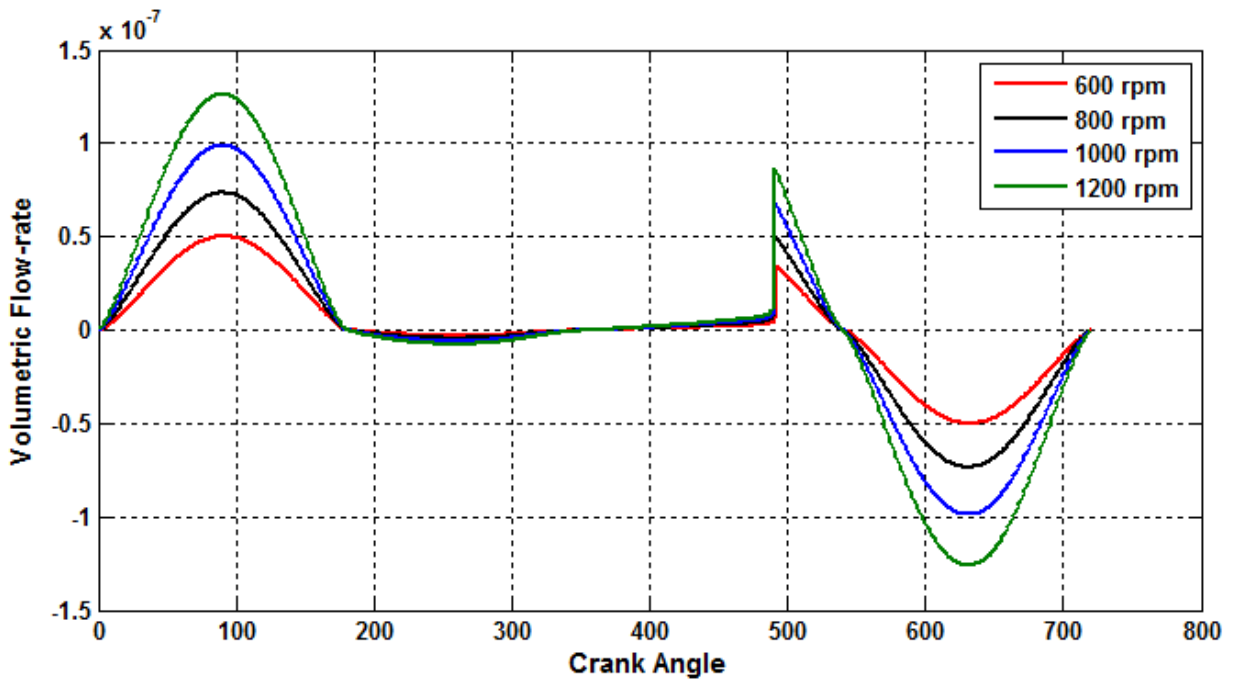


Fig 6.11: Volumetric Flow-rate (m³/s) Vs Crank Angle at Different Engine Speed

6.3 Parametric Study of Bore Distortion

6.3.1 Effect of Bore-Distortion on Lubricating Oil Film Thickness

Lubricating oil film thickness profiles at different of magnitude of bore distortion are shown in figure 6.12. Due to increase in circumferential distortion, flow of the lubricating oil increases in circumferential direction, hence decreasing the minimum film thickness value, resulting in relatively higher chances of wear.

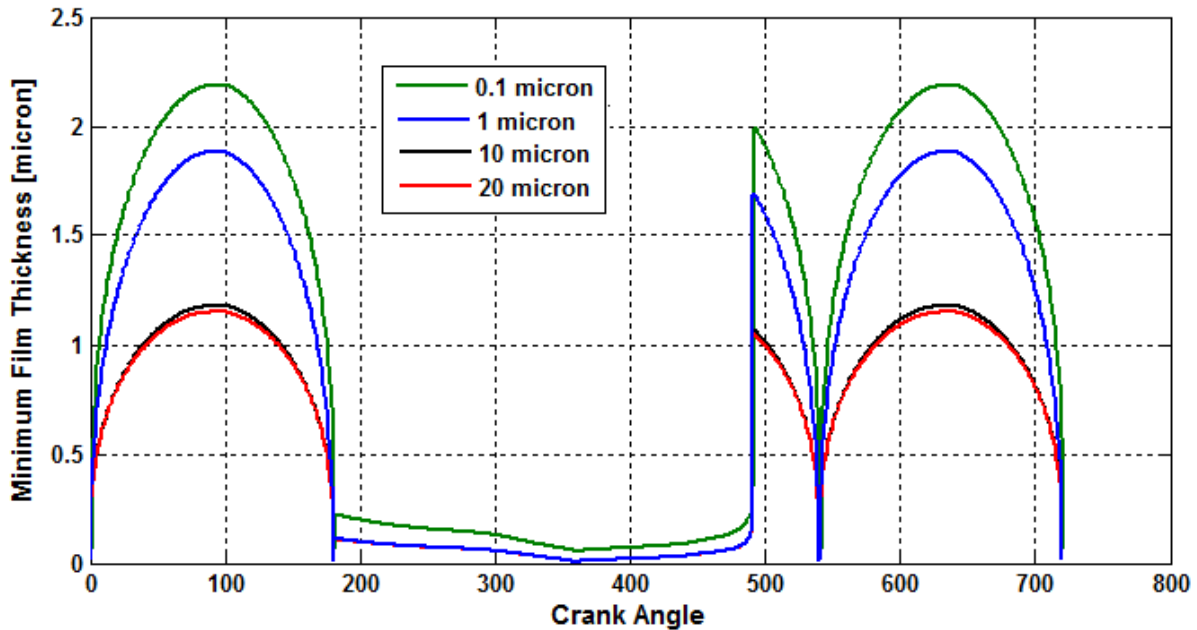


Fig 6.12(a): Minimum Film Thickness Vs Crank Angle at Different Degree of Bore Distortion

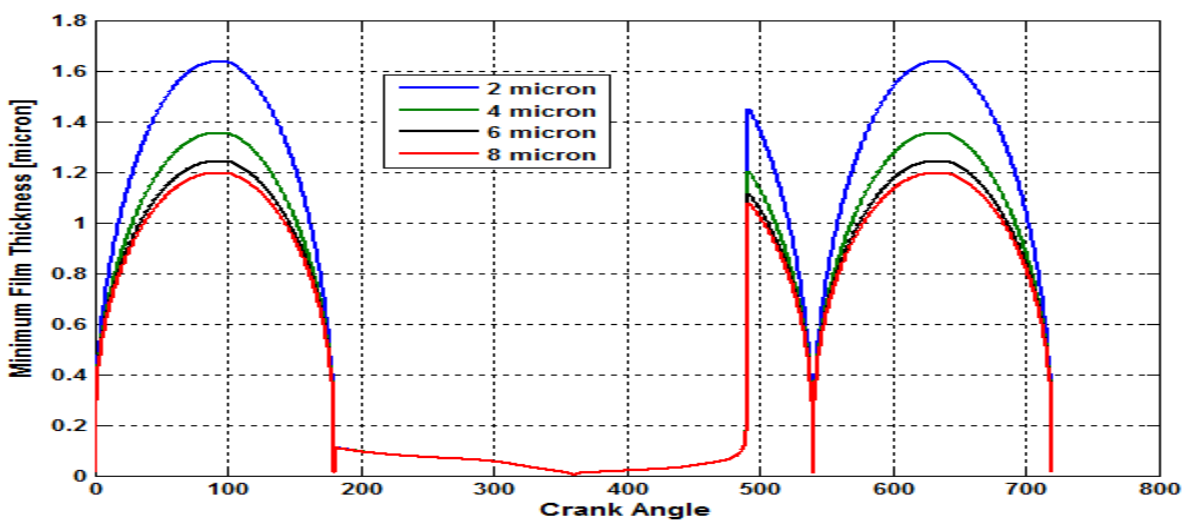


Fig 6.12(b): Minimum Film Thickness Vs Crank Angle at Different Degree of Bore Distortion

6.3.2 Effect of Bore-Distortion on Piston Ring Performance

6.3.2.1 Friction Force and Power Loss

Relation of friction force and power loss with minimum film thickness is discussed in detail in previous chapter (see section 5.3.1), hence, as bore distortion increases, clearance between piston ring and cylinder liner increases, resulting in decrease in minimum film thickness but due to overall increase in clearance, oil film fills the gap and results in decrease in viscous friction force and power loss, as shown in figure 6.13 and figure 6.14 respectively. Hence chances of wear are relatively higher, but increase in bore distortion improves the fuel efficiency and economy.

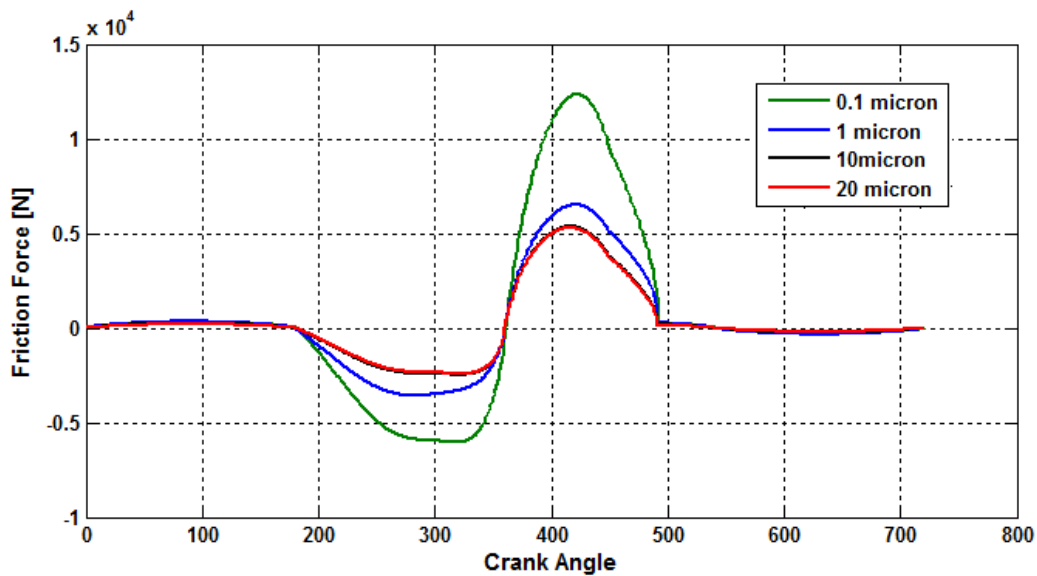


Fig 6.13: Viscous Friction Force Vs Crank Angle at Different Degree of Bore Distortion

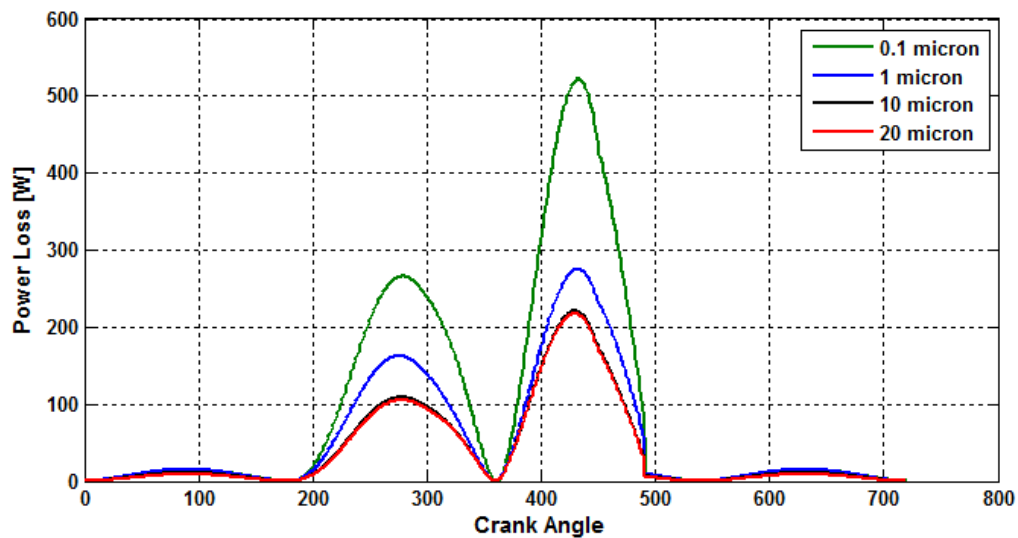


Fig 6.14: Mechanical Power Loss Vs Crank Angle at Different Degree of Bore Distortion

6.3.2.2 Volumetric Flow-rate

Profiles of oil transport to combustion chamber, and required at inlet of the piston ring to generate lubricating oil film thickness upon increasing magnitude of bore distortion are shown in figure 6.15. so if bore distortion increases volumetric flow rate of lubricant oil will increase to combustion chamber hence increasing health hazardous exhaust emissions, and relatively higher amount of oil at inlet region of piston ring will be required to generate hydrodynamic and elastohydrodynamic lubricating oil film thicknesses

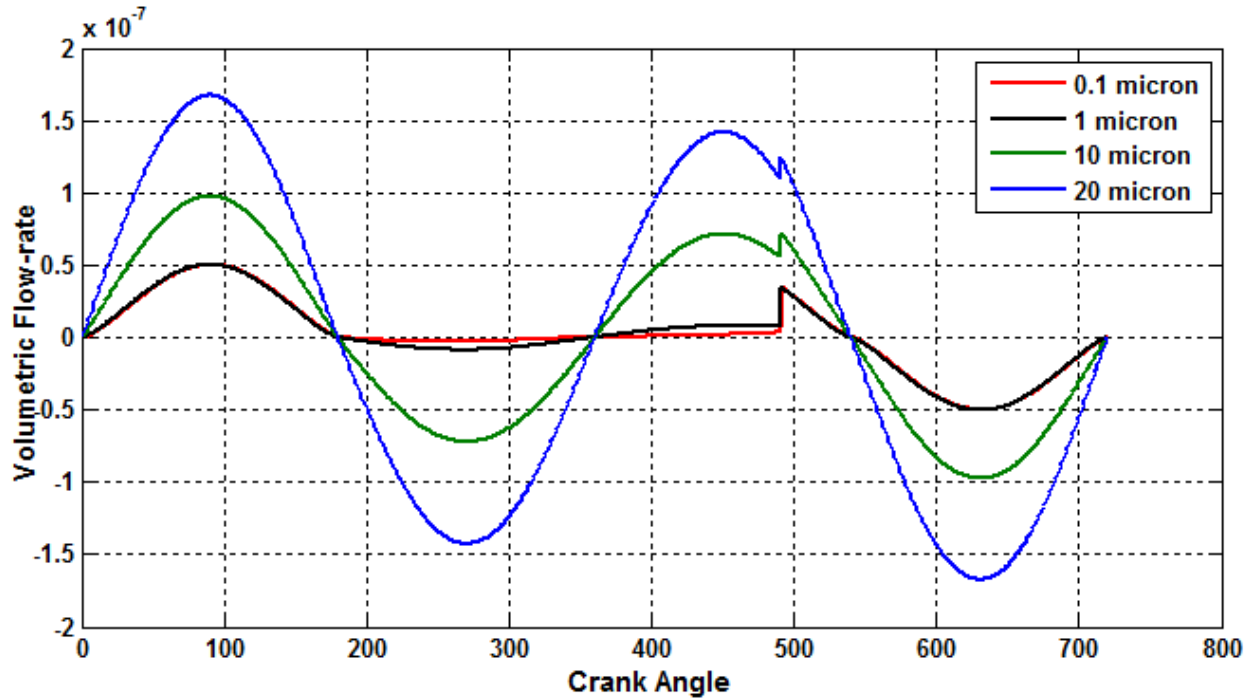


Fig 6.15: Volumetric Flow-rate (m³/s) Vs Crank Angle at Different Degree of Bore Distortion

CHAPTER-7

Conclusions

Though more in depth study is required, but after objective analysis of result presented and discussed in previous chapters, some conclusions can be made, that are

- Firstly, as far as development of Elastohydrodynamic lubricating film thickness and improvement in piston ring performance parameters are concerned, Parabolic running face profile is the best suited piston ring running face profile under the stated conditions, and, in initial engine start up conditions.
- Secondly, 600 rpm is the best suited engine speed for optimized Piston ring performance. With increase in speed, Elastohydrodynamic film thickness profile improves but friction force and power loss increases.
- Thirdly, with increase in magnitude of bore distortion, chances of wear and piston ring performances increases, except oil transport to combustion chamber which also increases and will cause more health hazardous exhaust emissions.

After studying piston ring lubrication on aforementioned optimized parameters, it can be stated that, Elastohydrodynamic lubricating oil film thickness can be developed in initial engine start up conditions, under the stated assumptions and conditions, but chances of wear are still there in compression and power stroke.

References

- [1] Simon C. Tung and Michael L. McMillan, "Automotive Tribology Overview of Current Advances and Challenges for the Future", *Tribology International* vol. 37, pp. 517-536, 2004
- [2] Gwidon W. Stachowiak and Andrew W. Batchelor, *Engineering Tribology*, Elsevier Butterworth-Heinemann, 2005, pp.103-112
- [3] Edward P. Becker, "Trends In Tribological Materials and Engine Technology", *Tribology International*, vol. 37, pp. 569-575, 2004
- [4] Peter, Jaana Tamminen and Sandstrom, "Piston ring tribology a Literature survey", VTT Research Notes, No. 2178, pp. 8, 2002
- [5] R.C. Coy, "Practical Applications of Lubrication Models in Engines", *Tribology International*, vol. 31, pp. 563-571, Nov 1998
- [6] Dong_Chul Han and Jae-Seon Lee, "Analysis of the piston ring lubrication with a new boundary condition", *Tribology International*, vol. 31, No. 12, pp. 753-760, 1998
- [7] ZHANG Yong, CHEN Cuohua and Li Bing, "Two Dimensional Numerical Analysis of Piston Ring Lubrication of an Internal Combustion Engine", SAE, Paper No. 1999-01-1222, 1999
- [8] Liang Liu, "Modeling the Performance of the Piston Ring-Pack with Consideration of Non-Axisymmetric Characteristics of the Power Cylinder System in Internal Combustion Engines" Massachusetts Institute of Technology, pp.15-23, 2005
- [9] Beauchamp Tower, First Report on Friction Experiments, *Proc. Inst. Mech. Engrs.*, Nov. 1883, pp. 632-659.
- [10] O. Reynolds, On the Theory of Lubrication and its Application to Mr Beauchamp Tower's Experiments Including an Experimental Determination of the Viscosity of Olive Oil, *Phil. Trans., Roy. Soc. London*, Vol. 177 (i), 1886, pp. 157-234.

- [11] G.M. Hamilton and S. L. Moore, "The Lubrication of Piston Rings--First Paper-- Measurement of the Oil-Film Thickness Between the Piston Rings and Liner of a Small Diesel Engine" IMechE, vol. 188, pp. 253-261, 1974
- [12] G.M. Hamilton and S. L. Moore, "Comparison between Measured and Calculated Thicknesses of the Oil-Film Lubricating Piston Ring", IMechE, vol 188, pp. 262-268, 1974
- [13] S. R. Brown and G.M. Hamilton, "The Partially Lubricated Piston Ring", IMechE, vol. 19, pp. 81-89, 1977
- [14] S. L. Moore and G. M. Hamilton, "The Piston Ring at Top Dead Center", Pro IMechE, vol. 194, pp. 373-381, 1980
- [15] Sherrington and E. H. Smith, "Experimental methods for measuring the oil-film thickness between the piston-rings and cylinder-wall of internal combustion engines", Tribology Transactions, vol. 85, pp. 315-320, Dec 1985
- [16] Y. Wakuri, T. Hamstake, M. Soejima and T. Kitahara, "Piston Ring Friction in Internal Combustion Engines", Tribology International, vol. 25 No. 5, pp. 299-308, 1992
- [17] M-T Ma, E H Smith and Sherrington, "A Three-Dimensional Analysis of Piston Ring Lubrication Part 1: Modeling", IMechE, vol. 209, pp. 1-14, September 1995
- [18] Masaaki Takiguchi, Hajume Ando, Takahiro Takimoto and Akiyoshi Uratsuka, "Characteristic of Friction and Lubrication of Two-Ring Piston", JSAE9541362, 1996
- [19] Yang, Q. and Keith, T.Jr., "Two-Dimensional Piston Ring Lubrication—Part I: Rigid Ring and Liner Solution,", Trib. Trans., vol. 39, pp. 3, 1996
- [20] G R Paul and I J Sixsmith, "A New Method of Investigating Piston Ring Friction under Firing Condition", IMechE, vol. 210, pp. 179-182, May 1996
- [21] Mohsen Esfahanian and Bernard Hamrock, "On the Hydrodynamic Lubrication Analysis of Piston Rings", Lubrication sciences 10-4, pp. 265-286, August 1998

- [22] K Liu, Y B Xie and C L Gui, "Two-Dimensional Lubrication Study of the Piston Ring Pack", IMechE, vol. 212 Part J, pp.215-220, 1998
- [23] Sanjay D. Gulwadi, "Analysis of Tribological Performance of a Piston Ring Pack", Tribology Transaction, vol. 43, pp. 151-162, May 1999
- [24] Sung-Woo Cho, Sang-Min Choi and Choong-Sik Bac, "Frictional Modes of Barrel Shaped Piston Ring under Flooded Lubrication", Tribology International, vol. 33, pp. 545-551, 2000
- [25] Jinglei Chen, D. E. Richardson, "Predicted and Measured Ring Pack Performance of a Diesel Engine", SAE Inc., paper No. 2000-01-0918, 2000
- [26] D. Dowson, B. L. Ruddy, P. N. Economou, "The Elastohydrodynamic Lubrication of Piston Rings", Proceedings of the Royal Society of London. Series A, Mathematical and Physical Science, vol. 386, No. 1791, pp.409-430, April 8, 1983
- [27] Chu-Jung and Cheng-I Weng, "Elastohydrodynamic Lubrication Of Piston Rings", Wear, vol. 151, pp. 203-215, 1991
- [28] Qingmin Yang and Theo G. Keith, JR., "Two-Dimensional Piston Ring Lubrication—Part II: Elastic Ring Consideration", STLE PREPRINT No. 96-AM-3G-3, 1996
- [29] Chenbo Ma and Hua Zhu, "The Minimum Film Thickness of Piston Ring and Cylinder Liner Pair in Partial Elastohydrodynamic Lubrication", IEEE, Proceedings of International joint conference on computational sciences and optimization, 2009, pp. 323-237
- [30] Malcolm F. Fox, Craig J. Jones, D. James Picken and C.G. Stow, "The "limits of lubrication" concept applied to the piston ring zone lubrication of modern engines", Tribology Letters, vol. 3, pp. 99-106, 1997
- [31] M Afzal Malik, Syed Adnan Qasim, Badar Rashid, Shahab Khushnood, "Modeling and Simulation of Elastohydrodynamic Lubrication of Piston Skirts Considering Elastic Deformations in the initial Engine Startup," ASME/STLE International Joint Tribology Conference USA, October 2004, TRIB2004-64101.

[32] Ozgen Akalin and Golam M. Newaz, "Piston Ring-Cylinder Bore Friction Modeling in Mixed Lubrication Regime: Part I- Analytical Results", ASME Journal of Tribology, vol. 123, pp. 211-218, Jan 2001

[33] Yeau-Ren Jeng, "Theoretical Analysis of Piston-Ring Lubrication, Part I: Fully Flooded Lubrication", Tribology Transactions, vol 35, 4, pp 696 - 706, Oct 1992

MATLAB CODE FOR HYDRODYNAMIC FILM LUBRICATION

```

clear all
clc
% inode = input('How many nodes in x direction ???');
inode=11;
% jnode = input('How many nodes in y direction ???');
jnode=11;

ca=0; %crank angle initialization

%=====
% ring geometrical parameters
%=====
a1=0.5; a2=0.5; s1=2e-6; s2=s1; b=0.0015; Rad=0.0415; %radius of ring
L=2*pi*Rad;
%Rad=Rad/L;
slender=b/L;
deltac=0.0000001;
cp=0.00001;

%=====
% initializing computational Matrices & parameters
%=====
H=zeros(inode,jnode);
G=zeros(inode,jnode);
P=zeros(inode,jnode);
Ph=zeros(inode,jnode);
F=zeros(inode,jnode);
M=zeros(inode,jnode);
hminn=zeros(1,721);
pmaximum=zeros(1,721);
% reslim1=('Terminating value of residual for iteration to solav Vogelpohl
equation');
reslim1=0.000001;
% nlim1=('Max No. of iteration during solving Vogelpohl equation')
nlim1=100;
factor1=1.2;

% N=input('Engine speed in [rpm]');
N=2000;
visc=0.01600;
error=1; h0=1; % initializing so that it may enter in while loop
r=0.0418; % crank radius
l=0.15; % stroke length

V=2*pi*N*r/60;
w=V/r;
w=w/57.29578;

```

```

deltax=(1/(inode-1));
deltay=(1/(jnode-1));

lemda=Rad/(Rad+deltac);
lemda2=deltac/(Rad+deltac);

% while ((error>0)&&(error<=0.0001)) || (ca<190)
while (error>0.01) || (ca<=720)
for i = 1: inode,
    x = (i-1)*deltax;

    for j = 1: jnode,
        y = (j-1) * deltay;

        if x<=a1
            h1=s1*(x^2-2*a1*x+a1*a1);
            dh1dx=2*s1*(x-a1);
            d2h1dx2=2*s1;

        elseif x > a2
            h1=s2*(x^2-2*a2*x+a2*a2);
            dh1dx=2*s2*(x-a2);
            d2h1dx2=2*s2;

        else
            h1=0;
            dh1dx=0;
            d2h1dx2=0;
        end

%         h1=(1+x)^2;
%         dh1dx=2*(1+x);
%         d2h1dx2=2;

        theta=(y*L)/Rad;
%         theta=theta*pi/180;
        h2=Rad*((1/((1-(1-lemda)*sin(theta))^0.5))-1);
        h2=h2/cp;
        h2=abs(h2);
        dh2dy=0.5*lemda2*((1-(1-lemda)*sin(theta))^-1.5)*(cos(theta));
        d2h2dy2=(3/(4*Rad/(Rad+cp)))*((cos(theta)*lemda2)^2)*(1-(1-
lemda)*sin(theta))^-2.5)-((Rad/(Rad+cp))*0.5*lemda2*(1-(1-
lemda)*sin(theta))^-1.5));

        h=h0+h1+h2;

```

```

        h=abs(h);
        %h=abs(h);

        H(i,j) =h;
        G(i,j) = dh1dx/(h^1.5);
        F(i,j) = 0.75*(dh1dx^2 + ((b/L)*dh2dy)^2)/(h^2) + 1.5*(d2h1dx2 +
d2h2dy2*((b/L)^2))/h;

        end;
end;

coeff1 = 1/deltax^2;
coeff2 = (slender/deltay)^2;

%=====
%SUBROUTINE TO SOLVE THE VOGELPOHL EQUATION
%=====
sum2 = 0; n1 = 0; residp = reslim1 + 10;
while (residp > reslim1) && (n1 < nlim1),
    n1 = n1 + 1; sum = 0;
    for i = 2: inode-1,
        for j = 2: jnode-1,
            store = ((M(i+1,j) + M(i-1,j))*coeff1 + (M(i,j+1) + M(i,j-
1))*coeff2-G(i,j))/(2*coeff1 + 2*coeff2 + F(i,j));
            M(i,j) = M(i,j) + factor1*(store-M(i,j));
            if M(i,j) < 0, M(i,j) = 0.0; end;
            sum = sum + M(i,j);
        end;
    end;
    if(sum==0)
        sum=0.0001;
    end
    residp = abs((sum - sum2)/sum); sum2 = sum;
end;
car=ca*pi/180;    %converting to radian
B=cp+(r*sin(car));
U=r*w*sin(car)+r*w*B*cos(car)*(1^2-b^2)^0.5;
U=abs(U);
% =====
% FIND PRESSURE FIELD FROM VOGELPOHL PARAMETER
%=====
for i = 2: inode-1,
    for j = 2: jnode-1,
        if(H(i, j)==0)
            H(i, j)=0.0001;
        end
        P(i,j) = M(i, j)/(H(i,j))^1.5;
        Ph(i,j)=(P(i,j))*6*U*visc*b/(cp^2);
    end;
end;
end;

```

```

%=====
%SUBROUTINE TO CALCULATE Radial force
%=====
suminx=zeros(jnode,1);
suminy=0;
%rload=0;
for j=1:jnode

    for i=1:inode

        if i>1 && i<inode
            if rem(i,2)==0
                suminx(j,1)=suminx(j,1)+(4*Ph(i,j));
            else suminx(j,1)=suminx(j,1)+(2*Ph(i,j));
            end
        end

        if (i==1)|| (i==inode)
            suminx(j,1)=suminx(j,1)+Ph(i,j);
        end
    end

    suminx(j,1)=deltax*suminx(j,1)/3;
end

for j=1:jnode
    if j>1 && j<jnode
        if rem(j,2)==0
            suminy=suminy +(4*suminx(j,1));
        else
            suminy=suminy+(2*suminx(j,1));
        end
    end

    if j==1|| j==jnode
        suminy=suminy+suminx(j,1);
    end
end

rload=(deltay*suminy/3)
% rload=mean(mean(Ph));
rload=rload+(rload==0)*eps;
% rload=abs(rload);
%     if rload==0
%         rload=0.01;
%     end
%=====
%Subroutine to calculate error term
%=====
    if ca>=0 && ca<180           %for crank angle 0 to 180
        FG=0.1;
    end

```

```

if ca>=180 && ca<=372          %for crank angle 180 to 372
    p1 = 1.9641e-020;
    p2 = -1.5914e-017;
    p3 = 4.3074e-015;
    p4 = -4.0552e-013;
    p5 = 5.6291e-012;
    FG = p1*ca^10 + p2*ca^9 + p3*ca^8 + p4*ca^7 + p5*ca^6;
end

if ca>372 && ca<=450          %for crank angle 372 to 450
    p1 = 0.0022685;
    p2 = -2.5086;
    p3 = 674.36;

    FG = p1*ca^3 + p2*ca^2 + p3*ca;
end

if ca>450 && ca<=540          %for crank angle 450 to 720
    p1 = 1.0565e-005;
    p2 = -0.025333;
    p3 = 22.624;
    p4 = -8919.9;
    p5 = 1.3101e+006;
    FG = p1*ca^4 + p2*ca^3 + p3*ca^2 + p4*ca + p5;
    if FG<0.1
        FG=0.1;
    end
end

if ca>540
    FG=0.1;
end

error=(abs(rload-FG))/rload    %error in ho asstimation
error=real(error)
error=error+(error==0)*eps;
%=====
% if error term satisfied to 0.005 or not
%=====
if error>0.01
    h0approx=h0*((FG/rload)^0.1);
    h0=h0-0.15*(h0approx-h0)

% h0=((rload-FG)*(Rad^2))/(0.005*cp*113.79e9)

end

if (error<0.01)
    ca=ca+1;
    hminn(1,ca)=(cp*h0);
    pmaximum(1,ca)=max(max(Ph));
end
end

```

MATLAB CODE FOR ELASTOHYDRODYNAMIC FILM LUBRICATION

```

clear all
clc
% inode = input('How many nodes in x direction ???');
inode=11;
% jnode = input('How many nodes in y direction ???');
jnode=11;

ca=0; %crank angle initialization

%=====
% ring geometrical parameters
%=====
a1=0.5; a2=0.5; s1=2e-6; s2=s1; b=0.0015; Rad=0.0415; %radius of ring
L=2*pi*Rad;
%Rad=Rad/L;
slender=b/L;
deltac=0.0000001;
cp=0.00001;

%=====
% initializing computational Matrices & parameters
%=====
H=zeros(inode,jnode);
G=zeros(inode,jnode);
P=zeros(inode,jnode);
Ph=zeros(inode,jnode);
Pe=zeros(inode,jnode);
F=zeros(inode,jnode);
M=zeros(inode,jnode);
hminn=zeros(1,721);
% viscl=ones(inode,jnode);
% reslim1=('Terminating value of residual for iteration to solav Vogelpohl
equation');
reslim1=0.000001;
% nlim1=('Max No. of iteration during solving Vogelpohl equation')
nlim1=100;
factor1=1.2;

% N=input('Engine speed in [rpm]');
N=600;
visc0=0.01600;
% viscl=visc*viscl;
error=1; h0=1; % initializing so that it may enter in while loop
r=0.0418; % crank radius
l=0.15; % stroke length

V=2*pi*N*r/60;
w=V/r;
w=w/57.29578;

deltax=(1/(inode-1));
deltay=(1/(jnode-1));

```

```

lemda=Rad/(Rad+deltac);
lemda2=deltac/(Rad+deltac);

Er=113.79e9;
Ec=200e9;
prc=0.3;
prc=0.3;
Eavg=0.5*((1-(prc^2))/Er)+((1-(prc^2))/Ec));

%while ((error>0)&&(error<=0.1))||(ca<720)
while (error>0.01)||(ca<=720)
    for j=1:jnode
        y=(j-1)*deltay;
        y=y*L;

        for i=1:inode
            x=(i-1)*deltax;
            x=x*b;
            if (x==0) && (y==0)
                pv=1;
            else
                pv=((x^2)+(y^2))^0.5;
            end

            Pe(i,j)=(1/pi)*Eavg*Ph(i,j)/pv;
        end
    end

suminx=zeros(jnode,1);
suminy=0;
%rload=0;
for j=1:jnode

    for i=1:inode

        if i>1 && i<inode
            if rem(i,2)==0
                suminx(j,1)=suminx(j,1)+(4*Pe(i,j));
            else suminx(j,1)=suminx(j,1)+(2*Pe(i,j));
            end
        end

        if (i==1)||(i==inode)
            suminx(j,1)=suminx(j,1)+Pe(i,j);
        end
    end

    suminx(j,1)=deltax*suminx(j,1)/3;
end

for j=1:jnode

```

```

        if j>1 && j<jnode
            if rem(j,2)==0
                suminy=suminy +(4*suminx(j,1));
            else
                suminy=suminy+(2*suminx(j,1));
            end
        end

        if j==1||j==jnode
            suminy=suminy+suminx(j,1);
        end
    end
    ed=(deltay*suminy/3);

for i = 1: inode,
    x = (i-1)*deltax;

    for j = 1: jnode,
        y = (j-1) * deltay;

        if x<=a1
            h1=s1*(x^2-2*a1*x+a1*a1);
            dh1dx=2*s1*(x-a1);
            d2h1dx2=2*s1;

        elseif x > a2
            h1=s2*(x^2-2*a2*x+a2*a2);
            dh1dx=2*s2*(x-a2);
            d2h1dx2=2*s2;

        else
            h1=0;
            dh1dx=0;
            d2h1dx2=0;
        end

        %         h1=(1+x)^2;
        %         dh1dx=2*(1+x);
        %         d2h1dx2=2;

        theta=(y*L)/Rad;
        %     theta=theta*pi/180;
        h2=Rad*((1/((1-(1-lemda)*sin(theta))^0.5))-1);
        h2=h2/cp;
        dh2dy=0.5*lemda2*((1-(1-lemda)*sin(theta))^-1.5)*(cos(theta));
        d2h2dy2=(3/(4*Rad/(Rad+cp)))*((cos(theta)*lemda2)^2)*(1-(1-
lemda)*sin(theta))^-2.5)-((Rad/(Rad+cp))*0.5*lemda2*(1-(1-
lemda)*sin(theta))^-1.5));

        h=h0+h1+h2+ed;

```

```

    %h=abs(h);

    H(i,j) =h;
    G(i,j) = dh1dx/(h^1.5);
    F(i,j) = 0.75*(dh1dx^2 + ((b/L)*dh2dy)^2)/(h^2) + 1.5*(d2h1dx2 +
d2h2dy2*((b/L)^2))/h;

    end;
end;

coeff1 = 1/deltax^2;
coeff2 = (slender/deltay)^2;

%=====
%SUBROUTINE TO SOLVE THE VOGELPOHL EQUATION
%=====
    sum2 = 0; n1 = 0; residp = reslim1 + 10;
    while (residp > reslim1) && (n1 < nlim1),
        n1 = n1 + 1; sum = 0;
        for i = 2: inode-1,
            for j = 2: jnode-1,
                store = ((M(i+1,j) + M(i-1,j))*coeff1 + (M(i,j+1) + M(i,j-
1))*coeff2-G(i,j))/(2*coeff1 + 2*coeff2 + F(i,j));
                M(i,j) = M(i,j) + factor1*(store-M(i,j));
                if M(i,j) < 0, M(i,j) = 0.0; end;
                sum = sum + M(i,j);
            end;
        end;
        if(sum==0)
            sum=0.0001;
        end
        residp = abs((sum - sum2)/sum); sum2 = sum;
    end;
    car=ca*pi/180;    %converting to radian
    B=cp+(r*sin(car));
    U=r*w*sin(car)+r*w*B*cos(car)*(1^2-b^2)^0.5;
    U=abs(U);
% =====
% FIND PRESSURE FIELD FROM VOGELPOHL PARAMETER
%=====
    for i = 2: inode-1,
        for j = 2: jnode-1,
            if(H(i, j)==0)
                H(i, j)=0.0001;
            end
            P(i,j) = M(i, j)/(H(i,j))^1.5;
            visc=visc0*exp(P(i,j)*2.8712e-4);
            Ph(i,j)=(P(i,j))*6*U*visc*b/(cp^2);
        end;
    end;
end;

```

```

%=====
%SUBROUTINE TO CALCULATE Radial force
%=====
suminx=zeros(jnode,1);
suminy=0;
%rload=0;
for j=1:jnode

    for i=1:inode

        if i>1 && i<inode
            if rem(i,2)==0
                suminx(j,1)=suminx(j,1)+(4*Ph(i,j));
            else suminx(j,1)=suminx(j,1)+(2*Ph(i,j));
            end
        end

        if (i==1)|| (i==inode)
            suminx(j,1)=suminx(j,1)+Ph(i,j);
        end
    end

    suminx(j,1)=deltax*suminx(j,1)/3;
end

for j=1:jnode
    if j>1 && j<jnode
        if rem(j,2)==0
            suminy=suminy +(4*suminx(j,1));
        else
            suminy=suminy+(2*suminx(j,1));
        end
    end

    if j==1|| j==jnode
        suminy=suminy+suminx(j,1);
    end
end

    rload=(deltay*suminy/3);
% rload=mean(mean(Ph));
rload=rload+(rload==0)*eps;
% rload=abs(rload);
%     if rload==0
%         rload=0.01;
%     end
%=====
%Subroutine to calculate error term
%=====
    if ca>=0 && ca<180           %for crank angle 0 to 180
        FG=0.1;
    end

```

```

if ca>=180 && ca<=372      %for crank angle 180 to 372
    p1 = 1.9641e-020;
    p2 = -1.5914e-017;
    p3 = 4.3074e-015;
    p4 = -4.0552e-013;
    p5 = 5.6291e-012;
    FG = p1*ca^10 + p2*ca^9 + p3*ca^8 + p4*ca^7 + p5*ca^6;
end

if ca>372 && ca<=450      %for crank angle 372 to 450
    p1 = 0.0022685;
    p2 = -2.5086;
    p3 = 674.36;

    FG = p1*ca^3 + p2*ca^2 + p3*ca;
end

if ca>450 && ca<=540      %for crank angle 450 to 720
    p1 = 1.0565e-005;
    p2 = -0.025333;
    p3 = 22.624;
    p4 = -8919.9;
    p5 = 1.3101e+006;
    FG = p1*ca^4 + p2*ca^3 + p3*ca^2 + p4*ca + p5;
    if FG<0.1
        FG=0.1;
    end
end

end

if ca>540
    FG=0.1;
end

error=(abs(rload-FG))/rload;      %error in ho asstimation
error=real(error)
error=error+(error==0)*eps;
%=====
% if error term satisfied to 0.005 or not
%=====
if error>0.01
    h0approx=h0*((FG/rload)^0.01);
    h0=h0-0.15*(h0approx-h0)

% h0=((rload-FG)*(Rad^2))/(0.005*cp*113.79e9)

end

% if ((error>0)&&(error<=0.0001))

if (error<0.01)
    ca=ca+1;
    hminn(1,ca)=(cp*h0)+ed;

```

end
end